CEPT ECC
Electronic Communications Committee

ECC Report 363

Aggregated interference from satellite systems into radio astronomy service

approved 24 January 2025

0 EXECUTIVE SUMMARY

Radio astronomical research is geared to detect and characterize the farthest and smallest radio sources in the outer space: the sensitivity of the equipment used for radio astronomical experiments is very important, explaining why the level of unwanted emissions of the various systems of other services operating in bands that could have an impact on radio astronomy must be controlled. Therefore, astronomers usually construct radio telescopes in remote areas, ideally with natural shielding from surrounding terrain. Despite these efforts, air and spaceborne transmitters may represent a challenge, owing to their ubiquitous nature and the international (spectrum management) framework in which they are operated.

The main goal of this report is to study the aggregation of received power from multiple satellite constellations into radio astronomy receiving systems. For this, the equivalent power flux density (epfd) method has been applied, which is described in detail in section 5.1. The threshold levels of interference detrimental to different types of radio astronomy observations (continuum observations, spectral line and VLBI observations) are provided in Recommendation ITU-R RA.769-2 [4]. The protection criterion, given in Recommendation ITU-R RA.1513-2 [5], is met when the data loss is less than 2% for an individual non-GSO satellite system, i.e. when less than 2% of the epfd samples over the entire sky, each averaged over 2000 s, exceed the threshold value given in Recommendation ITU-R RA.769-2, using the methodology given in Recommendation ITU-R M.1583-1 [7] and ITU-R S.1586-1. Recommendation ITU-R RA.1513-2 also specifies that a criterion of 5% is to be used for the aggregate data loss to the RAS due to interference from all networks.

This Report also identifies the parameters of the radio astronomy station as well as the ones of the non-GSO satellite system(s) required in the analysis. Sensitivity analyses on some of those parameters are included as well.

To date, if technical parameters or deployment information (e.g. satellite antenna pointing directions) are not provided, no method is known to estimate the epfd and data loss at an RAS site caused by a single satellite system. Regarding aggregate data loss from multiple non-GSO satellite systems, it was found that it could not be directly inferred from the respective data losses corresponding to each of the individual non-GSO satellite systems. The aggregate data loss needs to be calculated from the summation of epfd of all considered non-GSO satellite systems for each time sample.

This Report also includes examples, including data loss calculations, and investigates the dependency of the outcomes of the simulations on single parameters (see section 6). Some key findings are as follows:

- the equatorial coordinate reference frame offers a potential alternative or complement to the usual calculations in the horizontal (topocentric) observer frame. Equatorial coordinates are more commonly used in astronomy to compensate for the Earth's rotation. Results in the equatorial and horizontal frames can differ, with the distribution of the power in the equatorial frame usually being smoother over the sky;
- boresight avoidance, which is the technique to switch off satellite transmissions when a satellite is moving through a RAS observing beam (assuming the beam pointing is known in real time) may help to mitigate interference and to reduce data loss but could require relatively large areas around the RAS beam to be kept free from transmission. Boresight avoidance would however always require close coordination between the operators of the non-GSO satellite system and all the RAS stations to be protected.
- the geo-arc avoidance concept, which is used to protect GSO from non-GSO systems, is estimated to have a limited impact on RAS epfd results and could be left out from calculations in order to simplify the studies.

The above findings are valid for the chosen example configurations and there may be certain sets of parameters and deployments for which different results could be obtained. Some of the required parameters are not publicly available, and the report lists examples of potential fall-back solutions that may be used when it is the case. Confidence in the results can only be achieved through the joint cooperation between radio astronomers and non-GSO system operators (and their respective notifying administrations), as they are the only ones in position to provide all the missing information on the operational characteristics of their respective systems.

TABLE OF CONTENTS

LIST OF ABBREVIATIONS -

Abbreviation	Explanation
AAS	Active Antenna Systems
BSS	Broadcasting-Satellite Service
CEPT	European Conference of Postal and Telecommunications Administrations
CCDF	Complementary Cumulative Distribution Function
ECC	Electronic Communications Committee
e.i.r.p.	Effective Isotropic Radiated Power
epfd	Equivalent Power Flux Density
FSS	Fixed-satellite Service
GPS	Global Positioning System
GSO	Geostationary Orbit
HPBW	Half-power Beam Width
IMT	International Mobile Telecommunications
IoT	Internet of Things
ITU	International Telecommunication Union
LEO	Low Earth Orbit
LOFAR	LOw Frequency ARray
MES	Mobile Earth Station
MMSS	Maritime Mobile-Satellite Service
MSS	Mobile-Satellite Service
NenuFAR	New Extension in Nançay Upgrading LOFAR
NOEMA	NOrthern Extended Millimeter Array
Non-GSO	Non Geostationary Orbit
OOB	Out-of-band
pfd	Power Flux Density
RAAN	Right Ascension of the Ascending Node
RAS	Radio Astronomy Service
RNSS	Radionavigation Satellite Service
RR	Radio Regulations
VHF	Very High Frequency
VLBI	Very Long Baseline Interferometry

1 INTRODUCTION

Radioastronomical research is geared to detect and characterise the farthest and smallest radio sources in the outer space. The extreme sensitivity required for radioastronomical experiments is achieved by optimising three factors:

- by employing antennas with a large effective area, the collected power is increased, as also indicated in Recommendation ITU-R SA.509-3 [1], Recommendation ITU-R RA.1631-0 [2] and Recommendation ITU-R S.1428-1 [3], with the latter being referred to in Recommendation ITU-R RA.769-2 [4]. Dish antennas with diameters of up to 500 meters are in use, and telescopes with up to 100 meters in diameter remain fully steerable (see e.g. Recommendation ITU-R SA.509-3 [1]);
- the low-noise amplification in the − mostly cooled − receiver systems makes it possible to detect tiniest differences in the received power;
- the signal is integrated and then averaged over long periods and partly over large bandwidths.

This results in systems with extraordinarily small noise figures of the order of 0.01 dB and an rms noise or sensitivity levels of −310 dBW/m2/Hz (equivalent to 10 µJy) and lower. Important radioastronomical sources can be characterised only at that level. Typical levels of interference which may be tolerable by other services may lead to the failure of radio astronomical experiments. The sensitivity of RAS to radio interference is taken into account in the RAS protection criteria recommended in ITU-R RA.769-2 [4]. While in principle the complete frequency spectrum is usable for radio astronomical measurements, there are some frequency bands of the highest interest, characterised by line emission of atoms or molecules especially abundant in space. In some of those bands, RAS has a primary or secondary allocation in the ITU Radio Regulations (RR). Some additional important frequency ranges are furthermore addressed in footnote No. 5.149, which urges administrations to consider RAS protection when making assignments to other services in these bands. For any RAS band it is not only a requirement to guard the allocated band from any in-band emission, but it is also required to keep out-of-band or spurious emissions from adjacent bands below the RAS protection limits.

A strategy to enable RAS to operate relatively unaffected by harmful interference originating from active services is to choose remote, geographically protected sites to operate radio telescopes (see also Recommendation ITU-R RA.611-4 [6]) This may work well to avoid interference from Earth-bound services, but after the most recent attempts to choose the most remote and protected sites for the RAS operation, it has soon been realised that even with such careful choices, interference by airborne- and especially satellite-borne transmitters may severely affect RAS experiments. This makes it very important that satellite services control any kind of emission into bands allocated to RAS to stay below acceptable limits, which are specified in Recommendation ITU-R RA.769-2 [4].

The importance of protection of RAS from interference caused by satellite services has increased in recent years. Modern technology has made a leap and, through very low payload cost in launching services, it is now possible to deploy a large number of satellites into a non-GSO orbit. In fact, several projects are underway to operate satellite constellations of up to tens of thousands of non-GSO satellites.

In addition to the thresholds for harmful interference defined in Recommendation ITU-R RA.769-2 [4], Recommendation ITU-R RA.1513-2 [5] recommends that RAS stations experience a maximum data loss of 2% per system and 5% for the aggregate effect of all systems. In Annex 1 to the latter Recommendation it is concluded that a loss of data for 2% of the time per system is a practical limit to comply with the 5% requirement for all systems, but that further studies of this assumption may be necessary. This could be of particular interest in the case of low Earth orbit (LEO) satellite constellations, where a multitude of satellite systems can be expected. This Report has the aim to provide the technical foundation and analyses how the aggregation of interference (and its resulting data loss) from multiple satellite systems into the RAS can be numerically determined based on methods in existing Recommendations such as ITU-R M.1583-1 [7] and ITU-R S.1586-1 [8]. However, while this Report describes and applies the methodology to compute the aggregate data loss, it is noted that addressing any regulatory aspect is beyond its scope.

2 PROTECTION THRESHOLD AND ACCEPTABLE DATA LOSS FOR RAS

Protection criteria used for radioastronomical measurements and the acceptable data loss levels are laid out in Recommendation ITU-R RA.769-2 [4] and Recommendation ITU-R RA.1513-2 [5] respectively.

Recommendation ITU-R RA.769-2 [4] provides the methods to calculate threshold interference levels as the received input power, power flux density, and spectral power flux density, for a given set of values for integration time, frequency, bandwidth, and antenna- and system temperature of the receiving radio astronomical system. It also provides a set of tables listing those values for continuum and line observations for a number of representative frequencies (with allocations to RAS in the ITU Radio Regulations (RR)). Recommendation ITU-R RA.769-2 assumes an integration time of 2000 seconds to calculate sensitivities and interference levels in Tables 1 and 2, but actual integration times used in astronomical observations cover a wide range of values and the calculated values could be adjusted accordingly.

Recommendation ITU-R RA.1513-2 [5] discusses and specifies the practicability of meeting the requirement of threshold interference levels for radio astronomy and recommends data loss percentages for interference ("levels of data loss"), in particular through unwanted emission, for which an interferer may exceed the levels recommended in Recommendation ITU-R RA.769-2 [4]. The total recommended data loss percentage for the aggregate interference from all systems, above the threshold from Recommendation ITU-R RA.769-2 [4], is 5 percent, while the recommended data loss percentage for a single system is 2 percent.

Further discussion on how to apply these criteria can be found in section 5.

3 EXAMPLES OF RAS STATIONS

The characteristics of RAS systems may differ strongly. In particular, their antenna technology can vary from classical parabolic dishes over simple antenna elements, which may be connected to a phased array or to an interferometer. In the latter, the data from several antennas (or even phased-array apertures) are correlated (complex multiplied) to synthesise an observation corresponding to an antenna with a much larger diameter than that of the single antennas. The synthetic beam from such an observation is significantly narrower than a single-dish beam. For the purpose of calculating data losses, several parameters are significant, which are discussed in detail in section 5. Table 1 provides an example overview of several RAS observatories in CEPT countries, listing some information and a few relevant parameters: country, in which the site can be found, name or place of the RAS station, geographical latitude and longitude, operational status, and minimum elevation angle.

The latter is relevant, because, due to the geographical surrounding of the RAS stations, it may not always be possible to point the antenna in any direction as topography or physical obstacles could be blocking the sky, ITU-R Resolution 739 (Rev.WRC-19) [9] specifies that only RAS pointing directions above the RAS station minimum elevation angle θ_{min} shall be taken into account in the epfd calculations (see section 5). It is noted, however, that satellites below the minimum elevation of the RAS station, and not shielded by the surrounding terrain, could still contribute to the overall epfd value via receiving-antenna side-lobes.

The examples listed in Table 1 are provided for information only, to illustrate the variation of the parameters shown for different radioastronomy sites. Since some of those values are subject to evolution, they should not be directly used for sharing and compatibility studies.

Table 1: Examples of RAS observatories in Europe

Country	Place	Number of telescopes	Geographical coordinates	Minimum and maximum frequency (MHz)	Minimum Elevations (°)	Comment
Austria	Lustbühel	2	15° 29′ 34″ E 47° 04′ 03″ N	15-81	42 0	
Belgium	Humain	1	05° 15′ 12″ E 50° 11′ 31″ N	45-11000	0	
Finland	Metsähovi	3	24° 23′ 36″ E 60° 13′ 05″ N	2-210-98000	0	
France	Bordeaux	1	00° 31′ 32″ W 44° 50′ 06″ N	1400-1700	0	Closed
France	Nançay	4	02° 11′ 50″ E 47° 22′ 24″ N	10-10700	3.6	
France	NOEMA	12	05° 54′ 28.5″ E 44° 38′ 02″ N	18700-373000	3	
Germany	Effelsberg	3	06° 53′ 01″ E 50° 31′ 29″	10-95500	8	
Germany	Wettzell	2	12° 52′ 38″ E 49° 08′ 42″ N	2100-14000	0	
Italy	Matera	1	16° 42′ 14″ E 40° 38′ 58″ N	2210-8980	5	VLBI Station
Italy	Medicina	2	11° 38′ 49″ E 44° 31′ 15″ N	400-26500	15	
Italy	Noto	1	14° 59′ 20″ E 36° 52′ 33″ N	256-86700	5	
Italy	Sardinia	1	09° 14′ 42″ E 39° 29′ 34″ N	270-116000	5	
the Netherlands	Westerbork	14	06° 36′ 15″ E 52° 55′ 01″ N	250-8650	0	

Country	Place	Number of telescopes	Geographical coordinates	Minimum and maximum frequency (MHz)	Minimum Elevations (°)	Comment
Poland	Kraków	1	19° 49′ 36″ E 50° 03′ 18″ N	275-1755	10	Ceased activity
Poland	Torun	2	18° 33′ 51″ E 52° 54′ 38″ N	1350-36000	2 6	
Portugal	Espiunca	1	08° 13′ 52″ W 40° 59′ 57″ N	150-650	24.5	Ceased activity
Portugal	Santa Maria	1	25° 07′ 33″ W 36° 59′ 07″ N	2000-15000	5	
Spain	Pico Veleta	1	03° 23′ 34″ W 37° 03′ 58″ N	73000-375000	0	
Spain	Robledo	4	04° 14′ 57″ W 40° 25′ 38″ N	1400-50000	6	
Spain	Yebes	2	03° 05′ 13″ W 40° 31′ 29″ N	2000-116000	5	
Sweden	Onsala	4	11° 55′ 04″ E 57° 23′ 35″ N	10-116000	7 6 0 0	
Switzerland	Bleien	2	08°06′ 44″ E 47°20′ 26″ N	10-10700	0 3	
Türkiye	Kayseri	1	35° 32′ 43″ E 38° 42′ 37″ N	406-10700	30	
United Kingdom	Cambridge	5	00° 02′ 20″ E 52° 09′ 59″ N	38-31800	0 30 0 55 2	
United Kingdom	Jodrell Bank	2	02° 18′ 26″ W 53° 14′ 10″ N	150-24000	-1 0	
Europe	LOFAR	52		10-240	0	

4 EXAMPLES OF SATELLITE SYSTEMS

There is an increasing number of non-GSO satellite systems operating nowadays or planning to operate in the near future, providing services that range from low data rate Internet of Things (IoT) connectivity to direct-to-home broadband. This section provides some examples of such non-GSO satellite systems. For illustration purposes, they are divided between systems operating in the mobile-satellite service (MSS) and systems operating in the fixed-satellite service (FSS).

Space stations, either operating in the MSS or in the FSS, have a potential of generating interference to the RAS if they are using adjacent or co-frequency bands. In sections 4.1 and 4.2, there are examples of non-GSO satellite systems operating or planning to operate in bands ranging from VHF to Ka band (it is worth mentioning that there are plans to operate in Q/V band too).

This section is intended for illustration purposes, these examples include both systems that operate close to RAS allocations (see Table 2) and also systems that operate far from any existing RAS allocation. The last column of the tables listing these systems in sections 4.1 and 4.2 indicates if the non-GSO systems listed are operating in the space-to-Earth direction in a band adjacent to RAS.

Table 2: Bands with primary RAS allocations that are adjacent to bands where non-GSO satellite systems operate in the space-to-Earth direction

Radio astronomy allocations (Primary)	Adjacent space-to-Earth allocations
150.05-153 MHz	137-138 MHz (MSS) 157.1875-157.3375 MHz and 161.7875-161.9375 MHz (MMSS)
406.1-410 MHz	400.15-401 MHz (MSS)
1610.6-1613.8 MHz	1613.8-1626.5 MHz (MSS)
10.6-10.68 GHz, 10.68-10.7 GHz	10.7-10.95 GHz (FSS)
42.5-43.5 GHz	41-42.5 GHz (FSS and BSS) 43.5-47 GHz (MSS potentially space-to-Earth)
76-77.5 GHz	75.5-76 GHz (FSS)

4.1 EXAMPLE MSS SYSTEMS

Table 3 provides several examples of MSS non-GSO systems. More information about the systems operating below 1 GHz can be found in ECC Report 322 [10]. Note that not all the bands below are available for MSS use in all countries[1].

[1] As an example within CEPT, the bands 1616-1621 MHz and 148-149 MHz are not available for MSS use in the United Kingdom

Table 3: Example non-GSO systems in the mobile-satellite service

Satellite System	Spectrum for uplink/downlink	No. of satellites	Altitude (km)	Application(s)	Operating in the space-to-earth direction in a band adjacent to RAS
LEOTELCOM-1 (ORBCOMM)	137-138 MHz (space-to-Earth) 148-150.05 MHz (Earth-to space)	48	950 [11]	IoT and M2M	Yes
ARGOS KINEIS	400.15-401 MHz (space-to-Earth) 401-403 MHz or 399.9-400.05 MHz (Earth-to-space)	>25	650 [12]	IoT	Yes
SWARM	137-138 MHz (space-to-Earth) 148-150.05 MHz (Earth-to-space)	150	450-550	IoT and M2M	Yes
MYRIOTA	137-138 MHz and 400.15-401 MHz (space-to-Earth) 148-150.05 MHz and 399.9-400.05 MHz (Earth-to-space)	208	450-600	IoT	Yes
FLEETSPACE	387-390 MHz and 400.15-401MHz (space-to-Earth) 399.9-400.05 MHz and [312-315 MHz] (Earth-to-space)	145	up to 587	IoT and M2M	Yes
IRIDIUM	1617.775-1626.5 MHz5	66	780 (Note 1)	Personal communications, travel & outdoor, boating, aviation etc.	Yes
GLOBALSTAR, Inc.	2483.5-2500 MHz (space-to-Earth) 1610-1621.35 MHz (Earth-to-space)	24	1414 [13]	Spot – track and trace	No
Note 1: https://eccwp.cept.org/WI_Detail.aspx?wiid=408					

4.2 EXAMPLE FSS SYSTEMS

Some example non-GSO FSS systems, several of which are often referred to as "mega constellations", is given in Table 4.

Table 4: Example non-GSO systems in the fixed-satellite service

Satellite System	Spectrum for downlink (space-to-Earth) (GHz)	Initial No. satellites	Orbital planes	Altitude (km)	Application(s)	Operating in the space-to-earth direction in a band adjacent to RAS
Kuiper [14] (Amazon)	17.7-18.6, 18.8-20.2	3236	98 [14]	590 610 630	Direct to home broadband	No
Kepler [15]	10.7-12.7	140	12 (30 satellites per plane) [16]	600 ±50	IoT	Yes
OneWeb (Eutelsat Group) [17]	10.7-12.7, 17.8-18.6,18.8-19.3	588	12 (49 satellites per plane)	1100-1200	Backhaul /mobility	Yes
Starlink Gen1 [18] (SpaceX)	10.7-12.7, 17.8-18.6, 18.8-19.3	4408	72 (22 satellites per plane at 540 km) 72 (22 satellites per plane at 550 km) 6 (58 satellites per plane at 560 km) 4 (43 satellites per plane at 560 km) 36 (20 satellites per plane at 570 km) Total=4408 [19]	540 550 560 570	Direct to home broadband	Yes
Lightspeed (Telesat) [20]	17.8-18.6,18.8-19.3,19.7-20.2	198	6 (13 satellites per plane at 1015 km) 20 (11 satellites per plane at 1325 km) [21]	1015 1325	Backhaul /mobility	No

5 METHOD TO CALCULATE THE DATA LOSS

5.1 EPFD CALCULATION

5.1.1 Basic description of the epfd method

For the epfd calculations, the first step is to calculate the satellite positions for a range of time steps. Recommendation ITU-R RA.769-2 [4] contains power- and power flux density threshold levels for the protection of the RAS. As radio astronomers often integrate for minutes or even hours on a sky position to reduce the radiometric noise in the data, the protection thresholds are also defined for a given observation time. Today, the de-facto standard for the RAS integration time to be used in regulatory processes is 2000 seconds (s). Consequently, for the epfd, a time interval of 2000 s is simulated, usually with time steps of the order of a second. The time resolution needs to be fine enough such that the angular distance travelled by a satellite in this time step is not too large compared to the angular resolution of the RAS receiving system. It is noted that for comparison with the Recommendation ITU-R RA.769-2 [4] levels, the received power must be averaged over the 2000 stime range, but only after the power received from all satellites (i.e. the total power) for each time step has been determined.

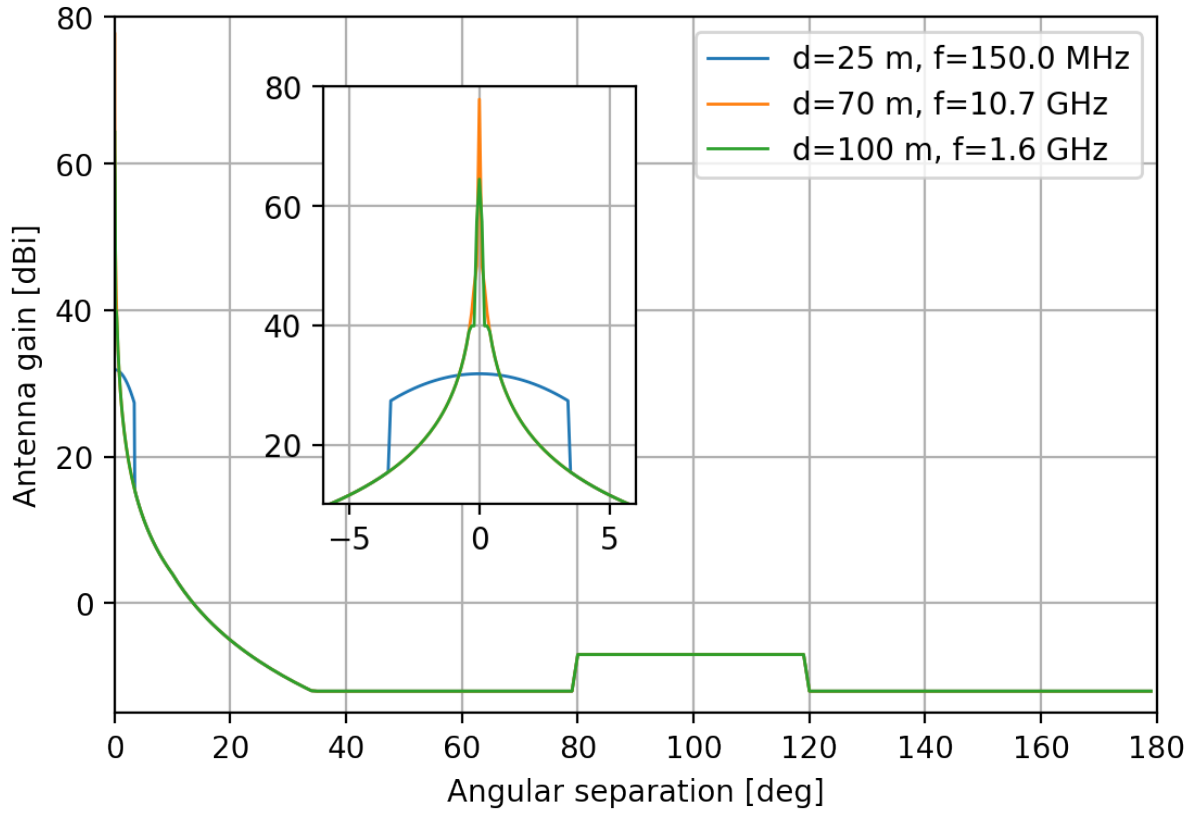

Figure 1: RAS antenna patterns according to Recommendation ITU-R RA.1631-0 [2] for a few example frequencies and antenna diameters

For the calculation of the total power in a single time step, the antenna diagrams of the transmitting satellite and the RAS station need to be considered. The transmitter patterns can vary a lot depending on the type of satellite. This can range from simple dipole-like types to active antenna systems, which provide beamforming capabilities in real time. For the RAS station, it is common to use the pattern as defined in Recommendation ITU-R RA.1631-0 [2], which is displayed in Figure 1 for a few example frequencies and antenna sizes. This pattern is that of a highly idealised paraboloid. There is a noteworthy feature at an angular distance of about 100° from the antenna boresight, which resembles the spill-over ring of the aperture. In reality, RAS antenna patterns are much more complicated, e.g. owing to feed support legs and primary focus cabins, which block part of the aperture. Furthermore, there are also completely different antenna designs in use, in particular for

low-frequency interferometers, such as LOFAR or NenuFAR, which employ arrays of dipole antennas that are electronically phased-up to form large, synthesised apertures. Still, from a statistical point of view, the results in an epfd simulation are expected to depend mostly on the size of the aperture, which also defines the width of the antenna main beam, thus the Recommendation ITU-R RA.1631-0 [2] model can be considered as suitable in regulatory calculations.

One very important aspect for satellite constellations is that the power received via the near- and far side-lobes of the RAS antenna can play a significant role. For large dish antennas, the main beam gain can be 30 dBi and more above the typical near side-lobe gain (even more compared to far side-lobes) as shown in Figure 1. However, the chances that a satellite crosses the main beam are low and the sheer number of satellites above the horizon can produce a significant contribution even via the side-lobes. In Figure 2, a snapshot of a simulation is visualised for three different times, in which the satellites of a large LEO constellation are shown in the topocentric frame (azimuth, φ, and elevation, ϑ) of the observer. The antenna pattern is shown as red-shaded area for a case when the antenna points to $(\varphi_0, \vartheta_0) = (31.62°, 30.44°)$. Again, the spill-over ring appears; as a large area at an angular distance of about 100° from the pointing position.

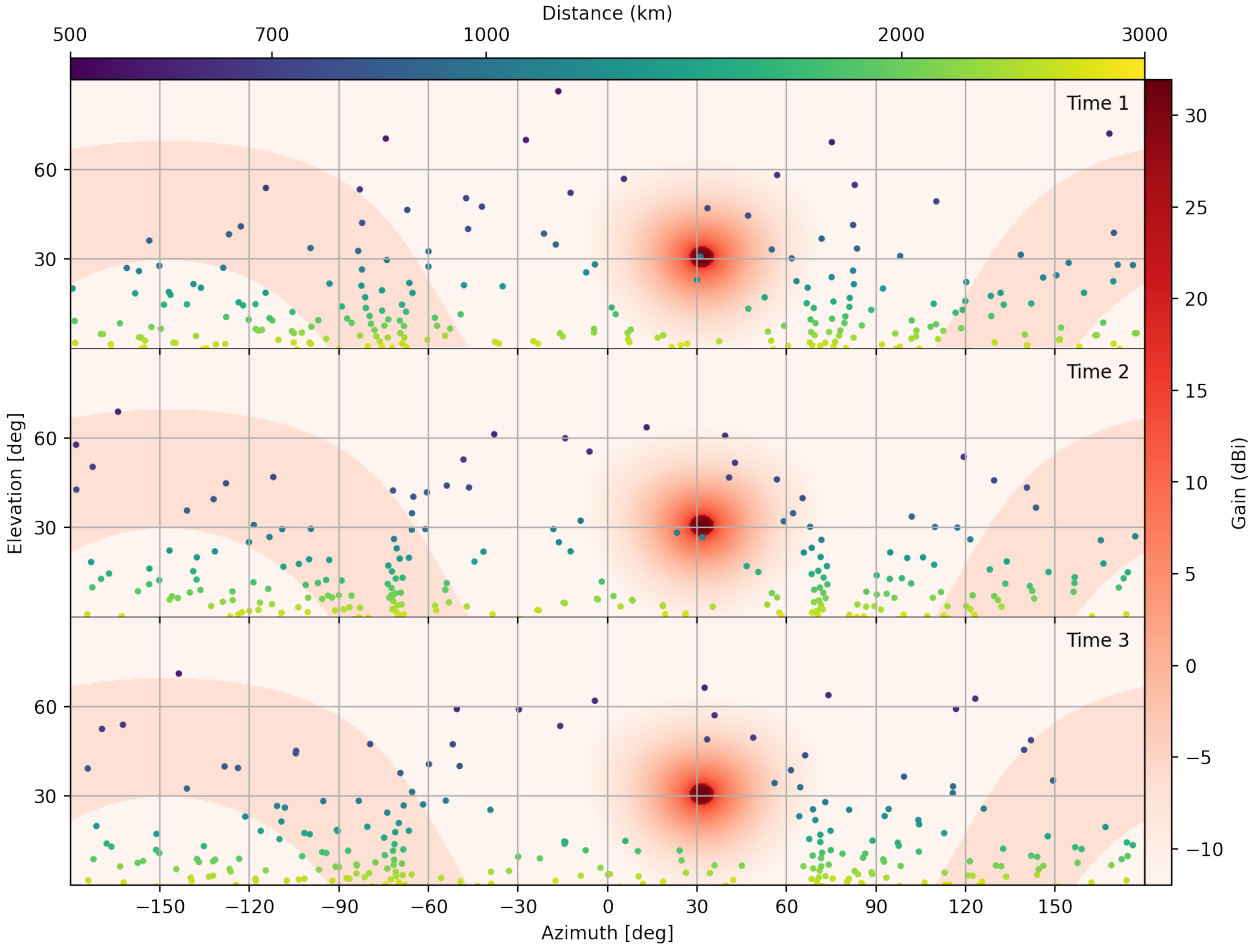

Figure 2: Snapshots of a satellite constellation simulation

The coloured circles mark satellite positions and distances in the topocentric (observer) coordinate frame. The red-shaded contours display the RAS antenna gain ($d = 25\ \mathrm{m}, f = 150\ \mathrm{MHz}$) with the telescope pointing to $(\varphi_0, \vartheta_0) = (31.62°, 30.44°)$.

For each time step, the received total power from all satellite transmissions in the band of interest can then be calculated as:

$$P_{\mathrm{rx}}(\varphi_0, \vartheta_0) = \sum_{i=0}^{n} \frac{c^2}{4\pi f^2} \frac{1}{4\pi d_i^2} G_{\mathrm{rx}}(\varphi_i, \vartheta_i; \varphi_0, \vartheta_0) G_{\mathrm{tx}}(\tilde{\varphi}_i, \tilde{\vartheta}_i) P_{\mathrm{tx}} \ . \quad (1)$$

Here, the coordinates $(\tilde{\varphi}, \tilde{\vartheta})$ refer to the antenna coordinate frame of the satellite (each being fixed to each of the individual satellites and thus moving with respect to the Earth or observer frames). Most of the quantities in the above equation are time-dependent and/or depend on the satellite[2].The result of this operation is shown in Figure 3 for a time span of 2000 s. The three snapshots of the constellation, which are shown in Figure 2, are marked with vertical red lines and were chosen to refer to different situations: (1) a satellite crosses very close to the main beam of the RAS telescope and causes a strong peak in the received power levels, (2) one or more satellites are close to the main beam, i.e. in the near side-lobe domain, and (3) the received emission is determined by the far side-lobe contributions. The "baseline" level in Figure 3 is not due to a system noise contribution (as with a spectrum analyser), but is the typical background contribution from all satellites in the sky above the local horizon entering via the far side-lobes.

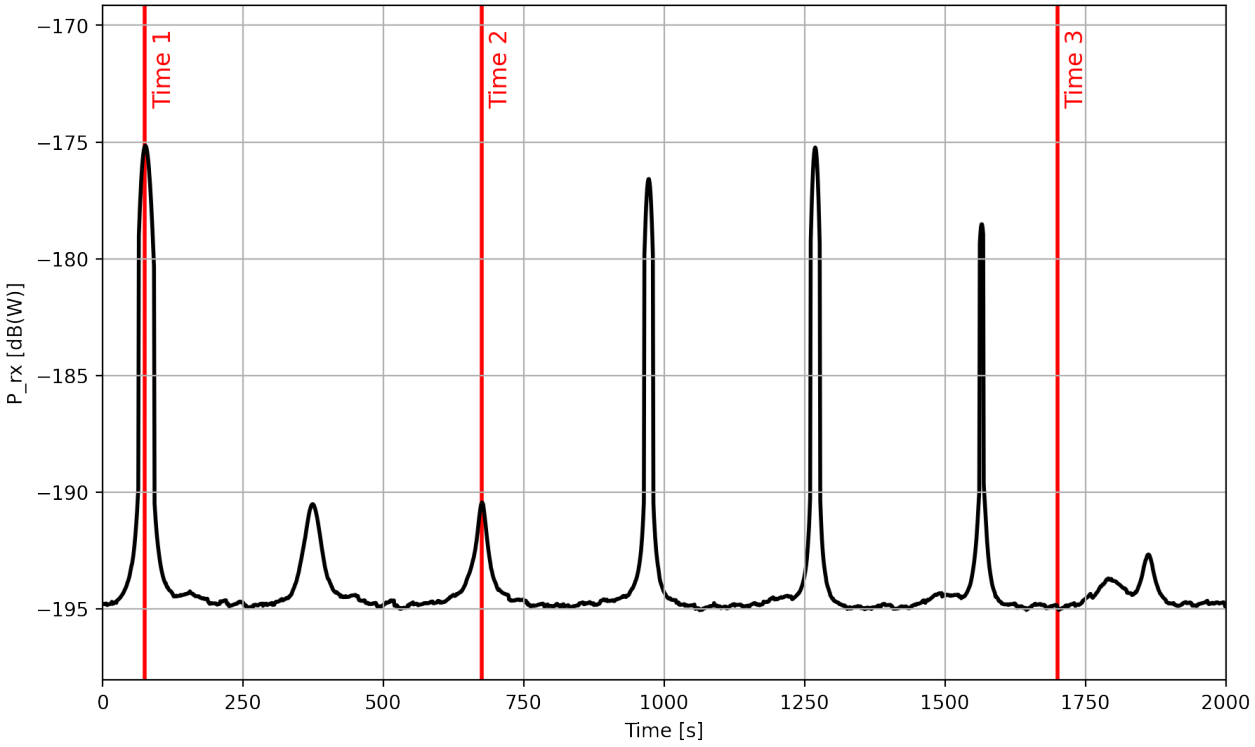

Figure 3: Total received power for an example satellite constellation

The three snapshots of the constellation, which are shown in Figure 2, are marked with vertical red lines.

It is noted that the total received power, as defined in Equation (1), is not the quantity, which is used in Recommendation ITU-R S.1586-1 [8] and Recommendation ITU-R M.1583-1 [7] as metric.

$$\mathrm{epfd}(\varphi_0, \vartheta_0) = \frac{4\pi f^2}{c^2} \frac{1}{G_{\mathrm{rx}}^{\max}} P_{\mathrm{rx}}(\varphi_0, \vartheta_0) = \sum_{i=0}^{n} \frac{1}{4\pi d_i^2} \frac{G_{\mathrm{rx}}(\varphi_i, \vartheta_i; \varphi_0, \vartheta_0)}{G_{\mathrm{rx}}^{\max}} G_{\mathrm{tx}}(\tilde{\varphi}_i, \tilde{\vartheta}_i) P_{\mathrm{tx}} \quad (2)$$

The equivalent-power flux density (epfd) is defined above. It is the power flux density (pfd) that a single satellite would have to radiate at the RAS station to produce the same received power if it was located in the pointing direction of the telescope. However, in practice, one usually converts this number to a 0-dBi reference, because the power flux density (pfd) threshold levels in Recommendation ITU-R RA.769-2 [4] are given for an isotropic receive antenna, i.e. one sets $G_{\mathrm{rx}}^{\max} = 1$. Then the above equation becomes

$$\mathrm{epfd}(\varphi_0, \vartheta_0)|_{G_{\mathrm{rx}}^{\max}=1} = \frac{4\pi f^2}{c^2} P_{\mathrm{rx}}(\varphi_0, \vartheta_0) = \sum_{i=0}^{n} \frac{1}{4\pi d_i^2} G_{\mathrm{rx}}(\varphi_i, \vartheta_i; \varphi_0, \vartheta_0) G_{\mathrm{tx}}(\tilde{\varphi}_i, \tilde{\vartheta}_i) P_{\mathrm{tx}} \,. \quad (3)$$

[2] Note that, in some cases, P_tx could be adapted based on phi_i, theta_i, phi_0, theta_0 (see section 5.1.2.5).

The threshold levels in Recommendation ITU-R RA.769-2 [4] are defined for an integration time of 2000 s, which means that the received power (or the epfd) has to be averaged over 2000 s of the simulation. Furthermore, Recommendation ITU-R S.1586-1 [8] and Recommendation ITU-R M.1583-1 [7] propose to split the sky in cells of equal area and repeat the analysis for random telescope pointings within these cells to assess the spatial distribution of received powers.

Recommendation ITU-R M.1583-1 [7] Annex 2 and Recommendation ITU-R S.1586-1 Annex 2 [8] describe a possible scheme to define the sky cells. The size of the cells was chosen to have a fixed solid angle. When one wants to sample a random position within the cell, k, it is important that the overall distribution of telescope pointings stays uniform on the sphere. This can be done by drawing the azimuths from a random uniform distribution, U, within the interval $[\varphi_k^{\text{low}}, \varphi_k^{\text{high}}]$. For the elevations, however, a correction needs to be applied to account for the spherical curvature, hence:

$$\varphi_k \sim U\left(\varphi_k^{\text{low}}, \varphi_k^{\text{high}}\right) \tag{4}$$

$$\vartheta_k \sim 90° - \cos^{-1} U\left(z_k^{\text{low}}, z_k^{\text{high}}\right) \tag{5}$$

$$\text{with } z_k^{\text{low/high}} = \cos\left(90° - \vartheta_k^{\text{low/high}}\right) \tag{6}$$

An additional consideration is the question which reference frame should be assumed for the epfd calculations.

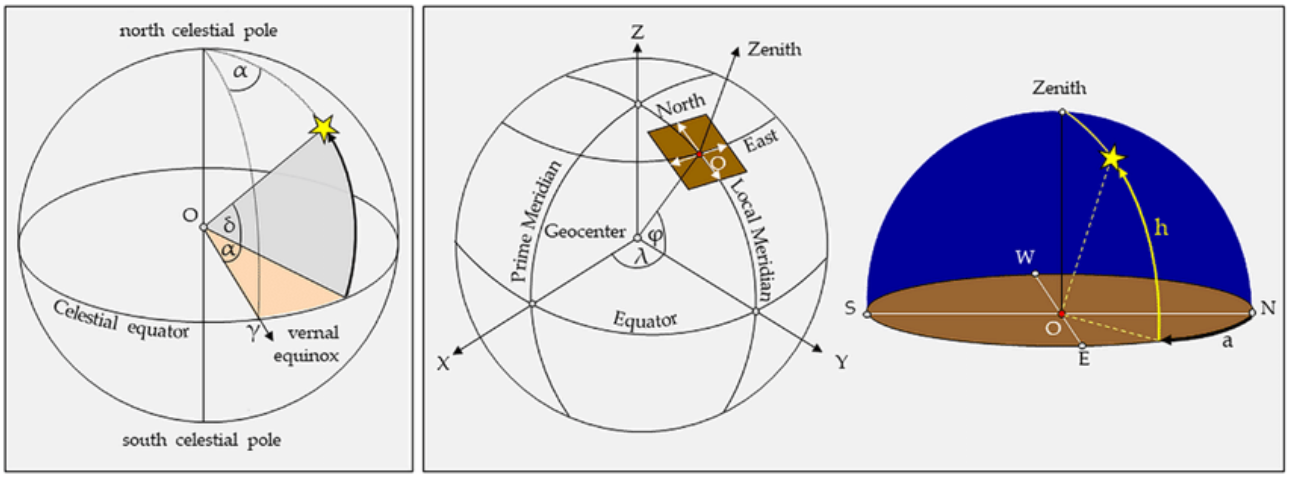

Figure 4: Two common reference systems used in astronomy

Figure 4 shows two alternative reference frames used in astronomy. On the left is the equatorial inertial or earth-centred inertial system, which is the most commonly used reference system. The position of an object on the sky is described in a reference frame fixed on the celestial sphere. The position of a (very distant) star is constant with time. It is described by the polar coordinate pair right ascension (RA) α and declination (Dec) δ.The origin for the declination is the celestial equator (great circle with 90° distance from the North or South pole), while the origin for the right ascension is given by the position of the Sun on the equator at the vernal equinox. The equatorial system is the most commonly used reference frame in astronomy, since the coordinates of most objects on the sky are constant or change very slightly.

On the right, Figure 4 shows the topocentric system. The position of an object on the sky is described from the viewpoint of the observer using the polar coordinates azimuth, a, and elevation, or height, h. Image from Richter, Teichert & Pavelka [36]. The height of an object is the angle with respect to the local horizon (great circle at 90° separation with respect to the zenith or upwards direction), while the azimuth is the angle between the local meridian (North or South direction) and the position of the object.

Recommendation ITU-R M.1583-1 [7] and Recommendation ITU-R S.1586-1 [8] do not explicitly prescribe the usage of a topocentric reference system. The usage of azimuth and elevation, however, suggests the topocentric coordinate system as a basis for the data loss calculations. In practice, however, the pointing

directions in astronomical observations are often not constant with respect to an earth-fixed system, but they are rather constant with respect to an earth-centred inertial system. In other words, radio telescopes often track observed objects on the sky rather than pointing to a fixed direction with respect to the Earth's surface. This is the case if a certain astronomical object is being observed. Opposed to that, observing modes with fixed directions in the topocentric system are used when mapping large areas of the sky. As a consequence, only if both situations are simulated, the result covers all fundamental cases of RAS operations.

This Report also includes epfd calculations in which the reference system is an earth-centred inertial system with the (celestial) coordinates right ascension, α, and declination, δ. The accessible latitude (declination) ranges depend on the geographical latitude ϕ of the observatory. In the northern hemisphere the range is $90° < \delta < \phi - 90°$ and in the southern hemisphere $-90° < \delta < \phi + 90°$. epfd calculations hence have to take a larger range of coordinates into account[3].

Regardless of the reference frame, the simulation should be repeated a large number of trials, often enough that the distribution of received powers in each sky cell converges. This repetition also offers the possibility to analyse the typical scatter, e.g. of the mean received power levels in each cell. Furthermore, Recommendation ITU-R RA.1513-2 [5] recommends an interference limit to RAS of 2% of the time for each system from other services. The statistical distributions resulting from iterated simulations allows to determine such percentiles (2% of data loss refer to the 98% percentile of the received power level, which then must not exceed the Recommendation ITU-R RA.769-2 [4] thresholds).

5.1.2 Parameters entering the epfd calculation

5.1.2.1 RAS station geographical location

The geographical position, usually provided as geographical latitude and longitude, as well as the altitude of the radio astronomy station determines the visibility and viewing angle of single satellites at a given moment in time. In particular, the latitude is an important parameter, as some constellations are designed to reach a maximum latitude, while optimising the distribution along the geographic longitude. This means that the outcome of the epfd calculations is expected to be similar with changing longitude, but differ depending on latitude.

5.1.2.2 RAS station antenna pattern

The gain of the RAS antenna is an input parameter to Equations (1)-(3). It should be noticed that it is not sufficient to consider the main beam gain only, but that the whole antenna pattern is required, as the effect of sidelobe coupling cannot a priori be neglected. Recommendation ITU-R RA.1631-0 [2] provides an antenna pattern to be used in the absence of a precise knowledge of the antenna pattern or for generalised calculations.

5.1.2.3 RAS station minimum elevation

From Table 1, it can be seen that minimum elevation θ_{min} is specific to each RAS station, due among other reasons to its mechanical capabilities and to the terrain surrounding it. Depending on the minimum elevation, observations cannot be made for some sky cells. As stated already in section 3, epfd statistics should be calculated only with pointing directions above the specified minimum elevation, if any, or 5° as indicated in ITU-R Resolution 739 (Rev. WRC-19) [9]. It is worth to mention that Resolution 739 (Rev. WRC-19) does not cover all frequency bands that may be used by RAS, but this value of 5° should be applicable by default. However, the emission from satellites below that elevation limit should not be omitted, as they may still couple with the radio telescope.

5.1.2.4 Satellite constellation orbital parameters

There are six elements (defined by Johannes Kepler in his "Laws of planetary motion") used to characterise an orbital plane (see Figure 5 for illustration), in which the Celestial body is a non-GSO satellite.

---

[3] Note that these formulas assume a minimum elevation angle of 0º, and that the actual minimum elevation of radio observatories also has to be taken into account.

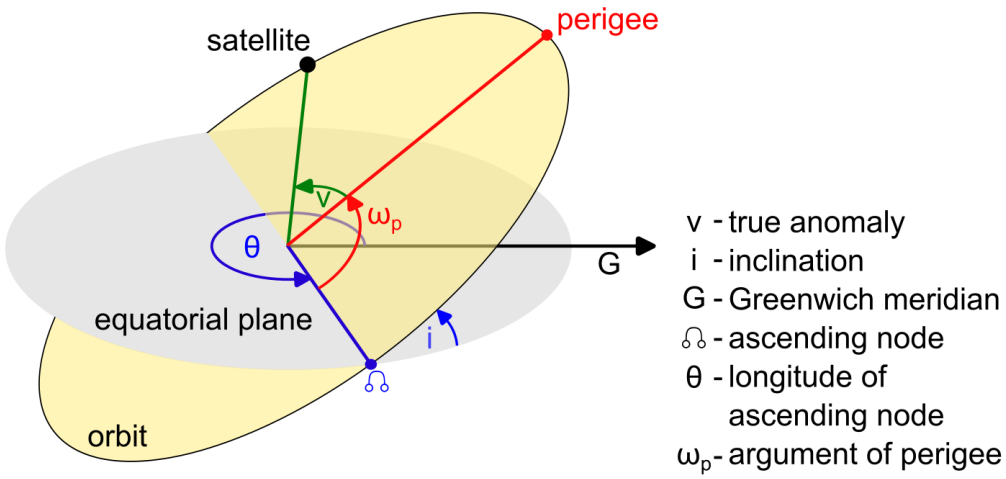

Figure 5: Orbital parameters

In Figure 5, the two first elements are used to describe the size and shape of the orbital plane: those are the semi-major axis (a) and the eccentricity (e). Two additional elements are used to describe the orientation of the plane, the inclination (i) and the longitude of the ascending node (θ), giving respectively the tilt between the orbital plane and the reference plane (usually Earth's equatorial plane for Earth-centred systems), and the longitude of the point where the orbit passes from south to north again compared to the reference plane. The two last elements are the argument of the perigee (ωp), providing the angle between the ascending node and the perigee, and the true anomaly (v) at epoch (t0), defining the position of the orbiting body along the ellipse at a specific time (the "epoch"), expressed as an angle from the perigee.

In term of interference, the two following parameters can have a significant impact:

- The altitude or orbital height;
- Inclination, when compared to the latitude of the RAS station, is a parameter that can have a dimensioning impact on the level of interference. By definition, the satellites of the non-GSO system with a given inclination "I" cannot go above a geographical latitude equal to "I". Depending on the latitude of the RAS station, there is a certain amount of sky cells for which alignment cases are not possible.

Those parameters cannot be considered independently from the rest of the parameters of the non-GSO satellite system.

5.1.2.5 Transmitted power

Entering as an input parameter to Equations (1)-(3) is the transmitted spectral power. As in the relevant compatibility studies and, consecutively, epfd simulations, often adjacent or spurious emission is studied, these characteristics may not be known.

It is noted that, in some cases, the satellite operator may be capable of changing the power of their emissions towards different directions. If that is the case, Ptx and other transmit parameter in Equation (1) may be adapted by the satellite operator if the telescope's pointing angles φ_0 and ϑ_0 are known in real time.

5.1.2.6 Satellite Antenna pattern

As for the RAS station antenna pattern, the epfd calculation requires the full antenna pattern of the transmitting satellite antenna, but currently no recommendation provides this approximation for the unwanted emission domain. This information, either the full pattern, or the approximation, would have to be provided by the satellite operators. The antenna pattern can change as a function of time. Alternatively, it may be provided as a function of pointing direction relative to the satellite orientation, as well as the satellite orientation as a function of time (which might be constant with respect to the Earth's centre or its surface) (see section 5.1.2.7). The effect of the satellite antenna pattern on the result of epfd calculations is further investigated in section 6.3.

5.1.2.7 Satellite pointing strategy and transmission schedule

For an ideal epfd simulation, a sufficiently accurate model of the pointing strategy and the transmission schedule may be required, i.e. the information of where the satellites are pointing and at which transmitted power they are operating, ideally as a function of time, as well as information on how the antenna pattern may change as a function of time.

If the satellite antenna pattern can be provided as a function of the pointing direction (relative to any reference system) and the transmitted power (see section 5.1.2.5) is known as a function of time, the missing information are the non-GSO satellite system pointing strategy for "non-Nco" satellites (see section 7.1.4) and the transmission schedule.

However, the pointing strategy and transmission schedule of a satellite system are generally considered proprietary and confidential to operators. A representative pointing strategy and transmission schedule could be used, and this would not require the precise knowledge of the actual values as a function of time. However, to date no recommendation or standard method exists to estimate such pointing strategy and transmission schedule, and could be provided by the satellite operator, in a deterministic or maybe a statistical format. Providing this information in a statistical format may require further consideration.

5.1.2.8 Assumed operational parameters of RAS stations

The scheme for the epfd calculation laid out in section 5.1.1 aims at determining the average level of interference of a non-GSO satellite constellation at an RAS station. To some extent, the operational parameters of radio telescopes play a role. In common operations of radio telescopes the integration time has a huge spread. Recommendation ITU-R RA.769-2 [4] uses 2000 s as an example integration time in their tables 1 and 2 and it has become a de facto standard in epfd studies. The starting time of the simulated observation may vary, and epfd samples should be repeated with differing starting times until the average epfd converges. Recommendation ITU-R S.1586-1 [8] stipulates that "… the number of trials multiplied by the 2 000 s integration time should be significantly higher than the period of the constellation. It is also necessary to ensure adequate statistical sampling over the full period of the constellation". However, in the typical operation of a RAS station, an observational campaign may be scheduled in a short timeframe or may happen over a schedule of months, such that no guidance can be sought from operational characteristics of radio stations. It seems reasonable to choose a range of start times such that no correlation between the propagated configurations in the single sample configurations exists. This is further studied in section 6.6.

5.1.3 Example and template configuration

In the following, an application of the method laid out in section 5.1 is demonstrated. For this, a reference configuration is defined, which represents a baseline for the rest of the Report. Figure 5 shows the average power flux density per cell for these default conditions.

The reference constellation for which the analysis has been done has the following main characteristics:

- 22 orbital planes with ascending nodes evenly distributed;
- In each plane, 22 satellites equally spaced;
- Orbital inclination of 55°;
- Satellite altitude of 500 km;
- Transmitted Power of -44 dBm;
- Isotropic antenna.

The RAS parameters are:

- Frequency band 1400-1427 MHz;
- Antenna diameter of 25 m;
- Latitude 50° N;
- Grid in the sky with size 3°x3°.

The grid in the topocentric calculations is chosen to have a cell size of approximately 3°x3° on average starting at an elevation of 0°, resulting in 2292 cells. The reason for the difference between the number of cells in our

calculations and Recommendation ITU-R M.1583-1 [7] and Recommendation ITU-R S.1586-1 [8], which cite 2334 cells for the same setup, is different rounding methods when calculating the cell size in azimuthal direction. Our calculations rely strictly on the formulas given in Recommendation ITU-R M.1583-1 [7] and Recommendation ITU-R S.1586-1 [8], allowing for an arbitrary value for the size of the cells in azimuthal direction, while in the example in Recommendation ITU-R M.1583-1 [7] and Recommendation ITU-R S.1586-1 [8] the rounding condition is that the cell sizes in azimuthal direction have an integer value in units of degrees. To achieve the goal for similar solid angles in the cells, the method used here is more accurate. In 5.3.1, the example sectorisation in Recommendation ITU-R M.1583-1 [7] and Recommendation ITU-R S.1586-1 [8] is used, which leads to slightly different results. The grid in the equatorial reference frame is chosen to have a cell solid angle of approximately 3°x3° square degrees on average. The declination ranges from -40° to +90º, resulting in a number of 3438 cells.

The experiment is repeated over 100 trials with different starting times, each simulation runs over 2000 s with a time resolution of 1 s. As a result, a hundred time-average epfd samples per cell were obtained. These can be compared to the power flux density level of -180 dB[W/m2] (Recommendation ITU-R RA.769-2 [4]). Figure 6 shows the average power flux density per cell, at the top for the topocentric reference frame, at the bottom for the inertial equatorial reference frame.

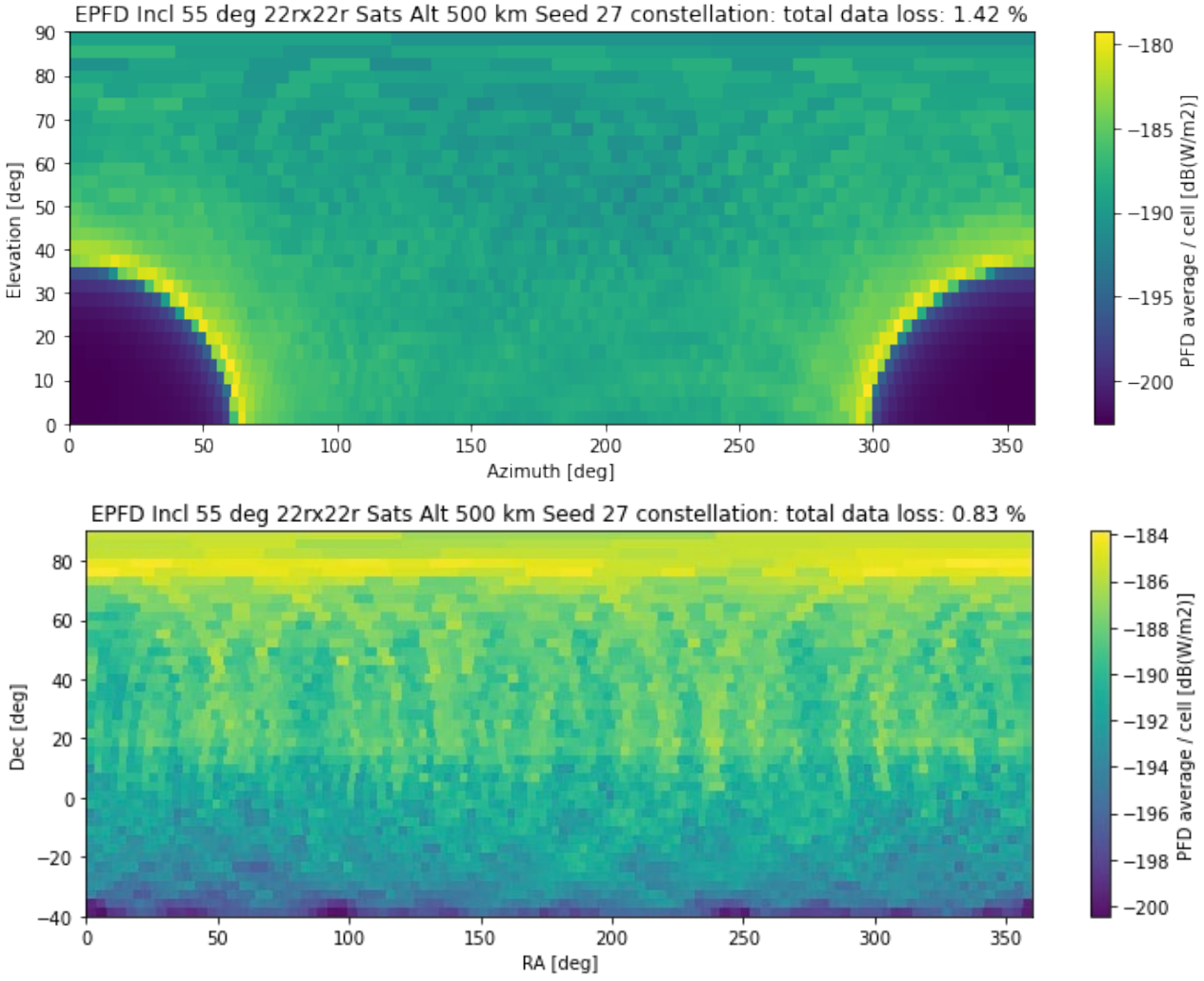

Figure 6: Average epfd per cell for the default satellite constellation used in this Report

5.2 EPFD METHOD AND DATA LOSS METRIC

In order to apply the acceptable data loss criteria defined in Recommendation ITU-R RA.1513-2 [5], a method is required to determine the (expected) data loss caused by a satellite constellation. Several reports and recommendations exist, which are summarised in the following. After careful analysis and comparison of the possibilities, a choice for the remainder of this Report is made.

5.2.1 Survey of existing ECC and ITU-R documents on epfd data loss

5.2.1.1 ITU-R Documents

There are several ITU-R documents about the EPFD method and compatibility studies using the method. Most importantly, one finds two recommendations, Recommendation ITU-R M.1583-1 [7] and Recommendation ITU-R S.1586-1 [8], which are introducing the epfd methodology for MSS/RNSS and FSS, respectively. Both include the same equations for calculating the epfd for a single radio astronomy telescope pointing but differ somewhat regarding the approach to calculate the overall data loss to the RAS. Furthermore, there is Recommendation ITU-R RA.1513-2 [5], which is about the acceptable levels of data loss to radio astronomy observations. In their section 3.2.2, an epfd formula is provided that is based on the same approach as in Recommendations ITU-R M.1583-1 [7] and ITU-R S.1586-1 [8], but is normalised for 0-dBi RAS antenna gain – making it easier to compare the resulting epfd samples with the power flux density (pfd) threshold levels defined in Recommendation ITU-R RA.769-2 [4]. However, when using this normalised approach, one ought to use the 0-dBi threshold power levels provided in Recommendation ITU-R RA.769-2 [4]. It may be confusing that Recommendation ITU-R RA.1513-2 [5] provides a formula for the epfd threshold (in their equation 2), which is valid for the unnormalised version of the epfd formula. It should be noted, that Resolution 739 (Rev.WRC-19) [9], which is about “Compatibility between the radio astronomy service and the active space services in certain adjacent and nearby frequency bands” only lists Recommendations ITU-R M.1583-1 [7] and ITU-R S.1586-1 [8] as sources for the epfd method, but quotes Recommendation ITU-R RA.1513-2 [5] only for the acceptable levels of data loss and does not mention the epfd section in Recommendation ITU-R RA.1513-2 [5].

In Resolution 739 (Rev.WRC-19) [9], the epfd threshold for RAS band 322-328.6 MHz (for example) are respectively -240 dBW/m2 for continuum observations and -255 dBW/m2 for spectral line observations. The pfd thresholds of ITU-R RA.769-2 [4] are -189 dBW/m2 for continuum and -204 dBW/m2 for spectral lines. This difference of 51 dB between epfd thresholds of Recommendation ITU-R RA.769-2 [4] and pfd thresholds of Resolution 739 (Rev.WRC-19) [9] correspond to the maximum gain of a 100 m antenna at 327 MHz computed with Recommendation ITU-R RA.1631-0 [2].

Surprisingly few ITU-R documents contain compatibility studies based on the epfd method. To our knowledge, only Report ITU-R SM.2091-0 [22] includes several case studies. Even Recommendations ITU-R SM.1542-0 [23] and ITU-R SM.1633-0 [24], which are both (in part) about non-GSO constellations and radio astronomy do not go into details. While Recommendation ITU-R SM.1542-0 [23] does not even mention epfd, Recommendation ITU-R SM.1633-0 [24] states that Recommendation ITU-R M.1583-1 [7] and Recommendation ITU-R S.1586-1 [8] should be applied. However, the maximum unwanted emission levels, which are quoted, are for GSO systems only (or represent single-entry analyses). Only for one non-GSO system at 10.7-10.95 GHz it is said that preliminary calculations were done, but no further information is provided.

In the following, the proposed/applied data loss metrics in the relevant documents are listed.

a) **Recommendation ITU-R M.1583-1**

Recommendation ITU-R M.1583-1 [7] includes two annexes. Annex 1 has two sections. The first lists the required parameters for an epfd simulation, the second section has the standard epfd equation (2), as well as the equation for 0-dBi receiver gain (3). Annex 2 has three sections. The first section shows how the sky could be divided into equal-area grid cells and the second section explains how the epfd samples in each sky cell are derived. Section 3 contains a sky map showing the data losses for each sky cell. Here, the data loss, d_i, of the i-th sky cell is the ratio of epfd samples, in the cell, where the Recommendation ITU-R RA.769-2 [4] threshold is exceeded and the number of trials in the cell. For the data loss, d_{sky}, of the whole sky, the ”percentage [...] is defined as the sum of these losses in all cells over the number of trials” This only makes sense, if the sum is calculated as the weighted sum with the solid area of the grid cells as weighting factors:

$$d_{sky} = \frac{\sum_i \Omega_i d_i}{\sum_i \Omega_i}, \qquad (7)$$

With Ω_i, the solid angle (area), and d_i, the data loss, of the i-th sky cell. As the sky cells are constructed in a way that they have approximately the same solid angles, d_{sky}, can be estimated by the average over all sky cell data losses:

$$d_{sky} = \frac{\sum_i \Omega_i d_i}{\sum_i \Omega_i} \approx \frac{\Omega_{\text{cell}} \sum_i d_i}{\sum_i \Omega_{\text{cell}}} = \frac{\sum_i d_i}{N_{\text{cell}}} \quad (8)$$

where:

- Ω_{cell} is the average solid angle of the cells;
- N_{cell} is the number of sky cells.

b) **Recommendation ITU-R S.1586-1 [8]**

This Recommendation is almost identical to Recommendation ITU-R M.1583-1, annex 2 [7], the third section is replaced by two new sections. The new section 3 contains a recipe on how worst-case pointing directions could be used to avoid performing the epfd calculations over the whole sky. Section 3 indicates that, if the worst-case pointing direction is known, the epfd results in the corresponding cell can give the following information, either for the entire sky or for a specific ring defined for a given elevation angle:

- If, in all M rings, the time-averaged epfd for the worst-case pointing directions is equal to or less than the threshold of detrimental interference for 98% or more of time (see Recommendation ITU-R S.1586-1, figure 2), then the criteria for avoidance of detrimental interference are met over the whole sky;
- If, in a ring defined for a given elevation angle, the time-averaged epfd for the worst-case pointing directions is equal to or less than the detrimental threshold for 98% or more of time (see Recommendation ITU-R S.1586-1, figure 2), then the criteria for avoidance of detrimental interference are met for the corresponding entire ring.

It is indeed quite straightforward to understand that in the case where a worst-case pointing direction has been identified, if the time-averaged epfd is equal to or less than the epfd threshold for 98% or more of time, then the time-averaged epfd is equal to or less than the epfd threshold for 98% or more of time for all the cells of the ring or for all sky cells, depending on the case. In that last situation, the protection criterion is met.

The first bullet states clearly that the protection criterion applies over the whole sky.

The last bullet attached to that paragraph starting by “Considering the 2% criterion in recommends 2 of Recommendation ITU-R RA.1513-2 [5]” indicates that:

- If the interference criteria are not met, then further investigation is needed.

This last bullet is once again making clear that if the epfd threshold is not met in one sky cell, no conclusion can be drawn with respect to the protection criterion. This also clarifies that the data loss metric is to be computed for all samples of epfd averaged over 2000 s for all useful sky cells.

Recommendation ITU-R S.1586-1 is the only document, which proposes such an approach.

c) **Recommendation ITU-R RA.1513-2, section 3.3.2 [5]**

As for Recommendation ITU-R M.1583-1 [7] and Recommendation ITU-R S.1586-1 [8], the sky is divided into a grid of cells and the epfd in each cell (random telescope pointings within cells) is determined for several simulation runs, which allows to infer the distribution of the epfd per cell. Recommendation ITU-R RA.1513-2 [5] then states that the calculated epfd distributions can be compared with the Recommendation ITU-R RA.769-2 [4] threshold levels, such ”that the percentage of trials during which this criterion is met may be determined for each of the cells which were defined”. It continues with” Over the sky, [...], the epfd threshold level defined above should not be exceeded for more than 2% of the time”.

Recommendation ITU-R RA.1513-2 [5] gives the practical steps of the approach:

- Divide the sky into cells;
- Random choice for the pointing direction of the RAS antenna;
- Starting time randomly chosen;

- Computation of epfd values for each time sample;
- Average epfd and obtain a statistical distribution of the epfd for the randomly chosen pointing direction;
- Repeat operation for other sky cells;
- Compare the "overall" epfd distribution (meaning the distribution for all sky cells) with pfd thresholds of Recommendation ITU-R RA.769-2 [4].

The protection criterion will be met if “Over the sky, for elevations higher than the minimum operating elevation angle of the radio telescope, the epfd threshold level defined above should not be exceeded for more than 2% of the time.”

Note: In Recommendation ITU-R RA.1513-2, figure 2 [5] provides a comparison between the pfd levels given in Recommendation ITU-R RA.769-2 [4] and the epfd distribution given for a cell. From the context of the Recommendation it is understood that this comparison is done for information only.

d) **Report ITU-R SM.2091-0**

Report ITU-R SM.2091-0 [22] contains several case studies regarding the compatibility between non-GSO systems operating at various frequency bands and the RAS, for which the epfd method was applied. The report refers to both Recommendation ITU-R M.1583-1 [7] and Recommendation ITU-R S.1586-1 [8]. It also contains orbital and transmitter parameters of the satellite constellations under study. The systems seem to be the same as for Recommendation ITU-R SM.1633-0 [24], which is noteworthy as Recommendation ITU-R SM.1633-0 [24] seems not to use the results of epfd studies from the Report.

In the Report ITU-R SM.2091-0 [22], there is a statement that ”simulations were performed considering an RAS antenna elevation angle of 0°, in order to get completely general results”, which seems to contradict that few sentences later the epfd levels for all sky cells were calculated. Therefore, it is likely that the above statement refers to the minimum elevation angle. In the Report the compatibility criteria are based on the metric that ”epfd threshold level during more than 98% of the time in average over the whole sky” is met. As the Recommendation ITU-R M.1583-1 [7] is referred to, it is likely that the same averaging procedure (see section 5.2.1.1 b)) is employed.

The Report also contains one case, where Recommendation ITU-R S.1586-1 [8] is applied to a single BSS satellite at 620-790 MHz. There is no mention of the different approaches in Recommendation ITU-R M.1583-1 [7] and Recommendation ITU-R S.1586-1 [8], and how these should be addressed. Furthermore, unlike for the studied MSS constellations, this case only displays the sky map of cell data loss (Figure 22 in the Report) but quotes no total data loss. However, it determines a maximum satellite pfd radiated at any RAS station, clarifying which metric was applied: ”This level ensures that the loss of data to the RAS over the part of the sky within which the radio astronomy station performs observations, taking into account the minimum elevation angle θ_{min} at which the radio astronomy station conducts observations in the frequency band [...], will be less than 2%”.

Report ITU-R SM.2091-0, figure 43 and figure 45 [22] refers to ”sky blockage” twice, by indicating that, the percentage of the time where the epfd threshold is exceeded goes up to respectively 14% and 18% per cell. The conclusion in the Report is that ”therefore it never causes any sky blockage in any part of the sky”. It is unclear what the term “sky blockage” refers to in this context, since it is not clear which limiting percentage is applied to identify a cell to be blocked.

Report ITU-R SM.2091-0, figure 48 [22] provides, for each sky cell, the percentage of time where the epfd threshold is exceeded (with a maximum of 64%) as well as the quantity of sky cells (12.4% of them, so 288 cells) where the epfd threshold is exceeded more than 2% of the time. This metric is very unusual compared to all other known cases, in which the number of blocked sky cells was counted when the average epfd in a cell exceeded the threshold, and not when the 98% percentile was exceeding the threshold. It is to be mentioned that the conclusions for the GPS, GLONASS, GALILEO and QZSS constellations are drawn from Report ITU-R SM.2091-0, figures 42, 44, 46 and 48 [22] where the epfd threshold is to be met ”for more than 98% of the time in average over the whole sky”.

5.2.1.2 CEPT/ECC Documents

CEPT had several work items in the past years, in which epfd simulations with RAS as the victim service were performed. Again, a brief compilation is provided in the following. All those reports consider the same interpretation of data loss metric, as the percentage of time-averaged (over 2000 s) epfd samples for all sky cells that exceed the RAS threshold.

a) **ECC Reports on Iridium**

ECC Report 171 [25], ECC Report 226 [26], ECC Report 247 [27] and ECC Report 349 [28] were all about Iridium (NEXT) and therefore, it is not surprising that the same data loss metric is applied. The method was to measure the pfd for some satellites, to then compute the data losses for all sky cells and the average data loss for the grand total. As no mention is made on a weighting/correction for the slightly different sky cell areas, it is assumed that a simple arithmetic average of the individual data losses was calculated.

Contrary to all other reports discussed here, these reports are based on actual measurements and not purely on simulations. The drawback is that the quantity of sample was lower, forcing the authors of the reports to deviate from the commonly accepted methodology.

b) **ECC Report 271**

In this Report, the OneWeb and SpaceX/Starlink constellations were analysed [29]. While maps of the data loss for the sky cell grid are shown for information, the overall data loss was determined as the fraction of all epfd samples (from all cells and all simulation runs) that exceeds the Recommendation ITU-R RA.769-2 [4] thresholds.

c) **ECC Report 322**

- Like for ECC Report 271, maps with cell data losses are shown but for the overall data loss, the full set of epfd samples was used [10]. In addition, this Report is the first one that also performed calculations in the equatorial coordinate frame, which is better suited to assess the interference potential on celestial astronomical sources. In addition, to assess the statistical scatter of the total data loss (i.e. its error bars), another approach was introduced, where the data loss is calculated as the median of the full-sky data loss of each simulation run. That is, for each iteration of the simulation, all epfd samples from all sky cells are considered; the fraction of samples exceeding the thresholds is computed, and based on the resulting data loss distribution, the median and desired error percentiles can be inferred.

5.2.2 List of data loss metrics

In summary of the above survey, one can identify the following existing data loss metrics.

5.2.2.1 (Weighted) average of "sky cell data loss"

In a first step, for each cell of the grid cell, the data loss is determined as the fraction of simulation trials, where the epfd samples in that grid cell exceed the Recommendation ITU-R RA.769-2 [4] threshold levels. Then the data loss for the whole sky is determined with the area-weighted sum or the (approximate) average of cell data losses according to the formula (see section 5.2.1.1 a), Recommendation ITU-R M.1583-1 [7], for more information)

$$d_{sky} = \frac{\sum_i \Omega_i d_i}{\sum_i \Omega_i} \approx \frac{\Omega_{\text{cell}} \sum_i d_i}{\sum_i \Omega_{\text{cell}}} = \frac{\sum_i d_i}{N_{\text{cell}}} \quad (9)$$

The finer the chosen sky grid, the better the approximation will be.

5.2.2.2 Using all epfd samples

Here, the epfd samples from every simulation trial and for all sky cells are considered. The grand-total fraction of epfd samples that exceed the RAS thresholds are counted.

This methodology is more accurate since it provides the entire statistic of all samples in all sky cells. The results obtained would be comparable to the ones obtained with the method above if the quantity of samples of 2000 used to compute d_i in section 5.2.2.1 are sufficient for each individual sky cell.

5.2.3 Alternative criteria that could be developed using the data loss metric

Other criteria based on the data loss could be developed in the future, examples are provided below.

5.2.3.1 Median of all-sky data losses per simulation run

For each simulation run/iteration of 2000 s, all sky cell epfd samples are used to calculate the fraction of all cells that violate the threshold. From the resulting data loss distribution (which is for all sky), the median and other percentiles (e.g. for determination of statistical errors) can be determined. The median data loss represents the grand-total data loss, in this case. This technique has been used in ECC Report 322 [10] to estimate the statistical scatter of the data losses.

5.2.3.2 Sky blockage

Here the data loss is defined as the fraction of sky cells:

- where 2% of the epfd samples from all simulation run/iterations in one cell exceed the RAS threshold (approach very similar to single sky cell criterion below);
- or where the average epfd (mean of all epfd samples in a cell from all simulation runs/iterations) in the cell violates the RAS thresholds.

While the latter seems to be a viable approach, the former would apply a 2% cut twice, which would make that criterion much stricter than the rest.

5.2.3.3 Single sky cell criterion

While not explicitly mentioned in any existing document, the consideration of individual cell statistics in some of the material would also allow the interpretation that not a single sky cell must exceed 2% data loss. This is a pure yes/no criterion and provides no immediate information on how much the thresholds are exceeded. Obviously, this is the most restrictive criterion compared to all of the above.

5.2.4 Comparison of the data loss metric with the alternative criteria

Using example satellite constellations, one can compare the various data loss metrics, which will help to judge on the most useful approaches.

Again, two satellite constellations are used. One is the default constellation with 484 satellites. To have a result close to 2% data loss (for the all-sky metrics), a transmit power of –47 dBm was used (using isotropic transmitters). In addition, a smaller constellation with only 20 satellites (4 orbital planes with 5 satellites each). To compensate for the lower number (and again to have results in the regime around 2% data loss), the transmitter power was set to –28 dBm. Notice that the data loss values from the first simulation cannot be directly compared to the second simulation owing to the different transmitter powers. For the default constellation, 50 runs/iterations were performed, for the small constellation 400 runs/ iterations of 2000 s each, were carried out.

Table 5 contains the results for all possible metrics and the various example epfd simulations. It is noted that for sufficiently many epfd samples, the metrics in sections 5.2.2.1, 5.2.2.2, and 5.2.3.1 are providing approximately the same values. While it appears that the “median of sky” metric is somewhat offset from the other metrics in sections 5.2.2.1 and 5.2.2.2, an analysis of the typical scatter of the results (which the “median of sky” approach delivers), shows that the typical errors (about 0.5%) are much larger than the deviation of the “median of sky” from the rest. Therefore, it can be said that the first four metrics differ insignificantly for all practical purposes. The remaining three metrics show huge discrepancies, and it must be concluded that these may not be suitable for regulatory purposes.

Table 5: Comparison of various data loss metrics

Metric	Data loss Topocentric Default	Data loss Topocentric Small	Data loss Equatorial Default	Data loss Equatorial Small
Weighted sum (section 5.2.2.1)	2.1247%	2.1828%	1.3092%	1.4121%
Approx. average (section 5.2.2.1)	2.1248%	2.1831%	1.3089%	1.4120%
All samples (section 5.2.2.2)	2.1248%	2.1831%	1.3089%	1.4120%
Median of sky (section 5.2.3.1)	2.1287%	2.0803%	1.3089%	1.3380%
Sky blockage, 2% (section 5.2.3.2)	24.53%	38.95%	15.68%	23.79%
Sky blockage, average epfd (section 5.2.3.2)	0%	6.63%	0%	2.18%
Single cell exceeded (section 5.2.3.3)	Yes	Yes	Yes	Yes

5.2.5 Conclusion on the data loss metric

The above survey indicates that the majority of the applications of Recommendation ITU-R M.1583-1 [7] and Recommendation ITU-R S.1586-1 [8] use all time-averaged epfd samples from all simulation trials to calculate the data loss, using some variants with apparently little difference in the numerical outcome.

The most consistent methodology to assess the compliance with the 2% criterion is to calculate the 98% percentile level of the average epfd trials in 2000 s over all sky cells and compare that number to the threshold value given in RA.769-2 [4] (hereafter called "total data loss"). This method is adopted in the consecutive sections unless explicitly stated otherwise.

5.2.6 Example calculation

The method to calculate the data loss using the example and reference calculation laid out in section 5.1.3 is used. Following Recommendation ITU-R RA.1513-2 [5], and as indicated in Recommendation ITU-R S.1586-1 [8], the total data loss is then calculated using all 100 iterations to generate a linear plot of the cumulative probability of the epfd to lie above a certain threshold, as shown in Figure 7. The central solid line shows the result for all simulations and every cell, the light blue lines close to solid line show the result per simulation for all cells. The top panel shows the results for the topocentric rest frame. Here, the Recommendation ITU RA.769-2 [4] threshold of an epfd of −180 dB[W/m2] is exceeded at a level of 98.6%, while 98% would be reached at an epfd level of −180.6 dB[W/m2]. The so-called RAS margin is 0.6 dB dB[W/m2]. The bottom panel shows the calculations for the inertial equatorial reference frame: the Recommendation ITU RA.769-2 [4] threshold of an epfd of −180 dB[W/m2] is exceeded at a level of 99.2%, while 98% would be reached at an epfd level of −181.2 dB[W/m2]. The so-called RAS margin is 1.2 dB[W/m2].

This is the adopted approach used for the decision whether a certain satellite constellation has an acceptable level of data loss in a RAS band in this document. The metric used here is the total statistical data loss as described in section 5.3.2 above and calculated for all samples of the time-averaged received power, regardless of position. As explained in section 5.1.1, most astronomical objects are fixed in the equatorial frame. It should be noted that in rare cases observations are performed in the so-called drift-scan mode, in which the telescope is observing a fixed position relative to the earth (see section 5.1.3). Under these circumstances the data loss in a given topocentric cell may be of interest. However, the possibility exists to point the telescope to a topocentric position that is less affected. This is not possible for an observation pointed to a position in the equatorial frame.

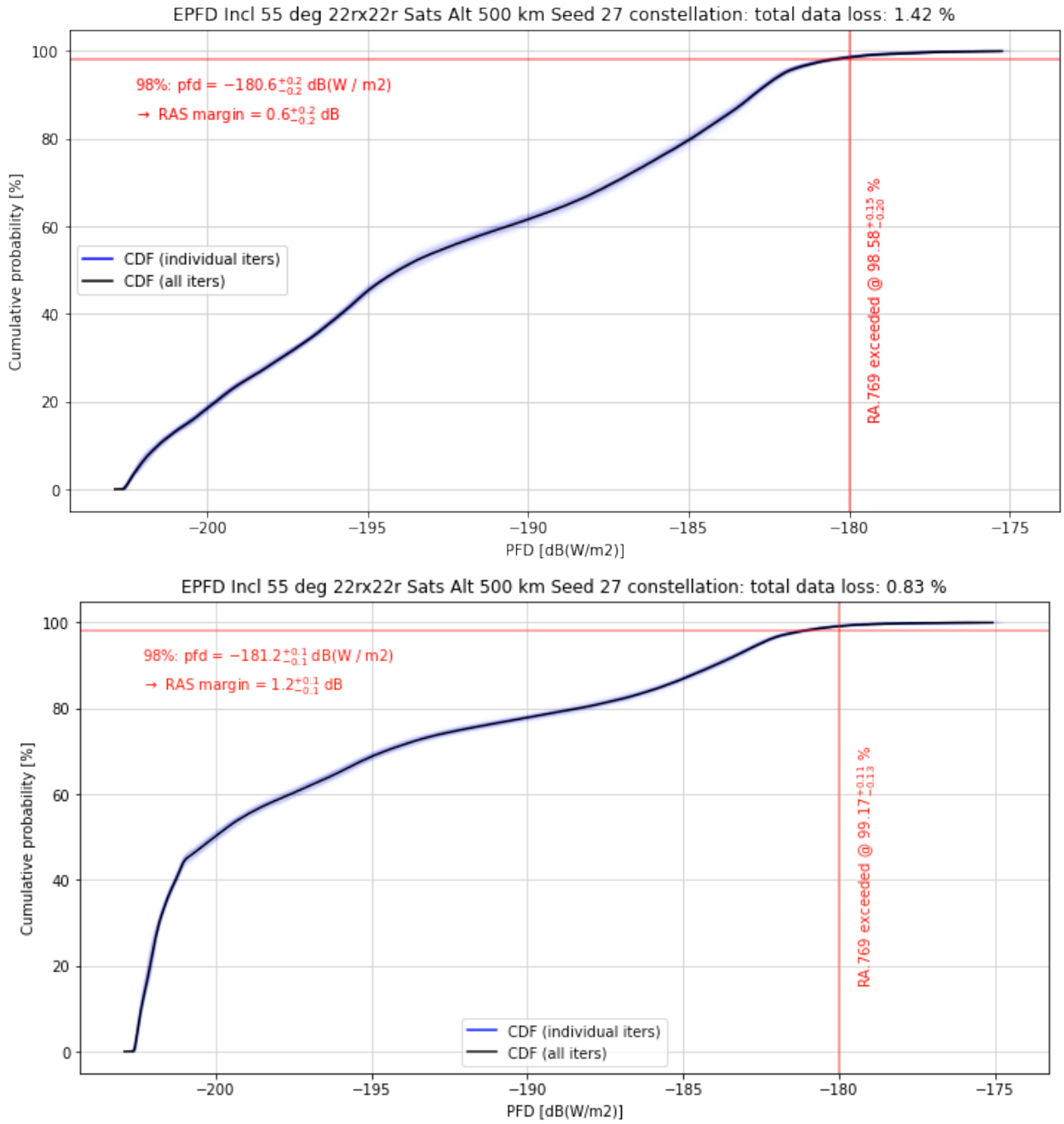

Figure 7: Cumulative probability for a cell exceeding a given power flux density

It is also possible, for additional information only, to calculate the single cell data loss, calculated for each individual cells as the number of trials for which the epfd level lies above the threshold in Recommendation ITU-R RA.769-2 [4] divided by the total number of simulation runs. Following Recommendation ITU-R S.1586-1 [8], this information can be used to visualise the distribution of data loss over the sky. This is shown in Figure 8.

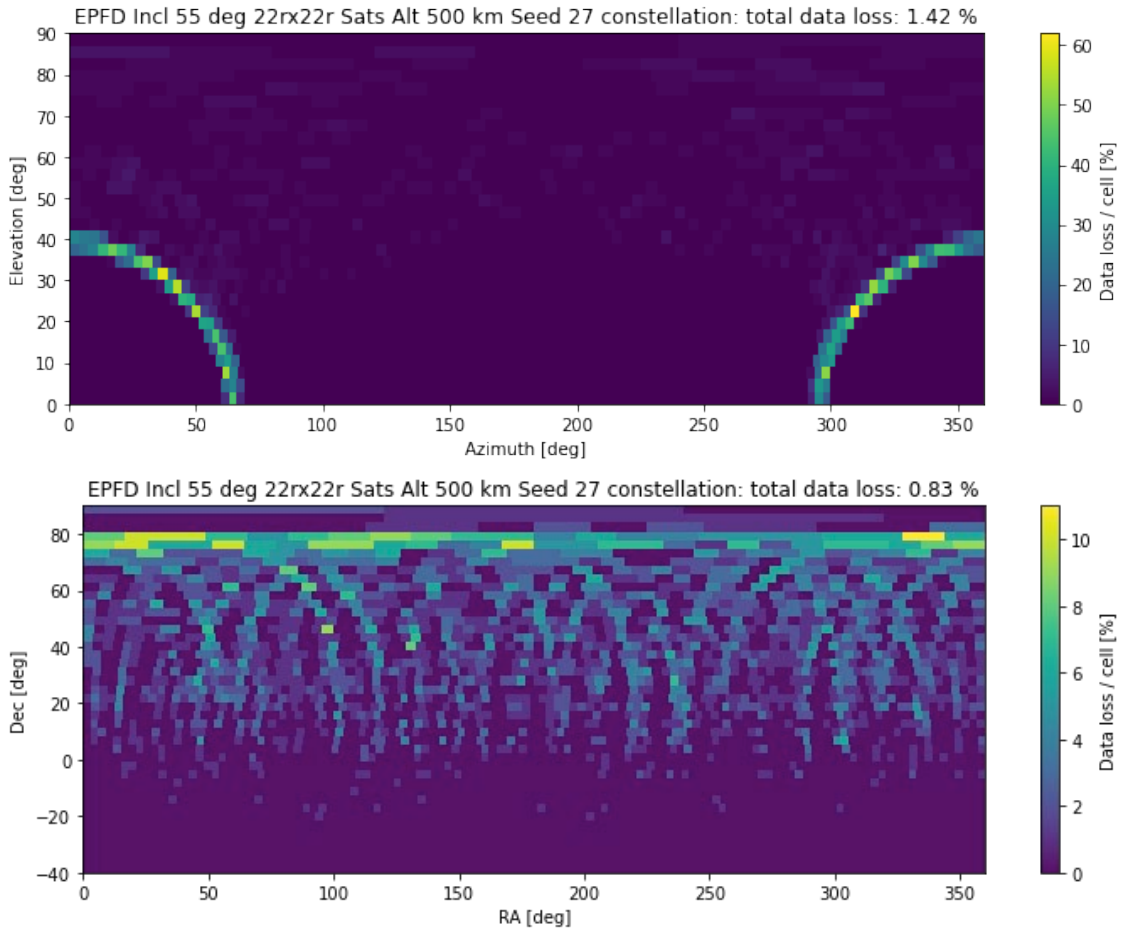

Figure 8: Single cell data loss for the example satellite configuration (as shown in Figure 6)

Figure 8 shows at top the results for the topocentric reference frame, and at the bottom it shows the results for the inertial equatorial reference frame.

5.3 AGGREGATE DATA LOSS OF MULTIPLE SATELLITE CONSTELLATIONS

The above approach can in principle easily be extended to incorporate more than one satellite constellation, to determine the total data loss caused by all constellations together. The sum in Equations (1) to (3) makes no difference on the type of satellite. The only difficulty could be that the memory of the computer might not suffice to hold all values at the same time − the problem space can become very large as the contributions to the received power depends on the combination of all sky cells with all satellite positions over hundreds or thousands of time steps; and all of this is repeated a number of times. However, it is straight-forward to do the simulations in batches and store intermediate results on disk for the final analysis.

The total data loss (independent on which data loss metric is used) is not necessarily a simple linear sum of the data losses caused by individual constellations. This is because the distribution of satellites on the sky can differ significantly, e.g. with respect to orbit altitudes or inclinations. As this has impact on the distribution and distances of the satellites in the topocentric observer frame, it could be that two very distinct constellations with 2% data loss each, will not cause exactly 4% together when they (partly) affect the same sky regions (whether the threshold in a cell is exceeded is a binary question). It is, however, obvious, that the overall data loss cannot be smaller than the larger data loss value of the individual constellations.

5.3.1 Full simulation

The methodology detailed in section 5.1 can be applied to assess the aggregated data loss, by the aggregated epfd from all non-GSO systems and applying the aggregated protection criterion.

The example given in this subsection illustrates the potential consequences in term of epfd exceedance when considering more than one constellation.

To do so, the respective impact in terms of data loss and affected sky cells for two non-GSO constellations was assessed independently, then altogether. One hundred iterations were simulated in each cell, starting at random time and lasting 2000 seconds each. The radio astronomy telescope diameter is 25 m, its antenna pattern is obtained through Recommendation ITU-R RA.1631-0 [2] and its geographic latitude is 50°N.

5.3.1.1 Constellation 1 (default)

The default constellation parameters are the same as the ones defined in section 5.1.3.

The results for the whole sky cells with constellation 1 are provided in Figure 9.

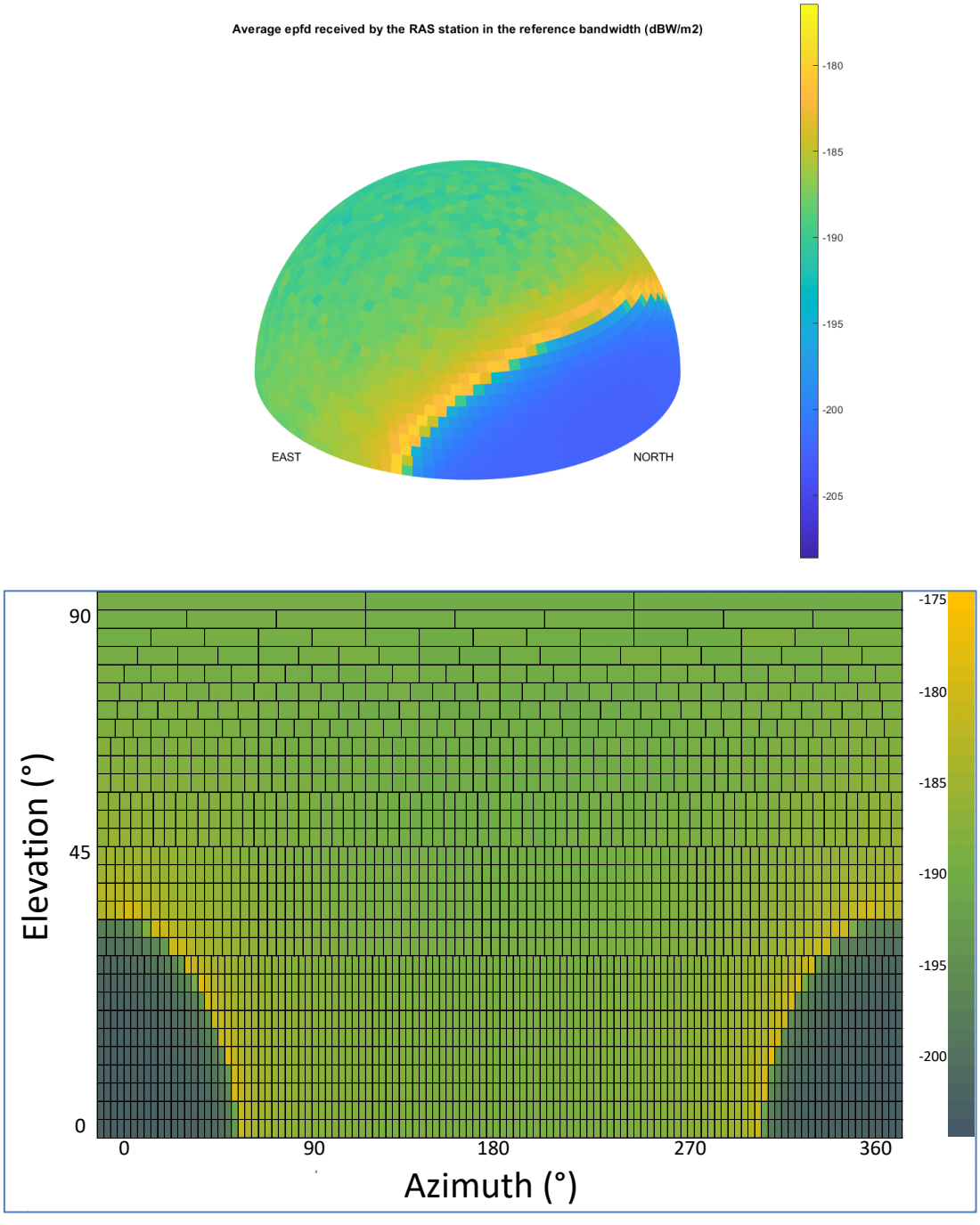

Figure 9: Epfd results for all sky cells with constellation 1

The data loss is 1.2% as shown in the complementary cumulative distribution function (CCDF) in Figure 10.

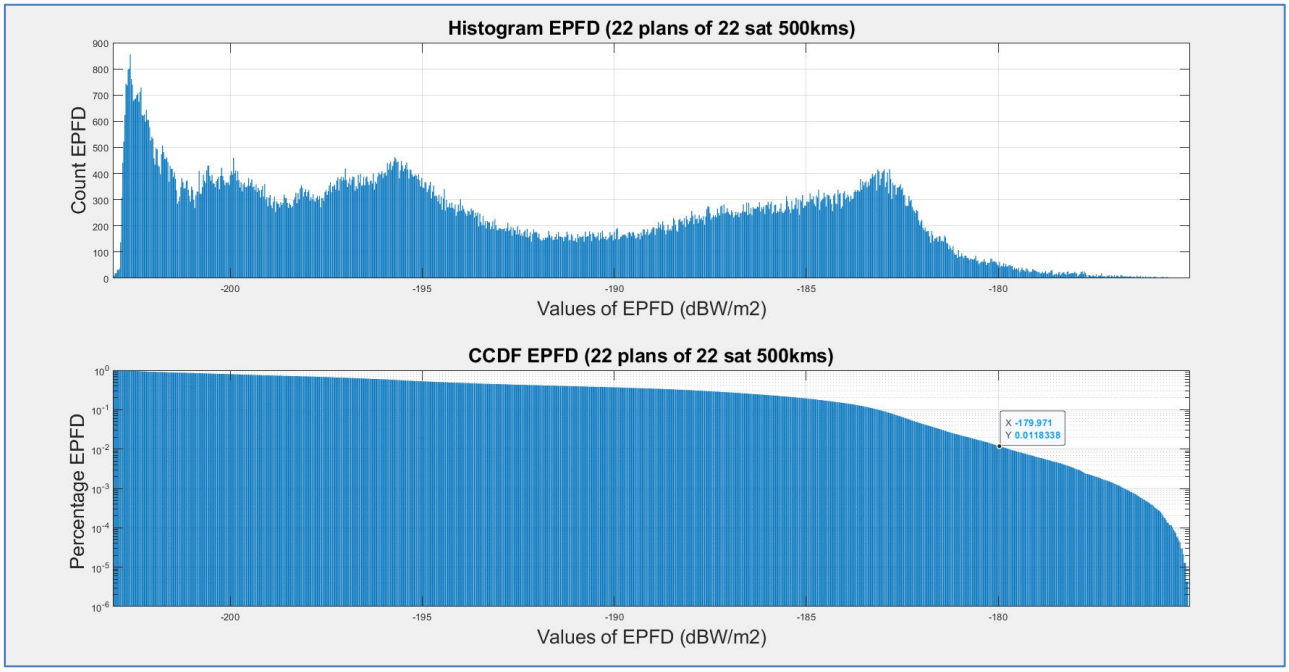

Figure 10: Constellation 1 - Histogram and CCDF of epfd samples for all sky cells

5.3.1.2 Constellation 2

A second constellation is considered, with the following parameters:

- 22 orbital planes with ascending nodes evenly distributed;
- In each plane, 22 satellites equally spaced;
- Orbital inclination of 30°;
- Satellite altitude of 1000 km;
- Transmitted Power of -38 dBm;
- Isotropic antenna.

The results for the whole sky cells with constellation 2 are provided in Figure 11.

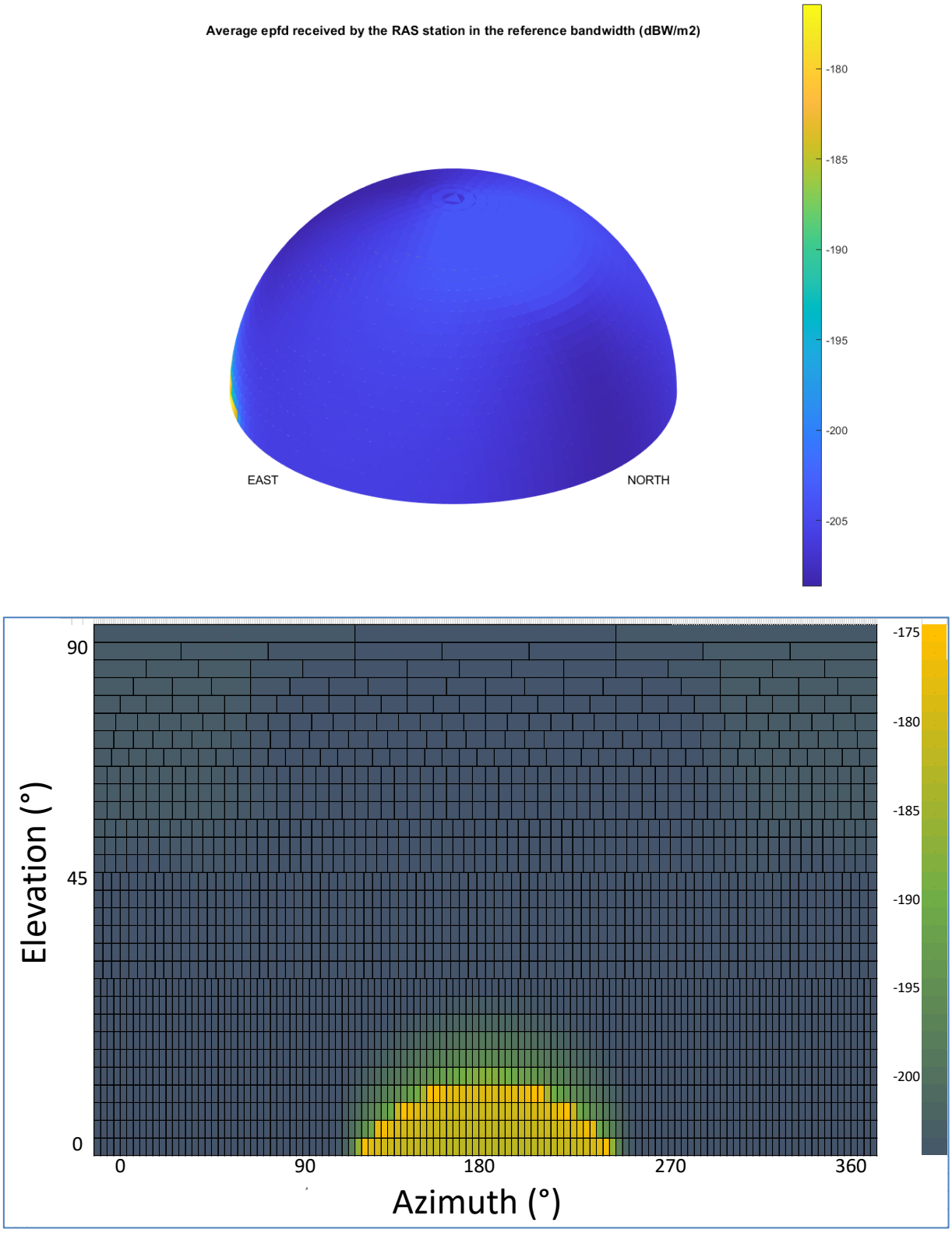

Figure 11: Epfd results for all sky cells with constellation 2

The data loss is 2.4% as shown in the CCDF in Figure 12.

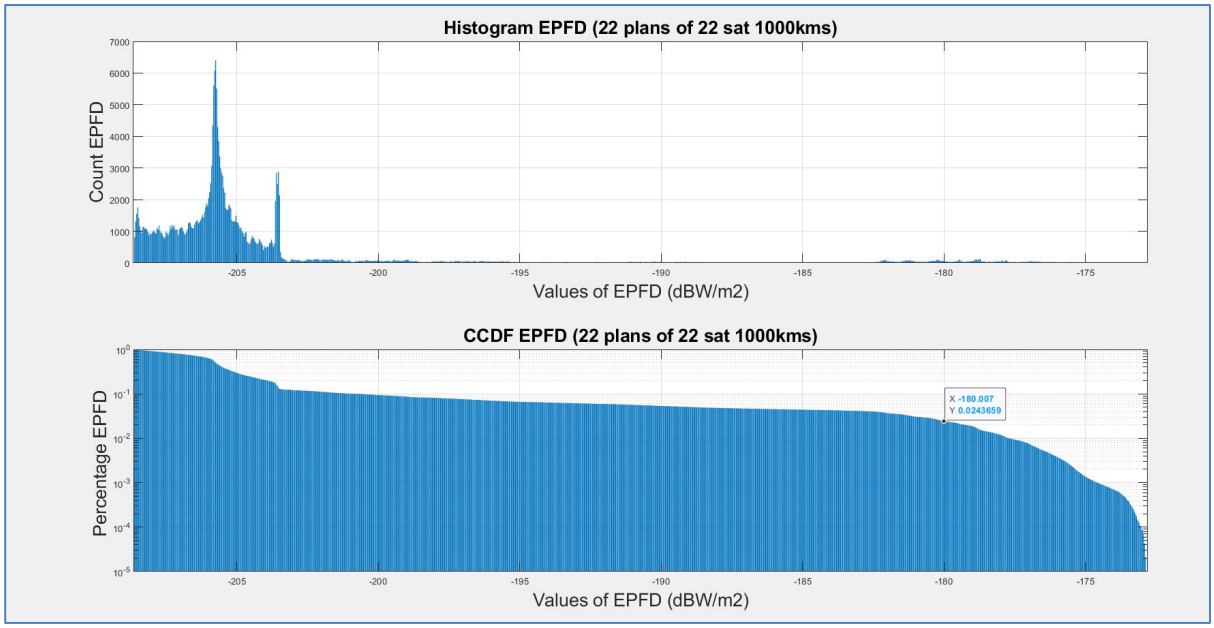

Figure 12: Constellation 2 - Histogram and CCDF of epfd samples for all sky cells

5.3.1.3 Constellation 1 + constellation 2

A third simulation is run with the 2 constellations operating simultaneously, the epfd results for the whole sky cells are shown in Figure 14.

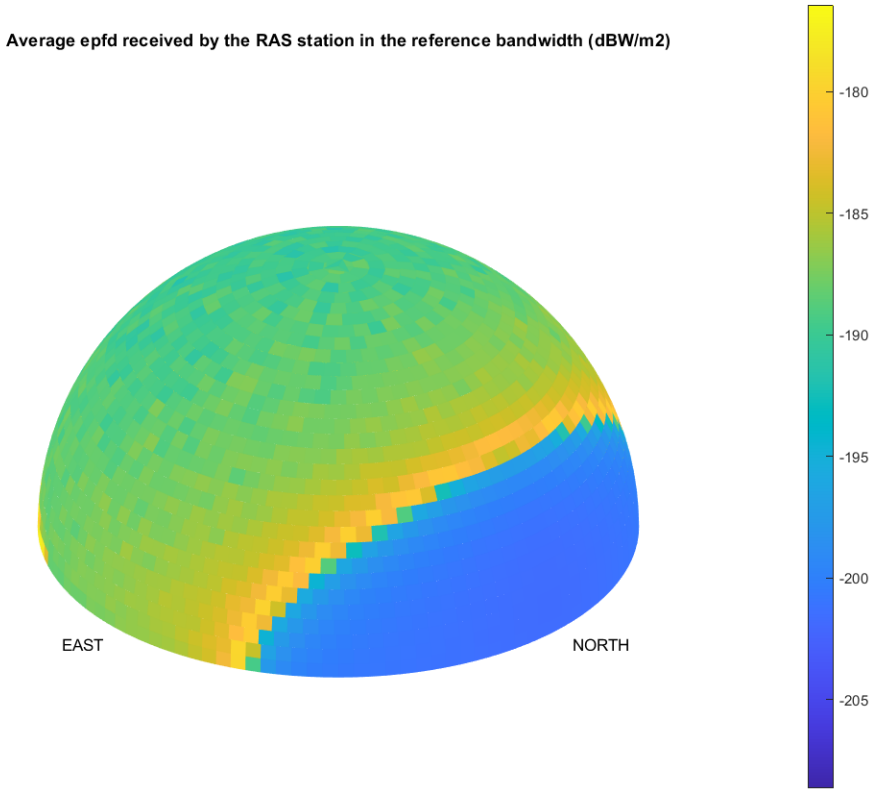

Figure 13: epfd results for the whole sky cells

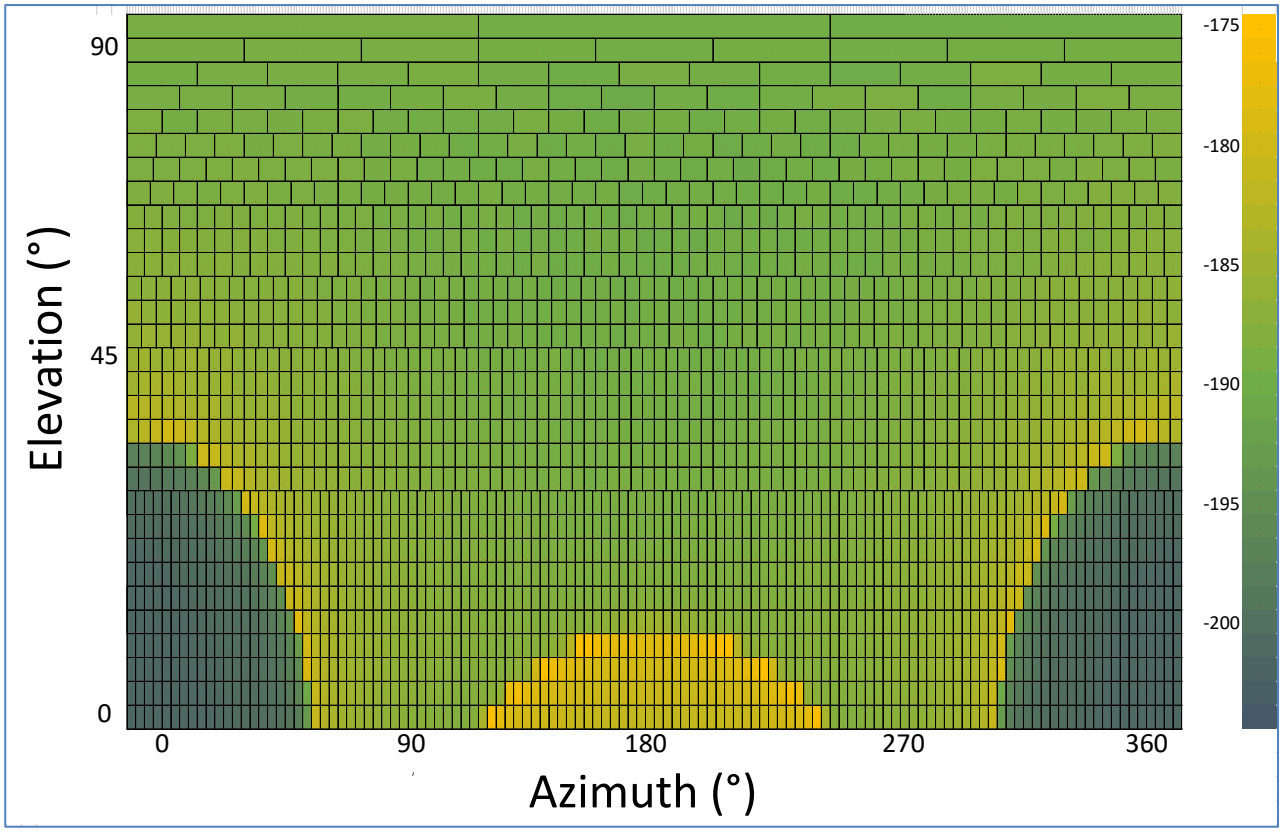

Figure 14: Epfd results for all sky cells with constellation 1 and 2

The Data loss is also computed for those 2 constellations and reaches 4.1% as it can be seen on the CCDF in Figure 15.

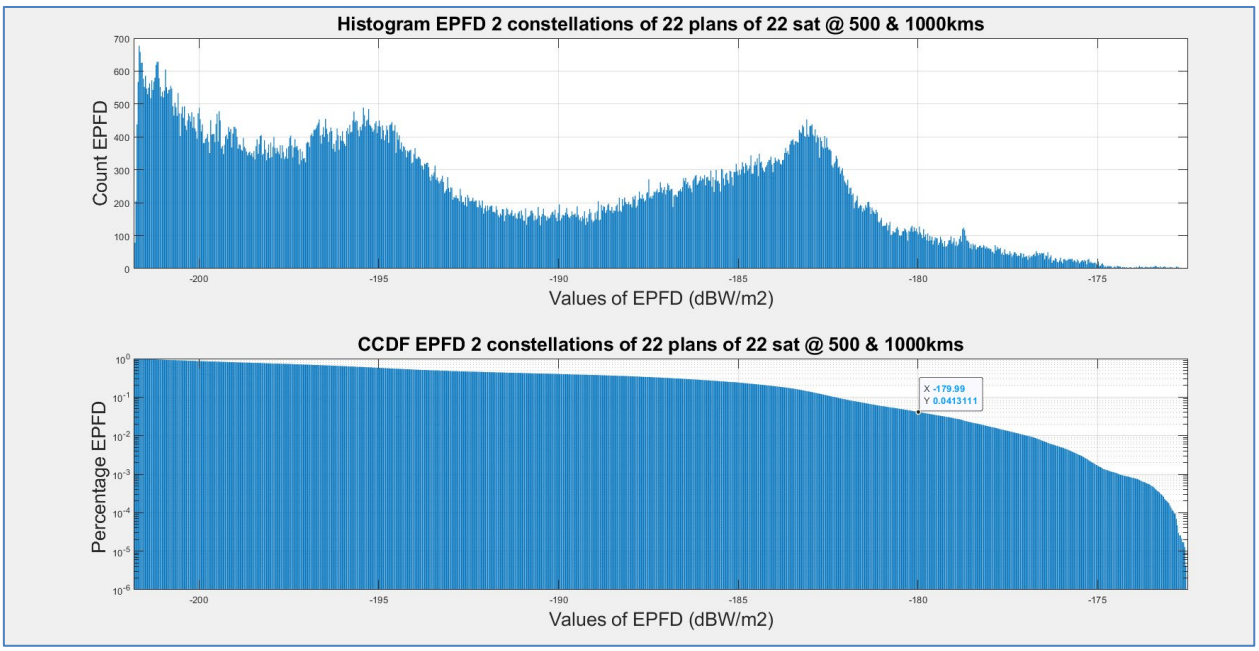

Figure 15: Constellations 1 and 2 -Histogram and CCDF of epfd samples for all sky cells

A summary of the statistics is given in Table 6.

Table 6: Summary of the simulation results

Metric	Constellation 1 @ 500 km	Constellation 2 @ 1000 km	Constellation 1 + Constellation 2
Total data loss (%)	1.2	2.4	4.1
Number of cells with more than 2% of the samples with epfd>-180 dBW/m2	98	118	220

Section 5.2.5 concluded that the metric to be used was the data loss over the whole sky, but it is to be noted that in the case of the number of cells with more than 2% of epfd samples above the Recommendation ITU-R RA.769-2 threshold the numbers for the simultaneous simulation and summing the results individually almost coincide. This result is a particular situation due to the significant difference in the geometry of the two constellations used in this example. If the two constellations have a similar geometry, the cells with data loss will coincide and the linear addition of single simulations will differ from the simultaneous simulation.

The results from the previous simulation indicate that the data loss due to the aggregate interference cannot be deduced from the simple addition of those constellations single entry data losses.

It was decided to run two additional simulations to confirm this conclusion:

- One simulation with exactly two times the constellation of 484 satellites at 500 km;
- A second simulation with exactly two times the constellation of 484 satellites at 1000 km.

All the other parameters remain unchanged. It is worth to mention that those configurations are unrealistic, since it would not be physically possible to have 2 identical satellites at the same position, and that constellations 1 (@500 km) and constellation 2 (@1000 km) are fictious systems, whose parameters were chosen specially to observe data loss with the epfd methodology given in Recommendation ITU-R M.1583-1 [7].

Those configurations with exactly twice the same constellation is in fact equivalent to an increase of 3dB in the satellite pfd, as it can be seen below on the epfd CCDF below.

5.3.1.4 Two times constellation 1

The results obtained are the following:

With constellation 1, as already seen in studies above, the data loss is 1.2%.

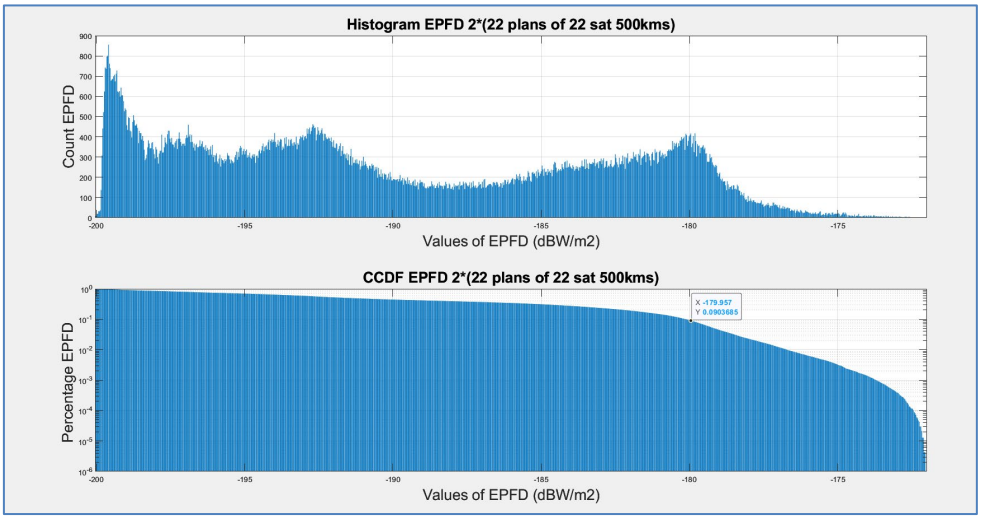

Figure 16: Results with two times constellation 1

The data loss, i.e. the percentile of epfd samples over the entire sky, each averaged over 2000s, that exceeds the threshold of -180dBW/m2 is increased to 9.0% with 2 times the same constellation at 500 km.

9.0% for 2*(constellation 1 @ 500 km) > 2 * (1.2% for constellation 1 @ 500 km)

5.3.1.5 Two times constellation 2

With constellation 2, as already seen in studies above, the data loss is 2.4%.

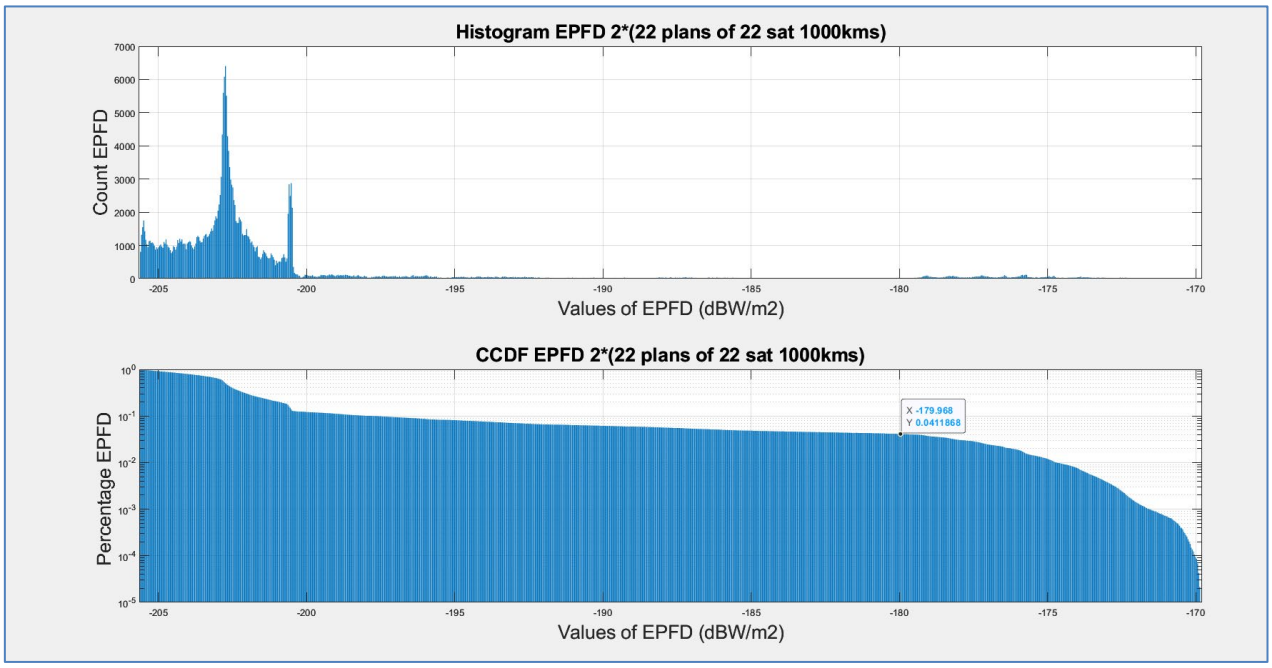

Figure 17: Results with two times constellation 2

The data loss, i.e. the percentile of epfd samples over the entire sky, each averaged over 2000s, that exceeds the threshold of -180dBW/m2 is increased to 4.1% with 2 times the same constellation at 1000 km.

4.1% for 2*(constellation 2 @ 1000 km) < 2 * (2.4% for constellation 2 @ 1000 km)

In these two simulations it can be seen that in one situation there is a major increase in the data loss while in the second one the data loss with twice the same constellation is less than twice the data loss with one constellation. It can therefore be concluded that it is not possible to approximate the aggregate data loss due to multiple non-GSO satellite systems based on the single-entry data losses due to each satellite system.

5.3.2 Conclusions on the calculation of aggregate data loss from multiple constellations

It can be concluded that the total data loss caused by more than one constellation cannot be obtained through the simple addition of those constellations single entry simulation results. The data loss has to be calculated from all samples resulting from the simultaneous transmissions of all satellite constellations at once, following the prescription in sections 5.1 and 5.2.

In the absence of receiver side nonlinear effects, and if the time ranges chosen for all samples are identical for two or more satellite constellations, the epfd values generated by each constellation can be added together for each sample to obtain the aggregate epfd level.

However, as this is generally not the case, the data loss due to multiple non-GSO satellite systems unwanted emissions has to be calculated from all samples resulting from the simultaneous transmissions of all satellite constellations at once, using the parameters listed in section 5.1 and following the methodology described in section 5.2.

6 SENSITIVITY ANALYSIS ON THE INFLUENCE OF VARIOUS PARAMETERS ON THE AGGREGATED DATA LOSS

This section explores the effect that variations in parameters have over the epfd results, for this the constellation described in section 5.1.3 is used as a starting point. To explore the influence of each parameter, the map of single cell average epfd value are produced for several points in each parameter and also the ratio of variation of the single cell average epfd with respect to the default constellation as control point.

To study the effect of the change of single configuration parameters, the first step consists in generating the average epfd distribution on the sky for a reference configuration, then in a second step to change single parameters of the reference configuration and finally study the effect by calculating the ratio of the epfd per cell on the sky grid. For the reference configuration the same parameters as in section 5.1.3 example were used.

Most of the calculations in the consecutive sections have been carried out using a Python [30] script in the form of a Jupyter [31] notebook, making use the pycraf [32] and cysgp4 [33] software packages.

While analysing the impact of the variation of the different parameters characterising a non-GSO satellite constellation does provide valuable insight, it is critical to keep in mind that they are all interdependent and it may prove challenging to deduce the impact of a given constellation without a detailed simulation. For instance, in the case of the inclination, in the current configuration the hypothesis has been made that the different orbital planes were always spaced in a similar manner whether the inclination of those planes was equal to 40° or 90°, with their respective RAAN spread over 360°. However, a satellite constellation using an inclination of 90° can only spread the RAAN of its orbital planes over 180° and not 360°. As a matter of fact, this is how the OneWeb and Iridium constellations are laid out, with an inclination of 87.9° and 86.4° respectively.

6.1 ORBITAL PARAMETERS

6.1.1 Satellite plane inclination

Figure 18 and Figure 19 show the ratios of the average epfd per cell for a few selected orbital inclinations and the reference configuration (orbital inclination of 55°) as displayed in Figure 6.

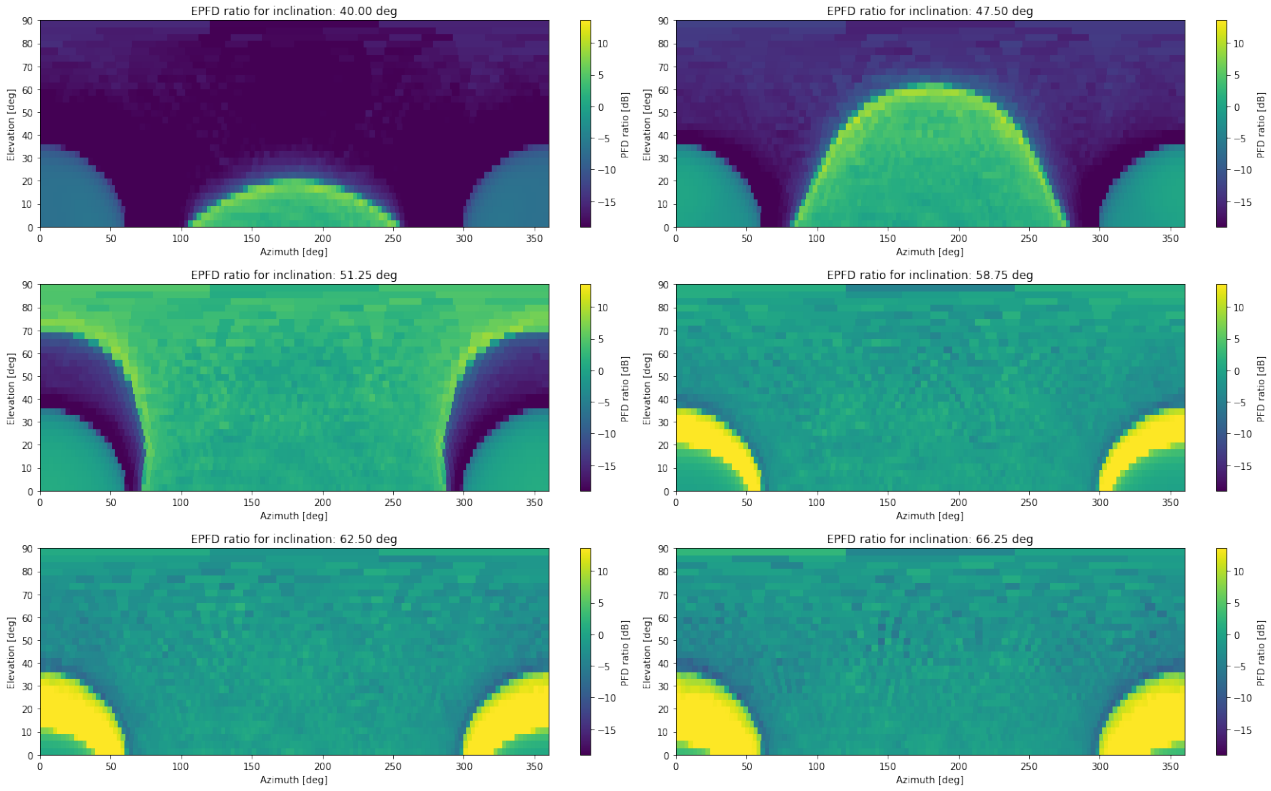

Figure 18: Ratio of epfd of a configuration changing in orbital inclination and a reference configuration (orbital inclination 55°), topocentric reference frame

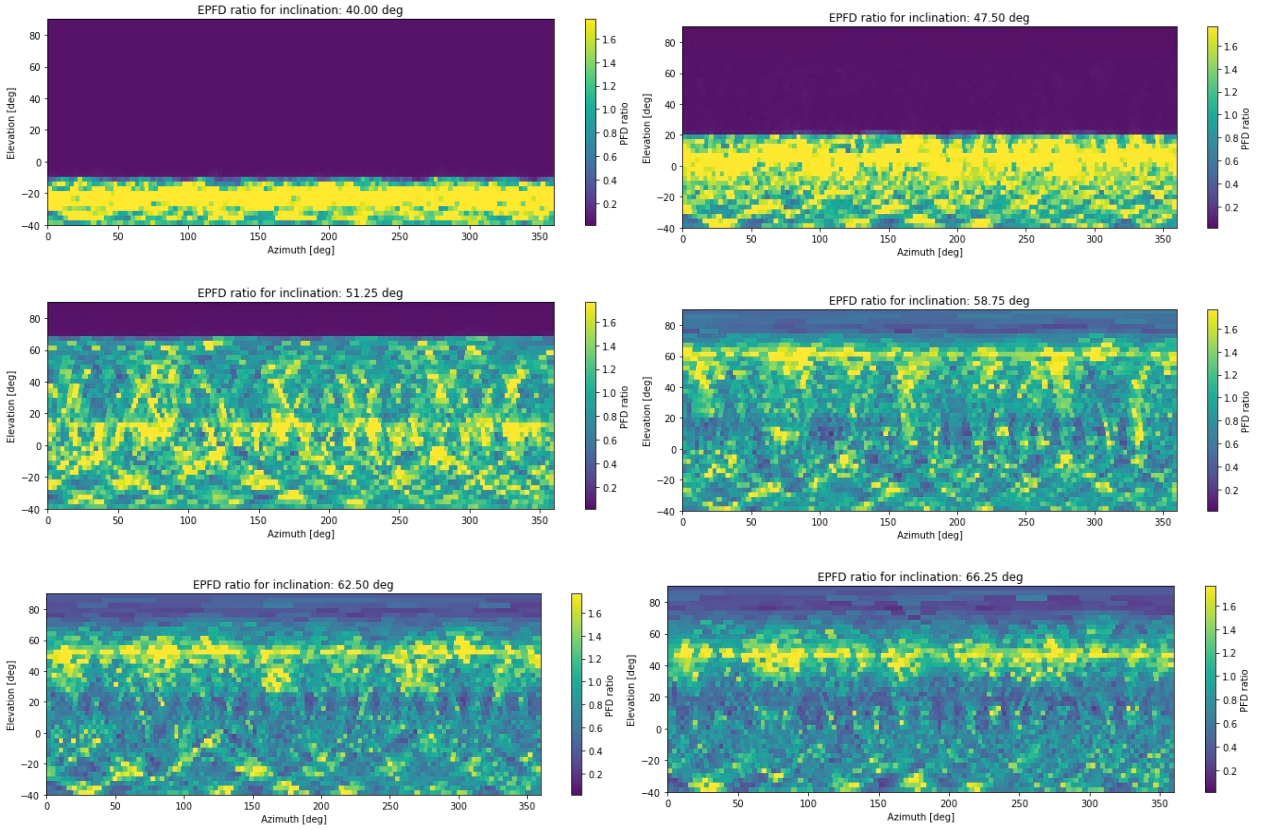

Figure 19: Ratio of epfd of a configuration changing in orbital inclination and a reference configuration (orbital inclination 55°), inertial equatorial reference frame

Since the altitude of the satellites is low (500 km) the position of the satellites on the sky never reaches the zenith, if the orbital inclination is much lower than the geographic latitude of the observatory. This only happens at an orbital inclination a few degrees below the geographic latitude of the RAS station. Above the value of the orbital inclination, the changes in the epfd ratio are significantly lower. Building the 5% and 95%-percentile of each plot shown in Figure 18 and Figure 19, as well as the mean and standard deviation of the cell values, one generates a linear plot of epfd statistics with inclination. This is shown in Figure 20.

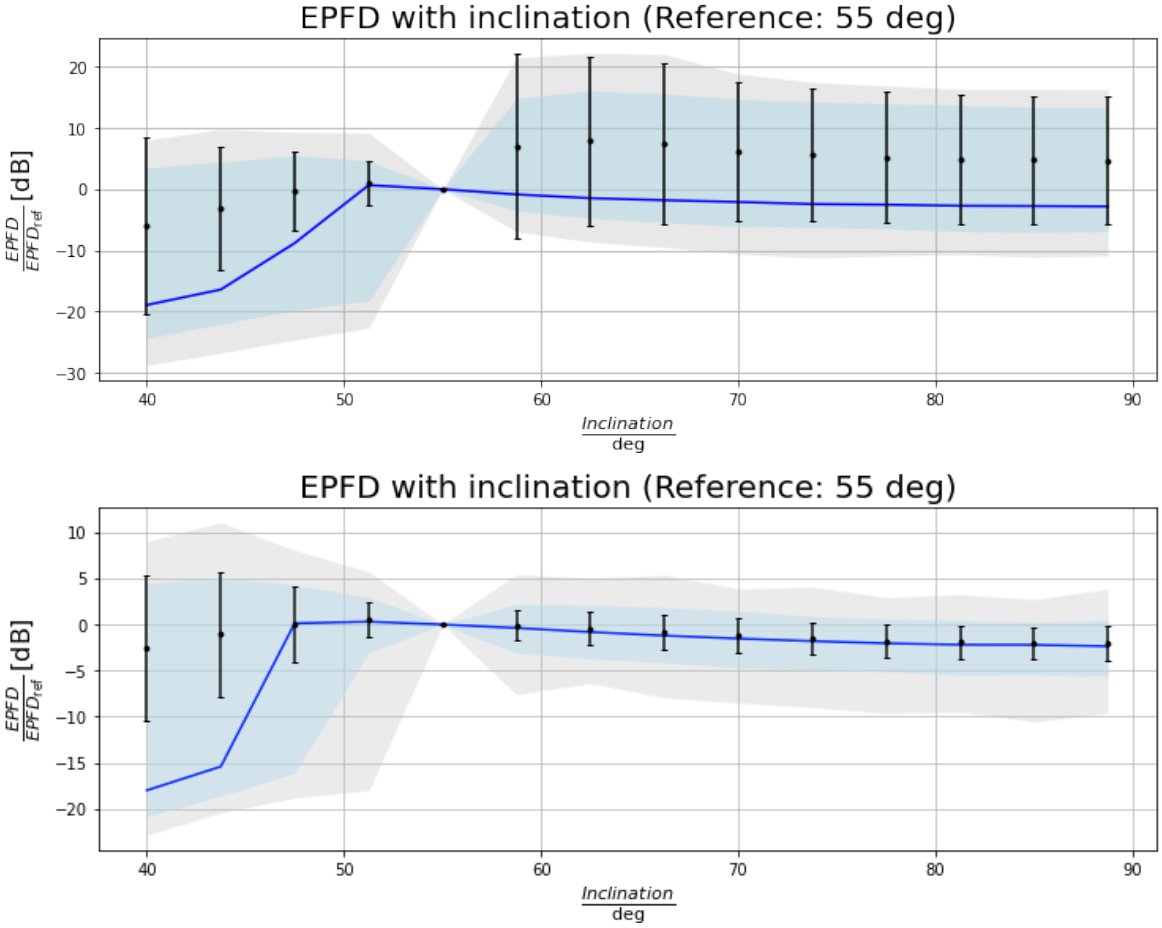

Figure 20: Ratio of epfd of a configuration changing in orbital inclination and a reference configuration (orbital inclination 55°).

In Figure 20, the black dots and error bars show the average and standard deviation. The blue shaded area comprises the area between the 5% percentile and the 95% percentile with the blue line indicating the median (50% percentile), the grey shaded area is the area between minimum and maximum in the plot. The top panel shows the results for the topocentric reference frame, the bottom one for the inertial equatorial reference frame.

Figure 20 reflects the tendency observed in the sky map plots: above an orbital inclination slightly below the geographic latitude of the RAS station, the epfd rises quickly as the satellites become visible at all elevations and then approximately saturates at a certain value above the geographic latitude of the RAS station. Already these viewgraphs show the effect of taking the inertial system into account for the epfd calculations: the equivalent power flux density is more evenly distributed over the sky.

6.1.2 Altitude

6.1.2.1 Change of altitude while keeping same power

Satellite altitude is changed from 300 km to 1500 km. Figure 21 shows the epfd ratios for two exemplary altitudes and the statistical plot in the topocentric rest frame, Figure 22 shows the same quantities in the equatorial frame. As the effective isotropic radiated power (*e.i.r.p.*) of the satellites was kept constant, the power flux density decreases quadratically with distance, this is a monotonic function. As however also the visibility of the satellites changes, the precise shape of the dependency remains to be studied in greater detail.

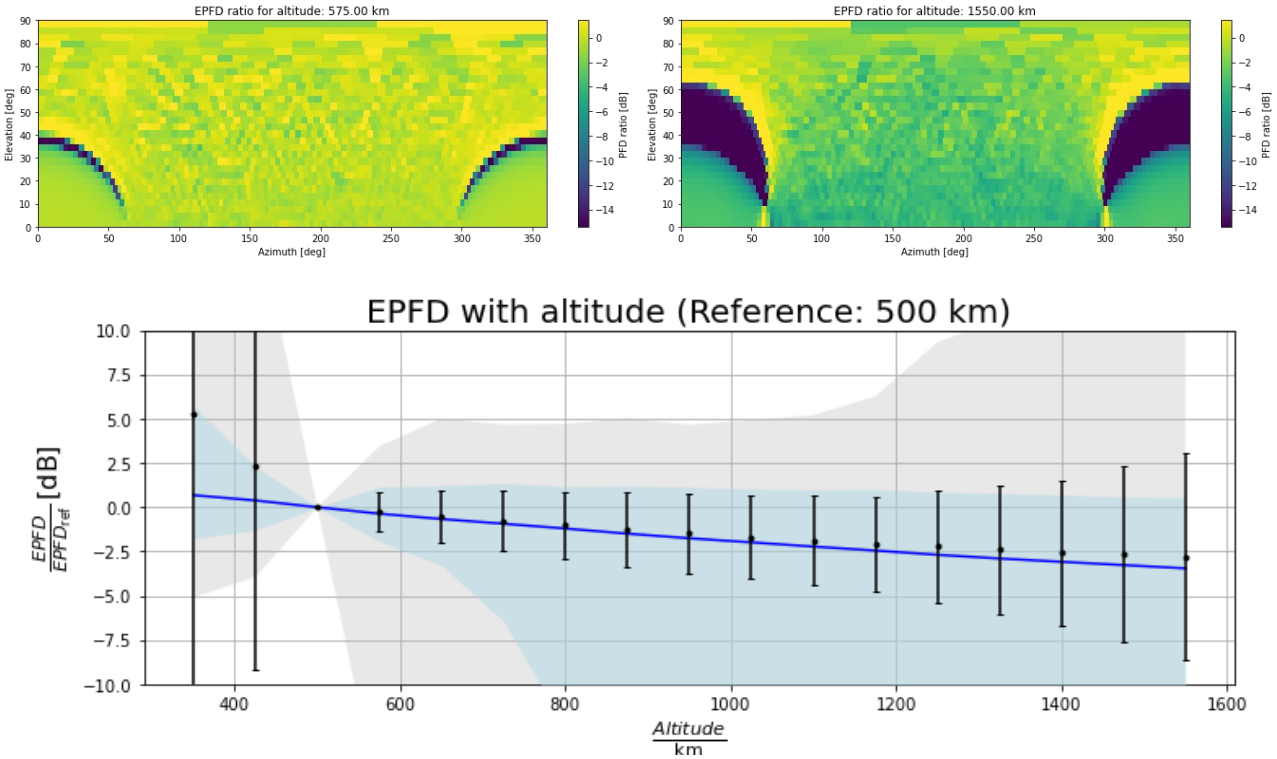

Figure 21: Ratio of epfd of a configuration changing in altitude and a reference configuration (altitude 500km), topocentric reference frame

In Figure 21, the top panels show the results per cell for two altitudes. The bottom panel shows the epfd ratios averaged over cells. Black dots and error bars show the average and standard deviation. The blue shaded area comprises the area between the 5% percentile and the 95% percentile with the blue line indicating the median (50% percentile), the grey shaded area is the area between minimum and maximum in the plot.

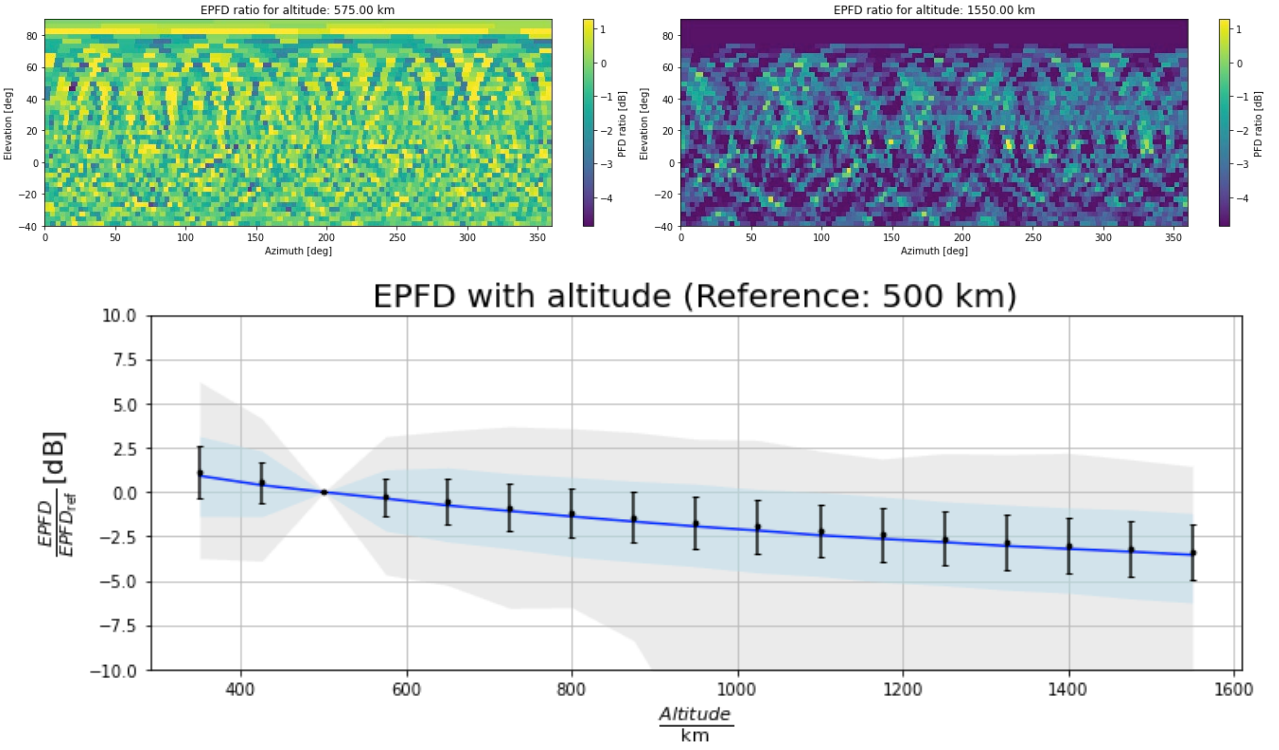

Figure 22: Ratio of epfd of a configuration changing in altitude and a reference configuration (altitude 500 km), inertial equatorial reference frame

In Figure 22, the top panels show the results per cell for two altitudes, and the bottom panel the epfd ratios averaged over cells. Black dots and error bars show the average and standard deviation. The blue shaded area comprises the area between the 5% percentile and the 95% percentile with the blue line indicating the median (50% percentile), the grey shaded area is the area between minimum and maximum in the plot.

6.1.2.2 Adjusted power

While instructive, the above example is not reflecting a realistic situation. Normally an operator needs to achieve a certain pfd level on the ground (required by terminals) and therefore will increase the power of the transmitters when the altitude is increased. Since the power flux density is inversely proportional to the square of the distance, it is expected that the transmitted power is changed proportionally to the square of the ground distance at nadir of a satellite in this case (considering isotropic transmitters). The effect of this is simulated in Figure 23 and Figure 24.

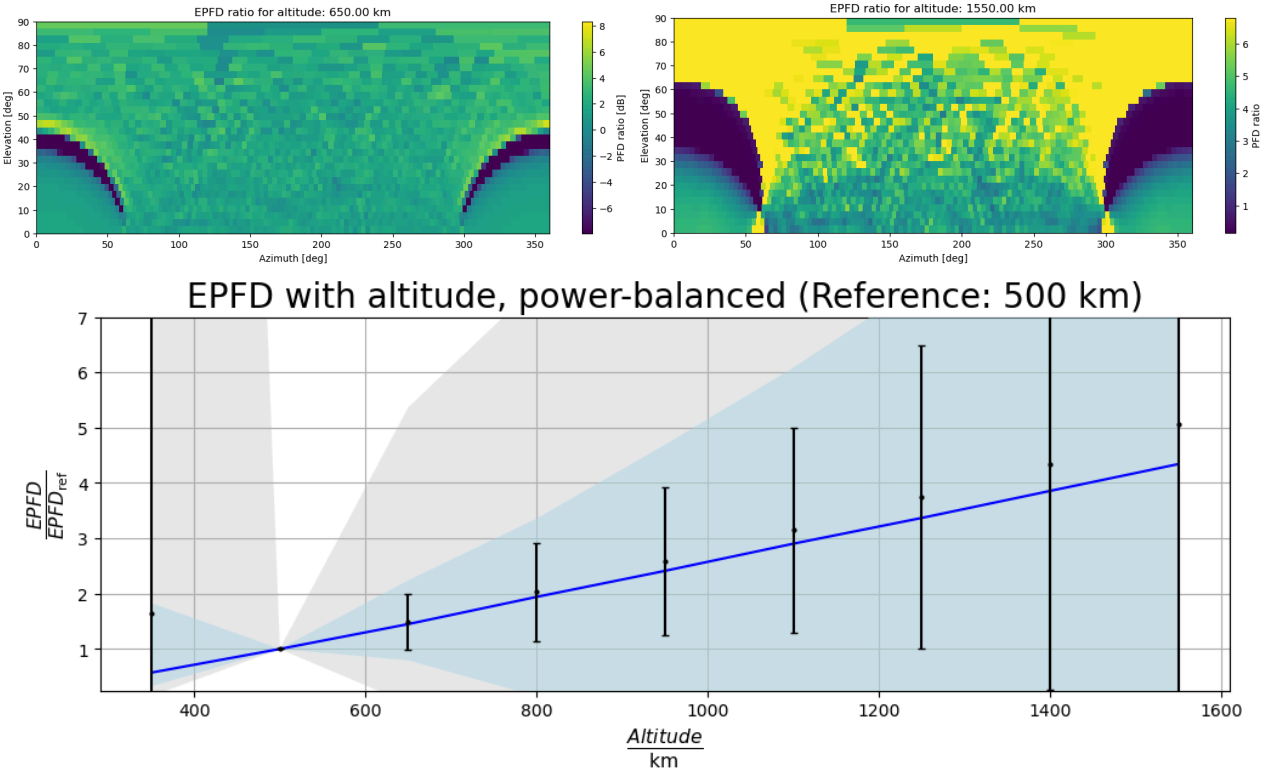

Figure 23: Ratio of epfd of a configuration changing in altitude and a reference configuration (altitude 500 km), while increasing the transmitted power proportionally to the square of the altitude above ground, topocentric reference frame

In Figure 23, the top panels show the results per cell for two altitudes. The bottom panel shows the epfd ratios averaged over cells. Black dots and error bars show the average and standard deviation. The blue shaded area comprises the area between the 5% percentile and the 95% percentile with the blue line indicating the median (50% percentile), the grey shaded area is the area between minimum and maximum in the plot.

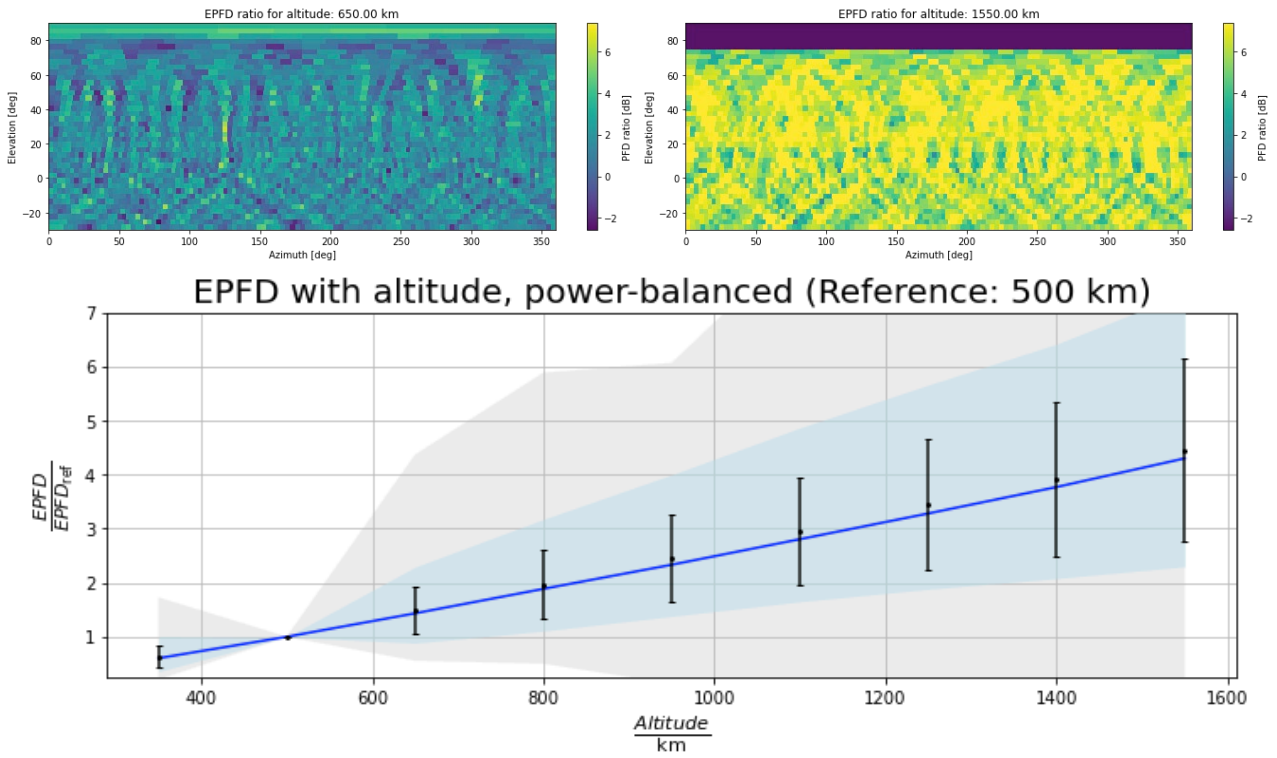

Figure 24: Ratio of epfd of a configuration changing in altitude and a reference configuration (altitude 500 km), while increasing the transmitted power proportionally to the square of the altitude above ground, inertial equatorial reference frame

In Figure 24, the top panels show the results per cell for two altitudes. The bottom panel shows the epfd ratios averaged over cells. Black dots and error bars show the average and standard deviation. The blue shaded area comprises the area between the 5% percentile and the 95% percentile with the blue line indicating the median (50% percentile), the grey shaded area is the area between minimum and maximum in the plot.

While per satellite the received power and hence the power flux density is constant, this is not true for the sum over many satellites. The cumulative interference level – given that all other parameters, in particular the number of satellites is constant – increases if the power flux density per satellite is kept constant through an increased transmitted power as a consequence of more satellites being in visibility of the RAS station.

6.2 NUMBER OF SATELLITES PER CONSTELLATION

The satellites of a given non-GSO satellite system are usually spread on several orbital planes. The spacing of the satellites within one plane can be regular or not. The number of satellites of the non-GSO system, as well as the distribution of the satellites on the different orbital planes, can have an impact on the level of interference.

A precise model of the non-GSO system is necessary, since each non-GSO satellite system has its own orbital characteristics that will have an impact on the epfd statistics. It is worth to mention that many non-GSO systems follow a Walker delta pattern constellation, for which:

- the inclination is the same for all orbital planes;
- the planes are equally spaced;
- the satellites are equally spaced within one plane.

An example is the Galileo navigation system, which is a Walker Delta 56°: 24/3/1 at 23222 km of altitude – 56° of inclination, 24 satellites, 3 orbital planes ("1" gives the change in true anomaly for satellites in neighbouring planes "1" * 360/24).

In that next set of simulations the number of orbital planes is chosen to be approximately equal to the number of satellites per plane and increase the total number of satellites. This results in a nearly perfectly linear dependency: the epfd can be assumed to be proportional to the number of satellites if no other parameter is changed (see Figure 25).

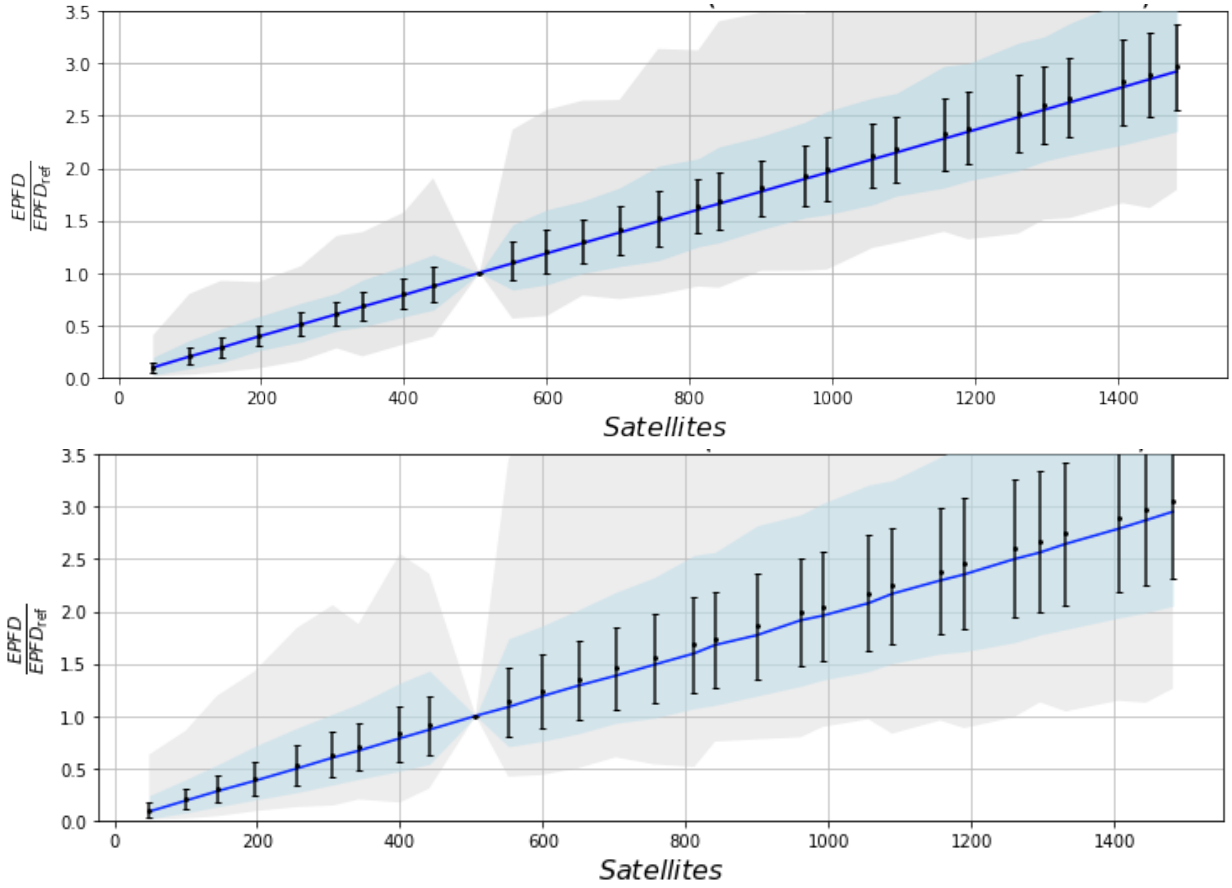

Figure 25: Ratio of epfd of a configuration changing in the number of satellites and a reference configuration (484 satellites)

In Figure 25, black dots and error bars show the average and standard deviation. The blue shaded area comprises the area between the 5% percentile and the 95% percentile with the blue line indicating the median (50% percentile), the grey shaded area is the area between minimum and maximum in the plot. Notice that this plot is linear and not logarithmic, to show the linear shape of the dependency. In the top panel of Figure 25 the topocentric rest frame was used, in the bottom panel the equatorial rest frame.

6.3 ACTIVE ANTENNA PATTERNS OF SATELLITES

To conduct the epfd calculations as described in section 5.1, the antenna pattern and pointing are required. However, non-GSO constellations nowadays often use active antenna arrays to form their synthetic beams, and for those no ITU-R recommendation exists to model the antenna gain in adjacent bands.

To approach the problem, here is given an example, where is used the description of an active array from Recommendation ITU-R M.2101-0 [34], which describes an IMT base station and user equipment beamforming antenna pattern in section 5. The assumption is that active antenna arrays aboard non-GSO satellites operate in a similar way. The software implementation from the pycraf software package was used. The layout of the simulated array is square. The single element maximum gain (7th row in Recommendation ITU-R M.2101-0, table 3 [34]) is chosen to be 5 dBi. The horizontal and vertical front-to-back ratio (3rd row in Recommendation ITU-R M.2101-0, table 3 [34]) is 30 dB, the horizontal and vertical 3 dB beam width of the single elements (2nd and 5th row in Recommendation ITU-R M.2101-0, table 3 [34]) is 65°. The separation of the single elements is chosen to be $\lambda/2$, Where λ is the wavelength, as suggested in Recommendation ITU-R M.2101-0, section 5 [34]. The array is directed towards Earth, with nadir being perpendicular to the array. The

nominal edge length of the array is varied as a parameter. This nominal edge length is then divided by twice the wavelength and rounded, resulting in the number of single elements. The physical size of the array is then $\lambda/2$ times the number of elements.

In the absence of any prescription, the pointing pattern is chosen as a uniform random pattern, considering that at the position where the satellite antenna points on Earth terminals will have a minimum elevation limit of 20° and no communication link will be established below that limit. In practice, from the perspective of the satellite this defines a cone within which the pointings can be chosen randomly. The pointing is kept constant in the satellite frame for 200 s, to then be changed. This is supposed to mimic the change in the pointings as the satellites move above Earth, although, in practice, such satellites may point at fixed locations on Earth to ensure a better service to user terminals. No GSO arc avoidance has been implemented, but this effect is studied further in section 6.7. It is assumed that a satellite which is seen from a point on Earth within the GSO arc will point into a slightly different direction but will be replaced by another satellite which lies not within the GSO arc to point at the same position, which probably balances the epfd statistics.

All other parameters, including $P_{e.i.r.p.}$, are kept as described at the beginning of this section.

The results are plotted in Figure 26 and Figure 27. The main effect is the reduction of the epfd with the edge length of the transmitter. This is because with increasing antenna aperture size, the boresight gain increases and hence the total transmitted power decreases.

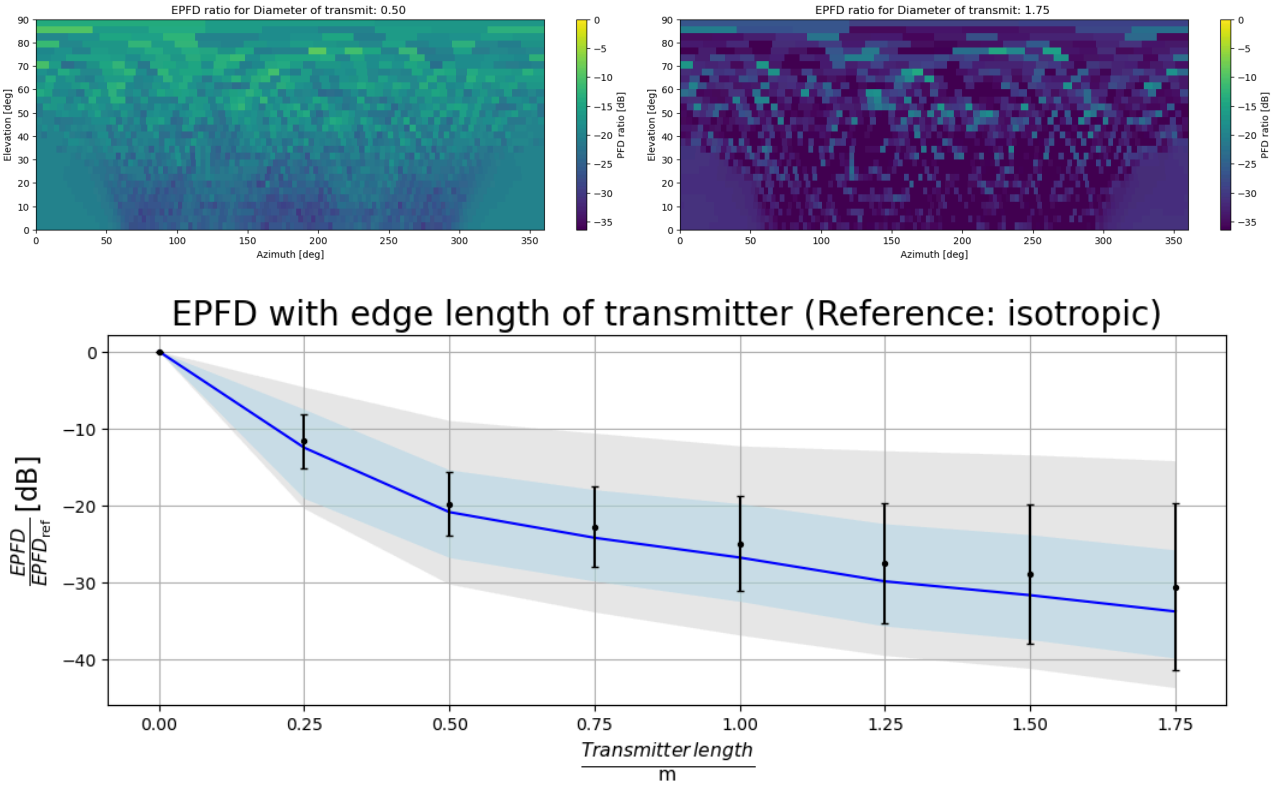

Figure 26: Ratio of epfd of a configuration changing in array size, and a reference (isotropic), inertial topocentric reference frame

In Figure 26, the top panels show the results per cell for two transmitter sizes, the bottom panel the epfd ratios averaged over cells. Black dots and error bars show the average and standard deviation. The blue shaded area comprises the area between the 5% percentile and the 95% percentile with the blue line indicating the median (50% percentile), the grey shaded area is the area between minimum and maximum in the plot.

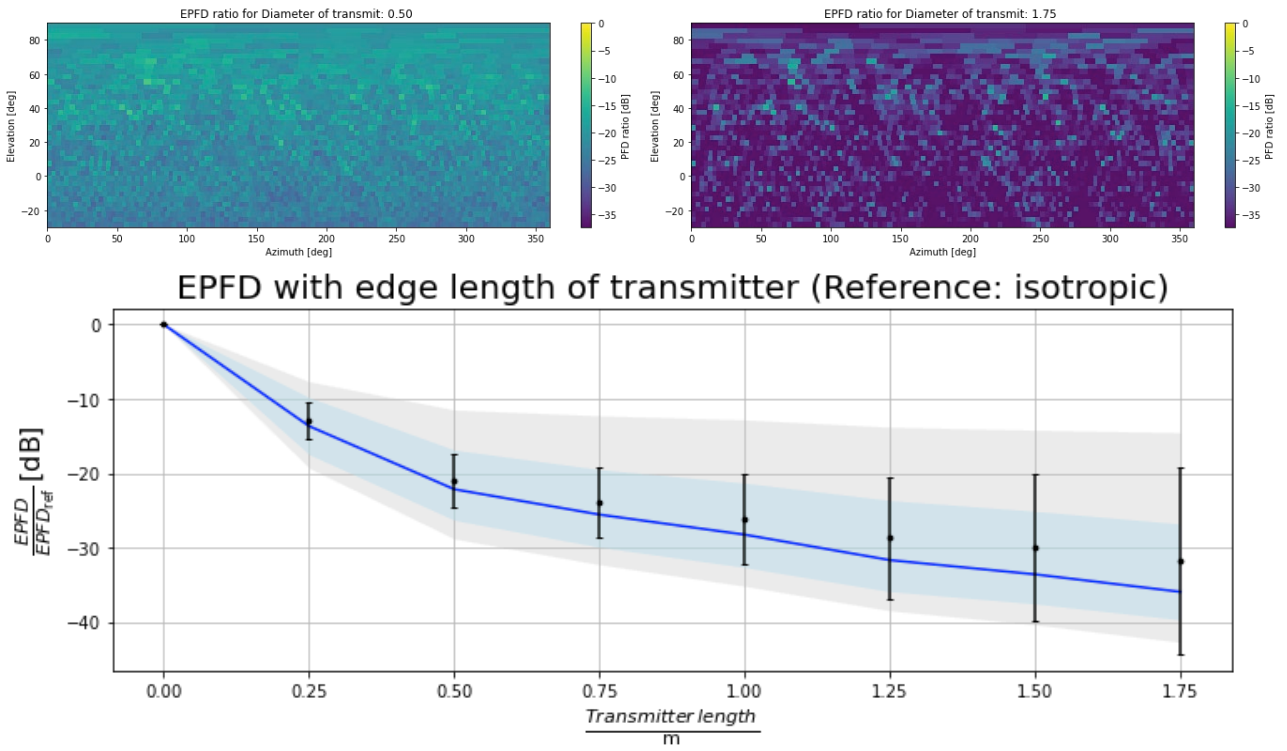

Figure 27: Ratio of epfd of a configuration changing in array size, and a reference (isotropic), inertial equatorial reference frame

In Figure 27, the top panels show the results per cell for two transmitter sizes, the bottom panel shows the epfd ratios averaged over cells. Black dots and error bars show the average and standard deviation with the blue line indicating the median (50% percentile). The blue shaded area comprises the area between the 5% percentile and the 95% percentile, the grey shaded area is the area between minimum and maximum in the plot.

6.4 TRANSMISSION PARAMETERS AND DUTY CYCLES

The duty cycle of the non-GSO satellite system is a parameter that has an impact on the level of interference received over time by an RAS station. However, it would certainly add a certain level of complexity in the computation since the different times of propagation between the different satellites and the victim RAS station would need to be appropriately considered.

6.5 SIZE AND SENSITIVITY OF RAS ANTENNA

6.5.1 Impact of RAS antenna size on epfd levels

As a final set of parameters was changed the size of the RAS antennas. With increasing antenna aperture not only the sensitivity increases but the antenna pattern becomes narrower, too. The consequence of this is visible in Figure 28 and Figure 29. With increasing telescope diameter the scatter of the cell values varies as a consequence of the much narrower beam. The epfd becomes much more stochastic. In addition, the average epfd increases slightly with telescope diameter, but while this is a clear trend the gradient is rather low. The epfd ratio between an antenna with a diameter of 300 m and an antenna of 25 m is lower than 1.25.

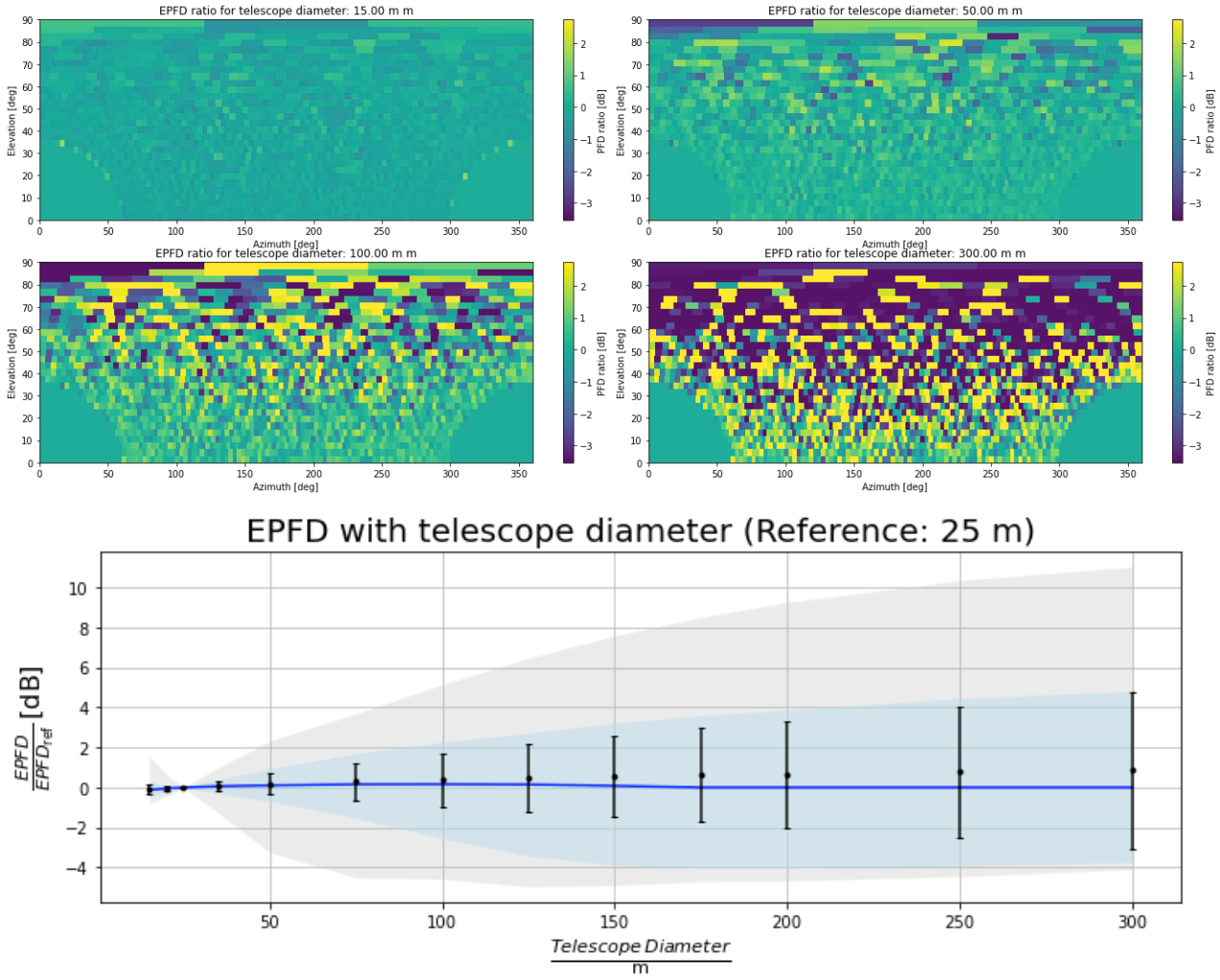

Figure 28: Ratio of epfd of a configuration changing in telescope diameter and a reference configuration (telescope diameter 25 m), topocentric rest frame

In Figure 28, the top and middle panels show the results per cell. The bottom panel shows the statistics of the epfd ratios taking into account all cells. Black dots and error bars show the average and standard deviation. The blue shaded area comprises the area between the 5% percentile and the 95% percentile with the blue line indicating the median (50% percentile), the grey shaded area is the area between minimum and maximum in the plot.

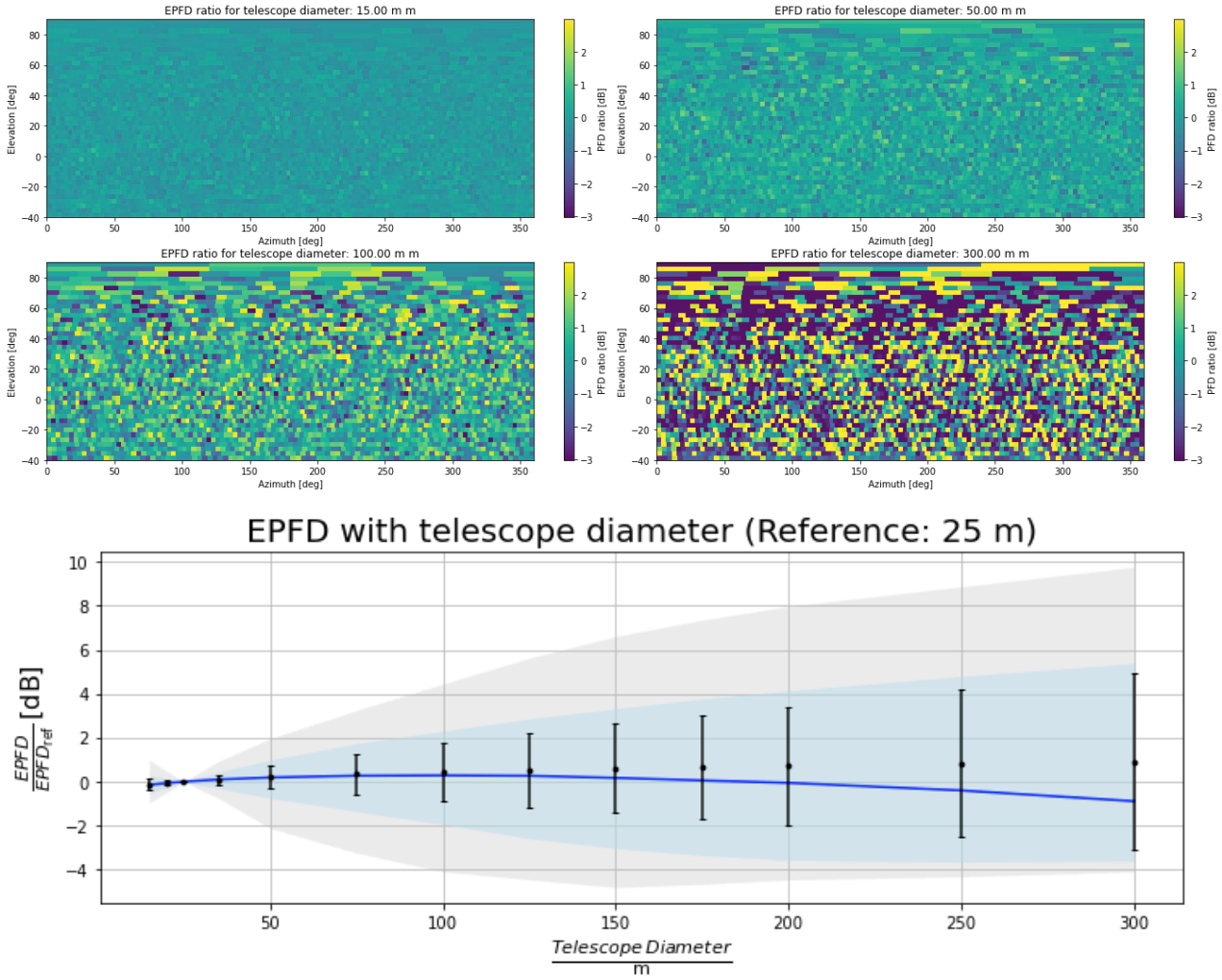

Figure 29: Ratio of epfd of a configuration changing in telescope diameter and a reference configuration (telescope diameter 25 m), equatorial inertial rest frame

In Figure 29, the top and middle panels show the epfd ratios per cell. The bottom panel shows the statistics of epfd ratios taking into account all cells. Black dots and error bars show the average and standard deviation. The blue shaded area comprises the area between the 5% percentile and the 95% percentile with the blue line indicating the median (50% percentile), the grey shaded area is the area between minimum and maximum in the plot.

6.5.2 Impact of RAS antenna size on the exceedance of the protection criteria

Another objective is to analyse the variation of the results not in term of variation of epfd ratio as done in section 6.5.1, but to assess the impact of changes of antenna diameter of the radio telescope in term of exceedance of the protection criteria.

The following antenna patterns in Figure 30 and Figure 31 have been obtained using ITU-R RA.1631-0 [2] with antenna diameters of respectively 7.5, 10, 15, 20, 25 and 30 m at 1.4135 GHz

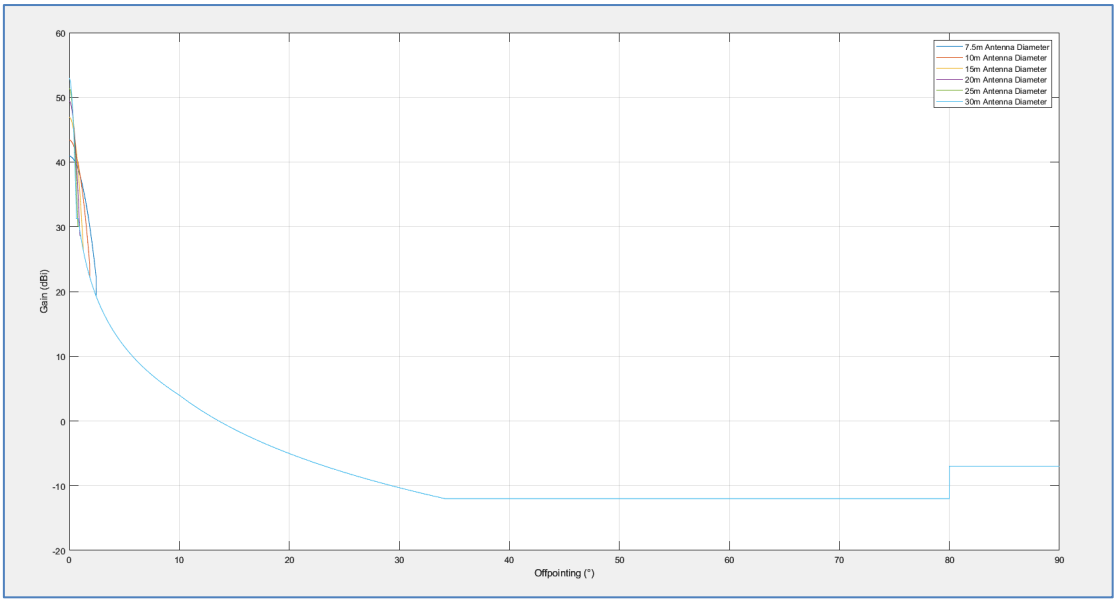

Figure 30: RAS antenna patterns for different antenna diameters

When focusing on the area close to boresight, the plot in Figure 31 is obtained.

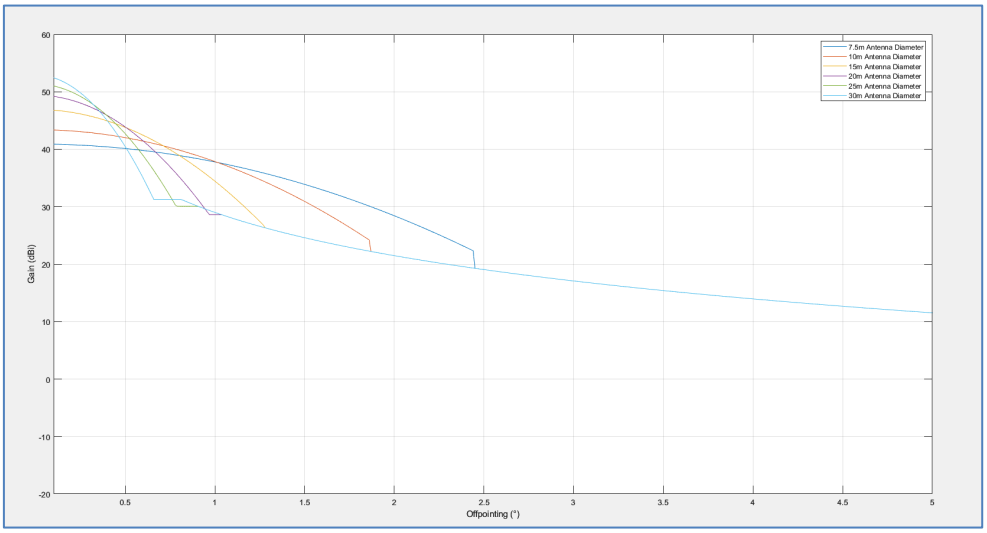

Figure 31: RAS antenna patterns for different antenna diameters - focus on small off-pointing angles

The differences in term of antenna gain are only seen for off-axis angles below 2.5°, and above 1° of off-pointing angle gains for all antenna diameters are below 38 dBi.

An analysis was conducted to observe the epfd results for a RAS antenna diameter of respectively 7.5, 10, 15, 20, 25 and 30 m, and the following non-GSO system:

- 22 orbital planes with ascending nodes evenly distributed;
- In each plane, 22 satellites equally spaced;
- Orbital inclination of 30°;
- Satellite altitude of 1000 km;
- Transmitted Power of -38 dBm;
- Isotropic antenna.

The results obtained are shown in Figure 32.

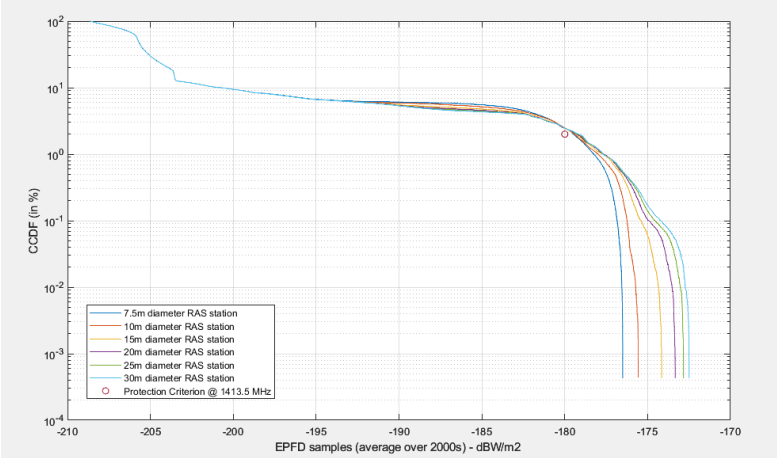

Figure 32: CCDF of interference into a RAS station for different antenna sizes at 1413.5 MHz

In Figure 32, it can be observed that the variation at 2%, depending on the antenna size, remains below 0.5 dBW/m^2. There is no significant difference in the results when various sizes of RAS antenna stations are considered. This is due to the fact that since the considered interfering non-GSO system is assumed to have an isotropic antenna pattern in the considered bandwidth, the only differences in the epfd statistics are due to the RAS antenna pattern variation.

It is shown above that differences in term of antenna gain patterns are only seen for off-axis angles below 2.5°: as a consequence, the antenna diameter of the radio telescope will have only an impact on epfd results for the non-GSO satellites relatively close to alignment.

It should be reminded that the considered non-GSO system has 484 satellite systems. With a higher density of satellites on orbital planes, and a higher number of orbital planes, the likeliness of alignments becomes higher, which in turn may increase the impact of the RAS antenna diameter.

6.5.3 Dependence on observing wavelength

Recommendation ITU-R RA.1631-0 [2] is the main reference antenna pattern used to perform the various analysis in this Report. While the antenna diameter D is undeniably a key parameter, it is important to clarify that the equations given in this Recommendation are all based on the quantity D/λ, λ being the wavelength at which the antenna gain is computed. In this study it is proposed to assess the impact of this quantity over a range of values that might be encountered in the real world.

All other studies in section 6.5.1 and 6.5.2 have been carried out for f = 1413.5 MHz, which leads, for a diameter D ranging from 10 m to 300 m, to a D/λ ranging from 47 to 1415. However, when considering for instance the case of a 100-m antenna at 10.65 GHz, this leads to a D/λ value of 3571, well above the range considered previously. It is therefore necessary to also study the impact of the antenna size on the exceedance of the protection criteria at higher frequency to best assess it.

The following parameters have been considered:

- A centre frequency of 10.65 GHz;
- 22 orbital planes with ascending nodes evenly distributed over 360 degrees;
- In each plane, 22 satellites equally spaced in anomaly;
- Orbital inclination of 55°;
- Satellite altitude of 500 km;
- Transmitted Power of -22 dBm;
- Isotropic Tx antenna;
- RA Rx antenna diameter from 20 m to 80 m every 10 m.

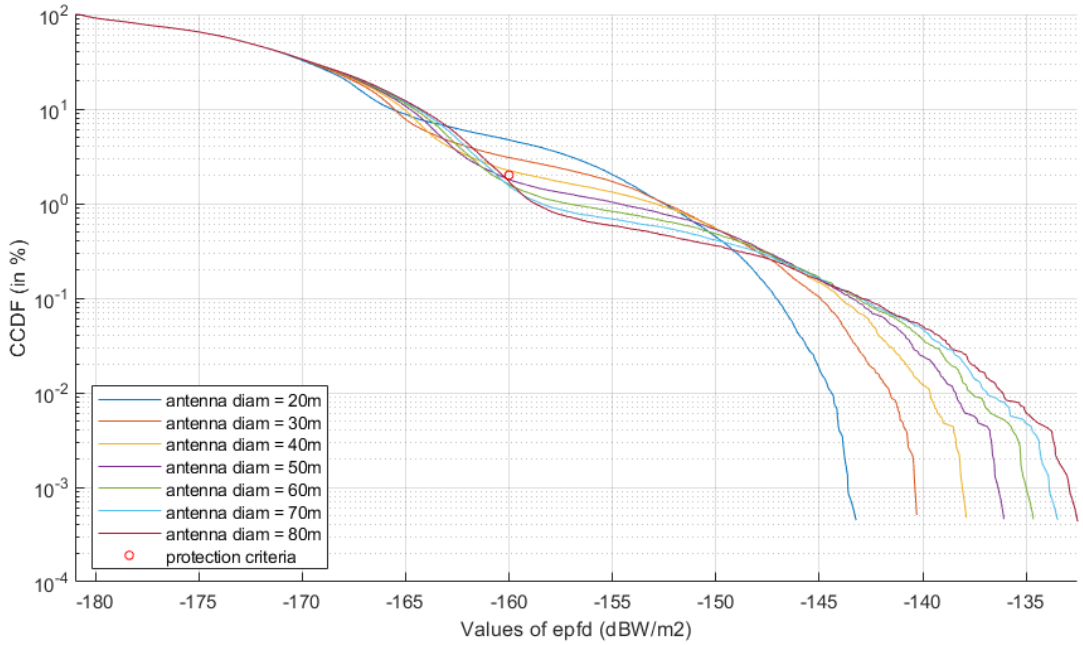

Figure 33: CCDF of interference into a RAS station for different antenna sizes at 10.65 GHz

Figure 33 shows that a variation of up to 6 dB can be observed depending on the antenna size, which appears to be a lot more important than what was previously observed through simulations performed at 1413.5 MHz, therefore demonstrating the importance of the antenna size as input parameter for such analysis.

These variations can be explained by the width of the RA antenna main beam which becomes narrower as D/λ increases while increasing the maximum gain, as can be seen in Figure 34.

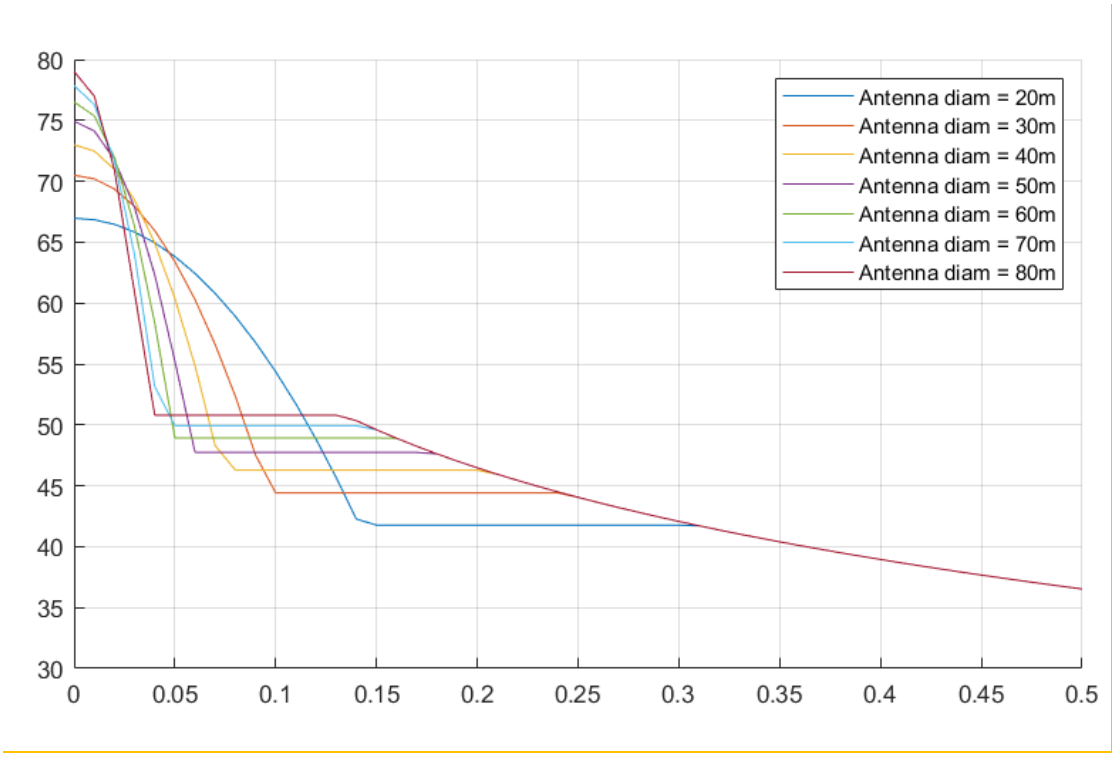

Figure 34: Main beam of the antenna radiation pattern for different antenna sizes as per Recommendation ITU-R RA.1631-0 [2]

6.6 SIMULATION STARTING TIMES AND IMPACT ON STATISTICAL PROPERTIES

The epfd calculations are usually repeated, i.e. several simulation runs/iterations are performed in order to control the statistical scatter of the Monte-Carlo type approach (compare section 5.1.1). There are many free parameters, which are randomly sampled (e.g. RAS antenna pointings within the grid cells, satellite beam pointings, orbit configuration/satellite positions). In particular for smaller constellations, the results can heavily depend on the state of the constellation. In practice, the simulation usually is performed for a given set of starting orbital parameters and then propagated with time to obtain different orbital states. It is noted that over the integration time of 2000 s (to comply with Recommendation RA.769-2 [4]) the satellite constellation is also propagated. This, however, is independent on the chosen starting time. If all simulation runs would start from the same start time, the final results would look very similar (ignoring the potential satellite beam forming). It is common to spread the start times of the simulations over a certain time span. While this obviously averages out some of the statistical scatter (in individual runs of smaller constellations one usually can see tracks of satellites in the sky maps), it is currently not well-established what time window for the starting times would be most appropriate. Often, a 24-hour window is used in studies involving the RAS as a victim service.

Before this is further discussed, it may be helpful to assess the potential impact on the results. Therefore, several epfd simulations were performed (using the default configuration introduced in section 5.1.3). This is a fairly large constellation with almost 500 satellites and a transmitter power of –50 dBm into the RAS band at 1410 MHz (isotropic). Start times were spread over 1, 24, and 720 hours (30 days). Furthermore, one simulation was performed with no change in starting times as a baseline. The RAS observer was placed at a geographical latitude of 50 degrees. As the effect of the chosen times could be different in horizontal and equatorial frames, results were determined for both frames. For an example, the results of the fixed-start time simulation in both frames are displayed in Figure 35. It shows the results for a baseline situation where all simulation runs were started at the same time (and thus with the same orbital configuration/satellite positions). The top panel shows the results in the topocentric frame, while the bottom panel shows the results in the equatorial frame.

As over the integration time of 2000 seconds, Earth does not perform a full rotation, the RAS station cannot access parts of the sky (which are below the horizon in the topocentric frame). This also has to do with the fact that Earth’s rotation axis is tilted with respect to the orbital plane of its motion around the Sun. Figure 36 has the results for starting times spread over 30 days and as a consequence the sky map is much smoother, especially in the equatorial frame where Earth’s rotation has a strong impact on the final distribution of the epfd values over the sky. It is noted that the overall data loss for the equatorial frame is also somewhat lower than for the topocentric frame, but this is mainly a consequence of the larger sky area over which the same power is then spread (the number of visible satellites at each instance of time is the same owing to the local horizon), as, owing to Earth’s rotation the signal is distributed more evenly across the cells. Notice that the effect can also result in a higher time loss in case of a stronger signal.

The resulting data losses for all these simulations are compiled in Table 7. While the sky maps appear very different, the data loss metric (for the whole sky) is rather stable. To test if this would also apply for constellations with much lower satellite numbers, a second setup was tested with only 20 satellites (5 satellites each in 4 orbital plans, Figure 37, Figure 38 and Table 8). To compensate for the lower number (and to have results in the regime around 2% data loss), the transmitter power was set to –30 dBm instead of –50 dBm used in the default constellation, so the data loss values from the first simulation cannot be directly compared to the second simulation owing to the different transmitter powers. This time, the data loss in the individual scenarios varies significantly, with the data loss being lowest when a start time window of 1 hour is used, while the 30-day scenario has much higher data loss – which is somewhat counterintuitive as it has the smoothed sky representation. While in the 1-hour case fewer cells are affected and the signal lies way above the threshold, the same power is distributed over a larger number of cells but still strong enough to cause a time loss.

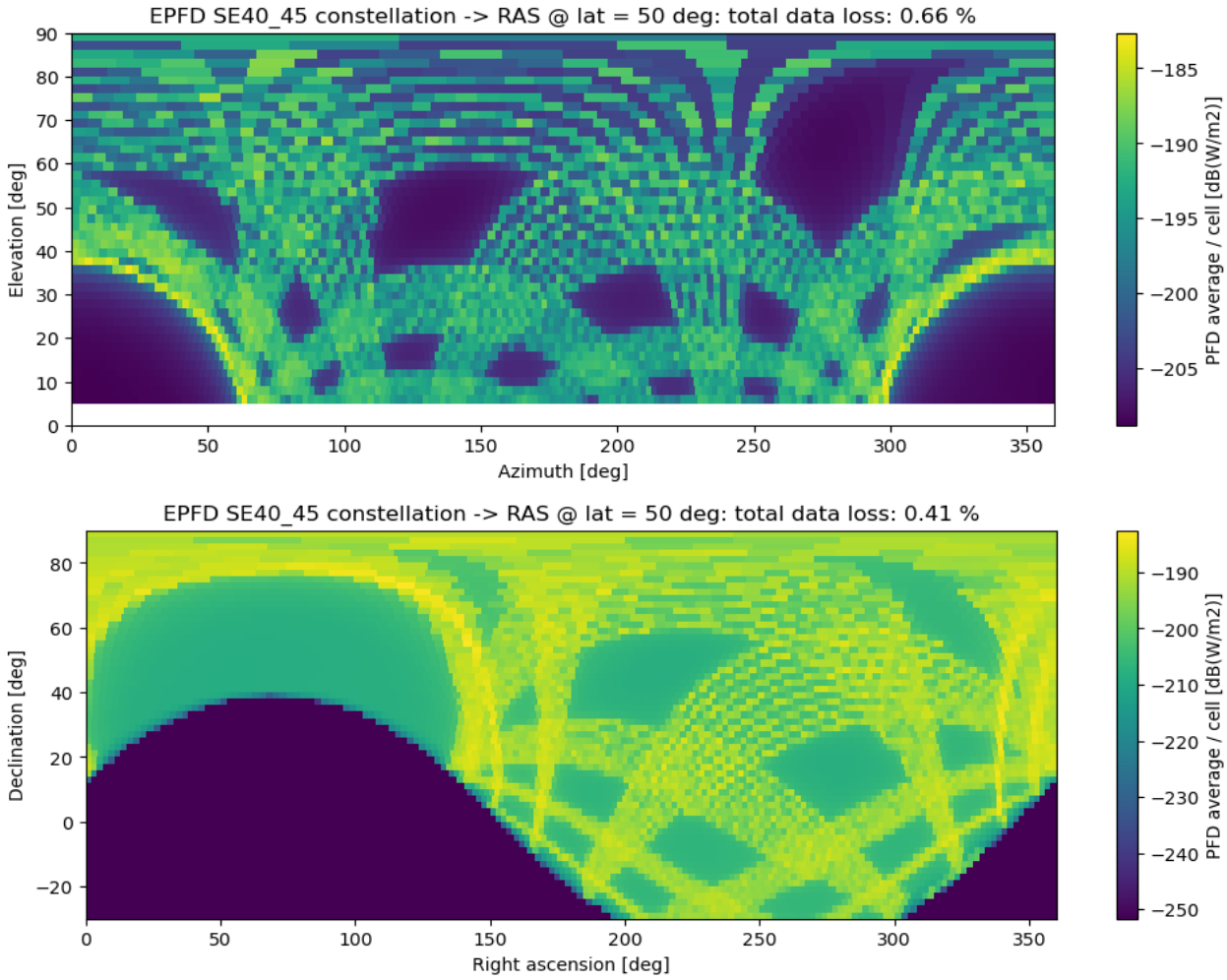

Figure 35: Effect of start times of the simulation runs

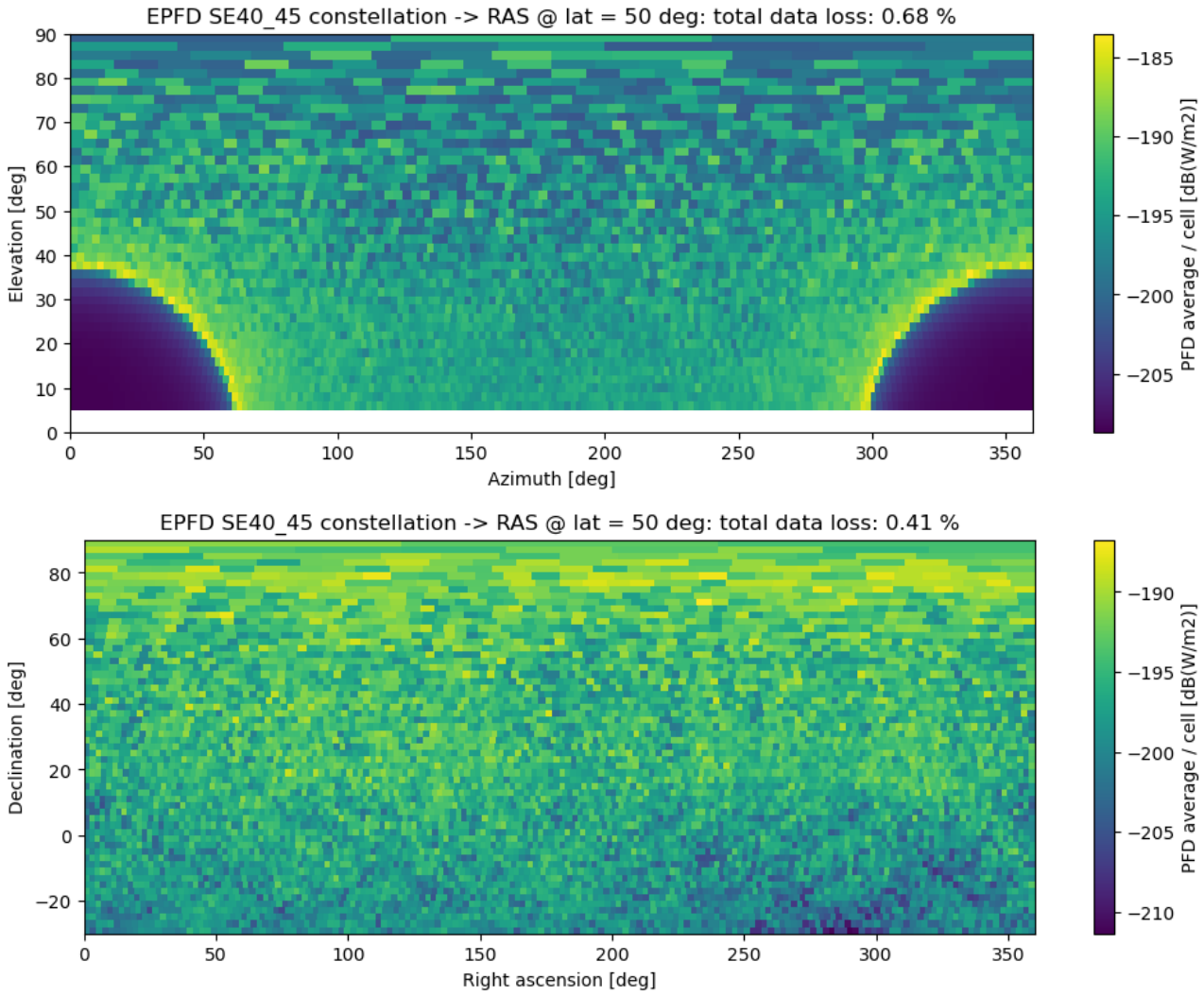

Figure 36: As Figure 35, but for a start time window of 30 days

Table 7: Influence of starting times on the data loss in topocentric and equatorial frames with a constellation with 484 satellites and Ptx = -50 dBm

Start time window	Data loss [%] (topocentric)	Data loss [%] (equatorial)
0 hours	$0.66^{+0.09}_{-0.10}$	$0.41^{+0.05}_{-0.06}$
1 hour	$0.66^{+0.09}_{-0.08}$	$0.41^{+0.08}_{-0.06}$
24 hours	$0.68^{+0.14}_{-0.13}$	$0.41^{+0.09}_{-0.07}$
30 days	$0.68^{+0.08}_{-0.07}$	$0.41^{+0.07}_{-0.07}$

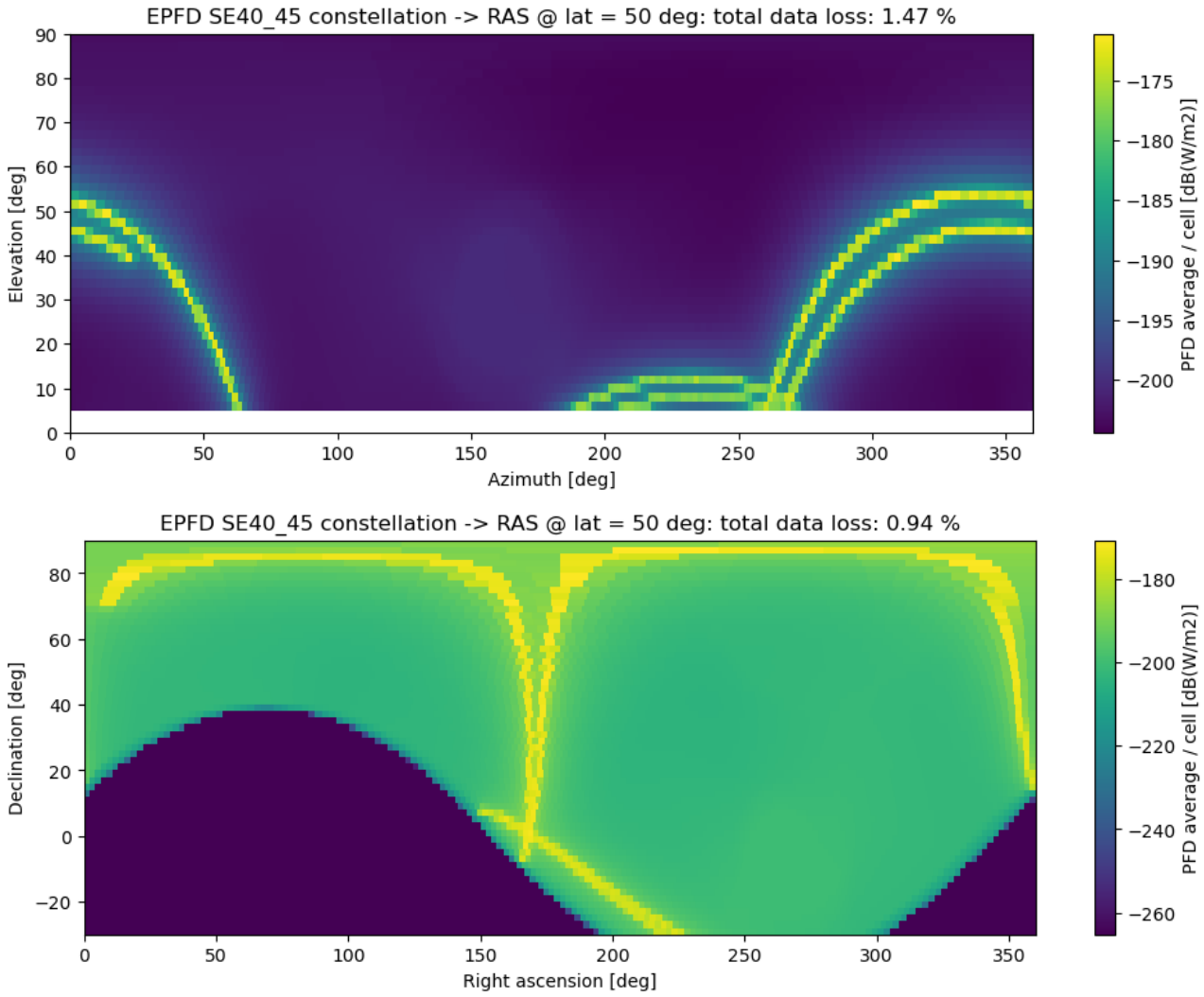

Figure 37: As Figure 35 but for a constellation with 20 satellites (4 orbital plans with 5 satellites each)

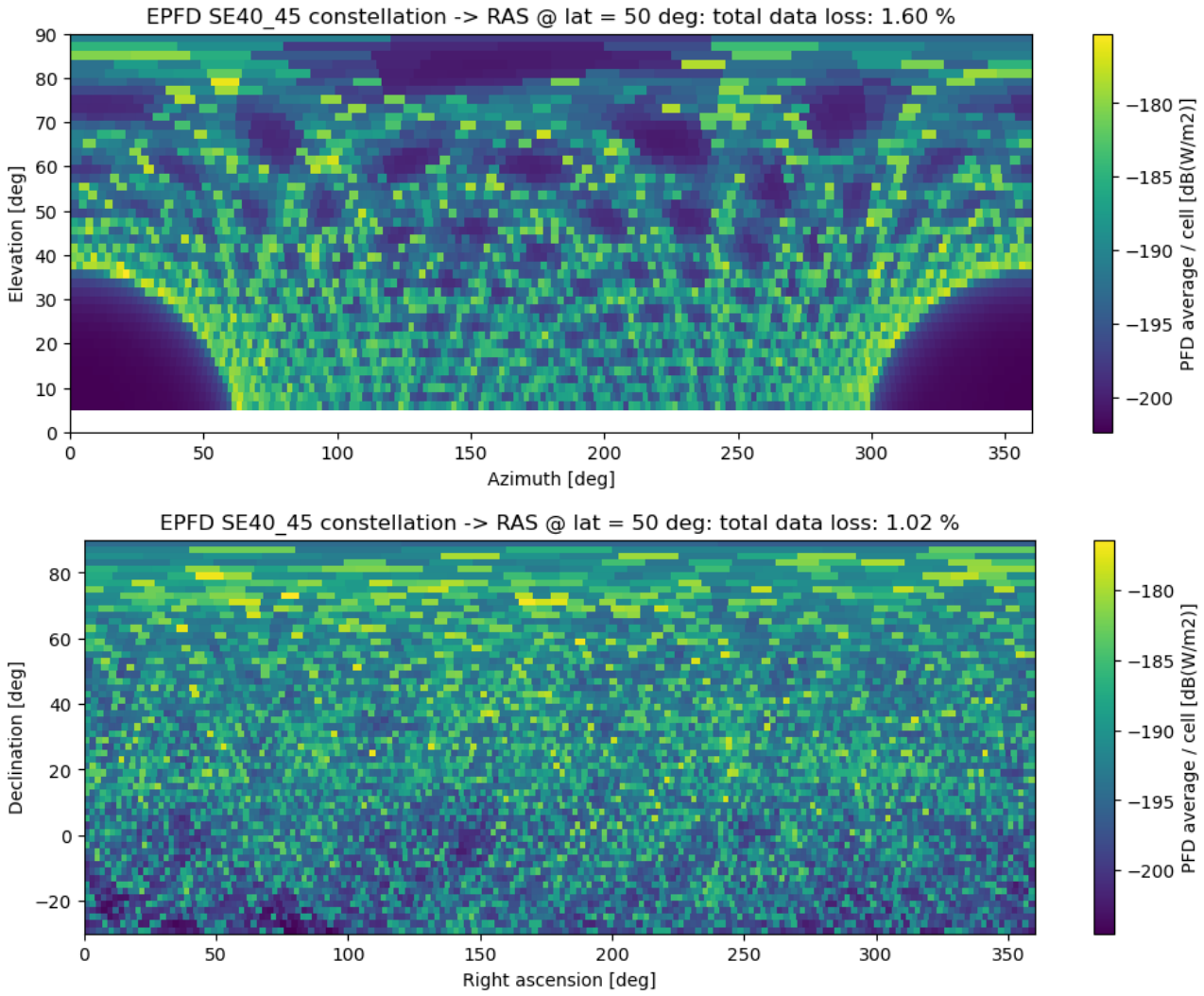

Figure 38: As Figure 37, but for a start time window of 30 days

Table 8: As Table 7 but for a constellation with 20 satellites (4 orbital plans with 5 satellites each) and Ptx = -30 dBm

Start time window	Data loss [%] (topocentric)	Data loss [%] (equatorial)
0 hours	$1.47^{+0.14}_{-0.14}$	$0.94^{+0.08}_{-0.08}$
1 hour	$1.18^{+0.29}_{-0.35}$	$0.82^{+0.20}_{-0.24}$
24 hours	$1.49^{+0.69}_{-0.58}$	$0.98^{+0.37}_{-0.32}$
30 days	$1.60^{+0.60}_{-0.55}$	$1.02^{+0.37}_{-0.32}$

6.7 INFLUENCE OF GEOSTATIONARY ARC AVOIDANCE ZONE

Non-GSO satellites constellation operators do not only need to consider the protection of RAS sites but also facilities of other spectrum stakeholders, including those of GSO satellite operators. For GSOs there are epfd requirements, too. On top of that there is a geostationary arc avoidance angle, which needs to be implemented by the non-GSO satellites (compare Recommendation ITU-R S.1325 [37]). For LEO satellites this usually means that any non-GSO Earth station cannot communicate with non-GSO satellites located between the position of that Earth station and the GSO arc (see Figure 39).

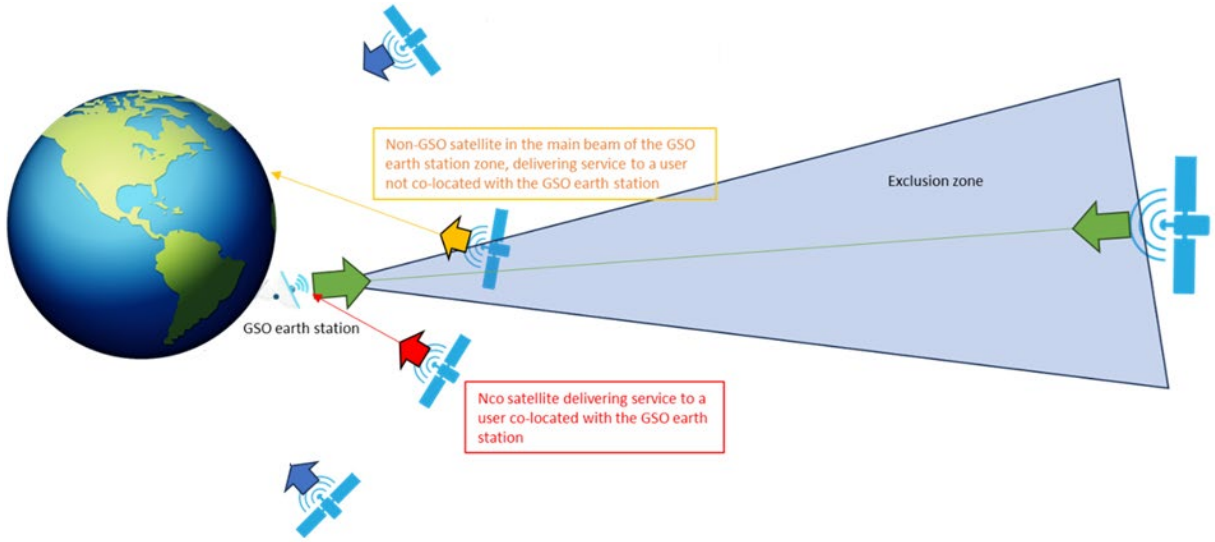

Figure 39: Illustration of GSO arc avoidance

For non-GSO satellites without active antenna systems (AAS), this can make it necessary to switch off transmissions for a given period of time. However, some modern systems utilize AAS, which allows the use of electronic beamforming. The pointing direction of the satellite and thus the served terminal on the ground could be steered in real-time. So, whenever a given terminal and satellite pair is subject to the geo-arc avoidance criterion, the satellite can simply steer its beam away to another terminal. From the radio astronomy perspective, the question is if this modified beam steering has a significant impact on the epfd levels received at a RAS station.

While there is a large space of parameters that will also have an impact on the answer to the above questions, in this Report at least a few prototypical scenarios are investigated. Based on the default satellite configuration (introduced in section 5.1.3), the geo-arc avoidance zone was implemented in the epfd calculations. As most real AAS non-GSO constellations also feature a maximum separation angle of the formed beams from the nadir direction, this constraint was also added to the simulation (maximum separation from nadir is set to 60º). While there are many types of AAS in operation, the choice was made to implement the antenna pattern model defined in Recommendation ITU-R M.2101-0 [34], as it offers a very convenient closed-form analytical model, with meta-parameters such as the number of antenna elements in both direction, beam widths of the single antenna elements, spacing between the elements and more, such that it can be tailored to a large variety of situations. However, it is assumed that other beam-forming models would show the same qualitative behaviour.

For the simulation, a 16×16 element AAS was assumed, with the parameters provided in Table 9. The ρ parameter controls how effective the beamforming is. For out-of-band and spurious domains, there will be some loss in the beamforming efficiency. Here, an in-band case with 100% beamforming efficiency is assumed. The HPBW of this model (assuming no tilt angles) is about 6.3 degree, which translates into a footprint of about 55 km for the satellites at 500 km altitude (if beam points to nadir). The *e.i.r.p.* (into maximum gain direction) was set to –15 dBm, thus the antenna pattern has been normalised to zero gain in forward direction. The *e.i.r.p.* power was chosen such that the results of the epfd simulations would lead to less than about 2% data loss in all scenarios, such that the relevant regime of the cumulative distribution (of the epfd values) was sampled.

Table 9: AAS parameters used for the beamforming (see Recommendation ITU-R M.2101-0)

Parameters	Values
$G_e^{\max}$	8 dBi
A_m, SLA_ν	30 dB, 30 dB

Parameters	Values
$\varphi_{3\mathrm{dB}}, \theta_{3\mathrm{dB}}$	65°, 65°
$d_{\mathrm{H}}, d_{\mathrm{V}}$	0.5 m, 0.5 m
$N_{\mathrm{H}}, N_{\mathrm{V}}$	16, 16
ρ	1.0

Regarding the sampling of the satellite beam pointings, there is not much known (in the public) for real systems. Here, the simplest approach is followed, which is to sample the pointings uniformly in the Azimuth/Elevation plane. However, for a system with only 484satellites, it seems unlikely that this would be able to cover the ground properly (the cells on the ground are relatively small). Therefore, the sampling scheme may need to be changed such that the density of beam positions increases towards larger separation. Studying this further is beyond the scope of this Report.

The simulations have been performed for two different RAS sites, one at a geographical latitude of 50° (in Figure 40) and one for a latitude of 0° (in Figure 41). The data losses and margins (average epfd with respect to the RAS threshold) are compiled in Table 10. In each of the two figures, the top panel contains the result for the simulation neglecting the geo-arc avoidance zone and the bottom panels show the results with the avoidance zone applied.

In the sky maps, the effect of the avoidance zone is visible as a somewhat darker area. However, the impact on the resulting metrics (data losses and margins) is relatively minor, with almost no significance on the data loss and much less than 1 dB on the margin. This shows that the effect is relatively minor and could in most cases be ignored for the sake to simplify the calculations (the impact on computing times is not large, but the code complexity is increased, which will require thorough testing in new implementations).

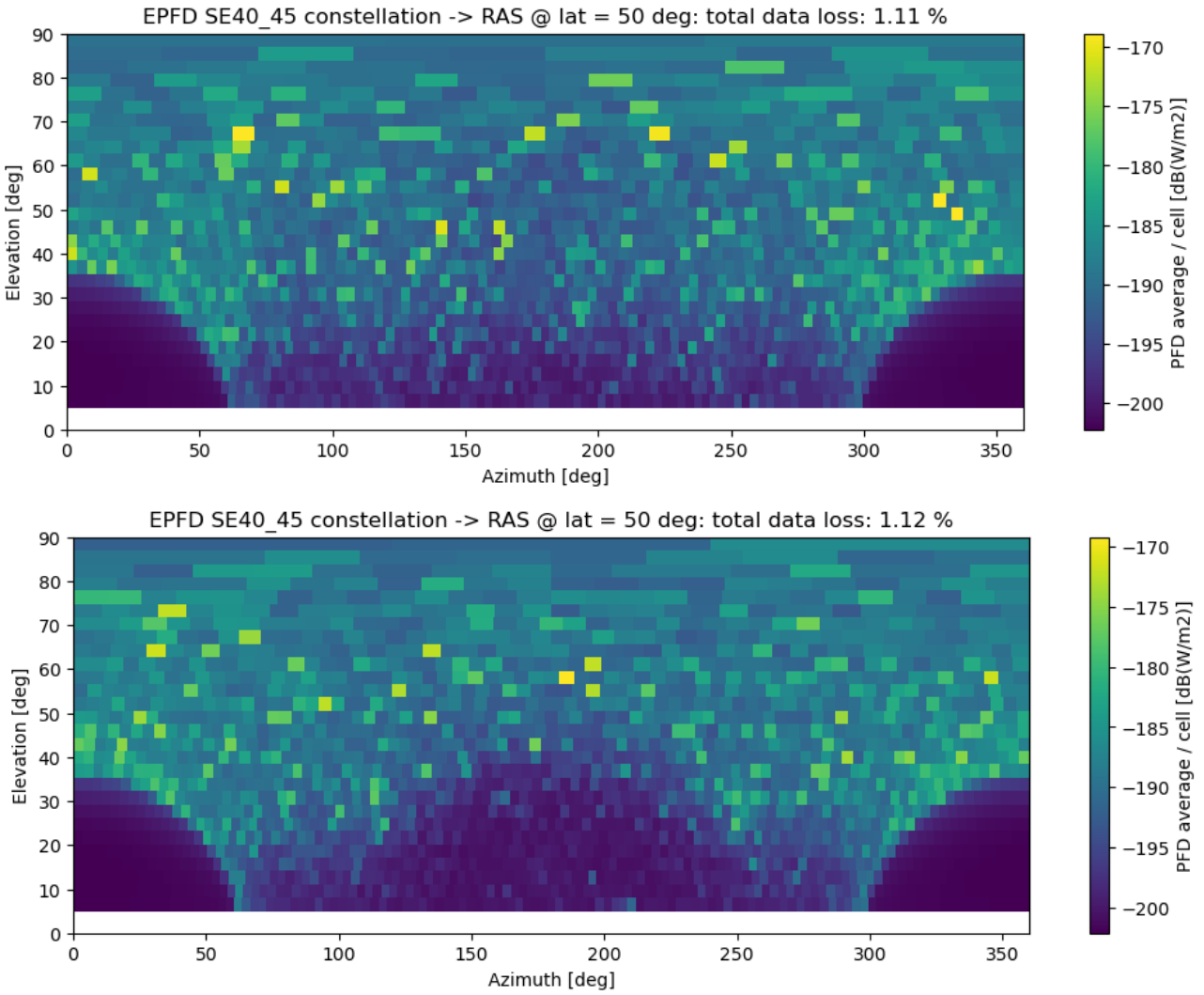

Figure 40: Results of an epfd simulation with (bottom panel) and without (top panel) geo-arc avoidance zone considered

Figure 40 shows that the satellite constellation consists of about 500 satellites in low-Earth orbit, which has beam-forming capabilities (see text for full set of parameters). The RAS site is situated at a geographical latitude of 50°.

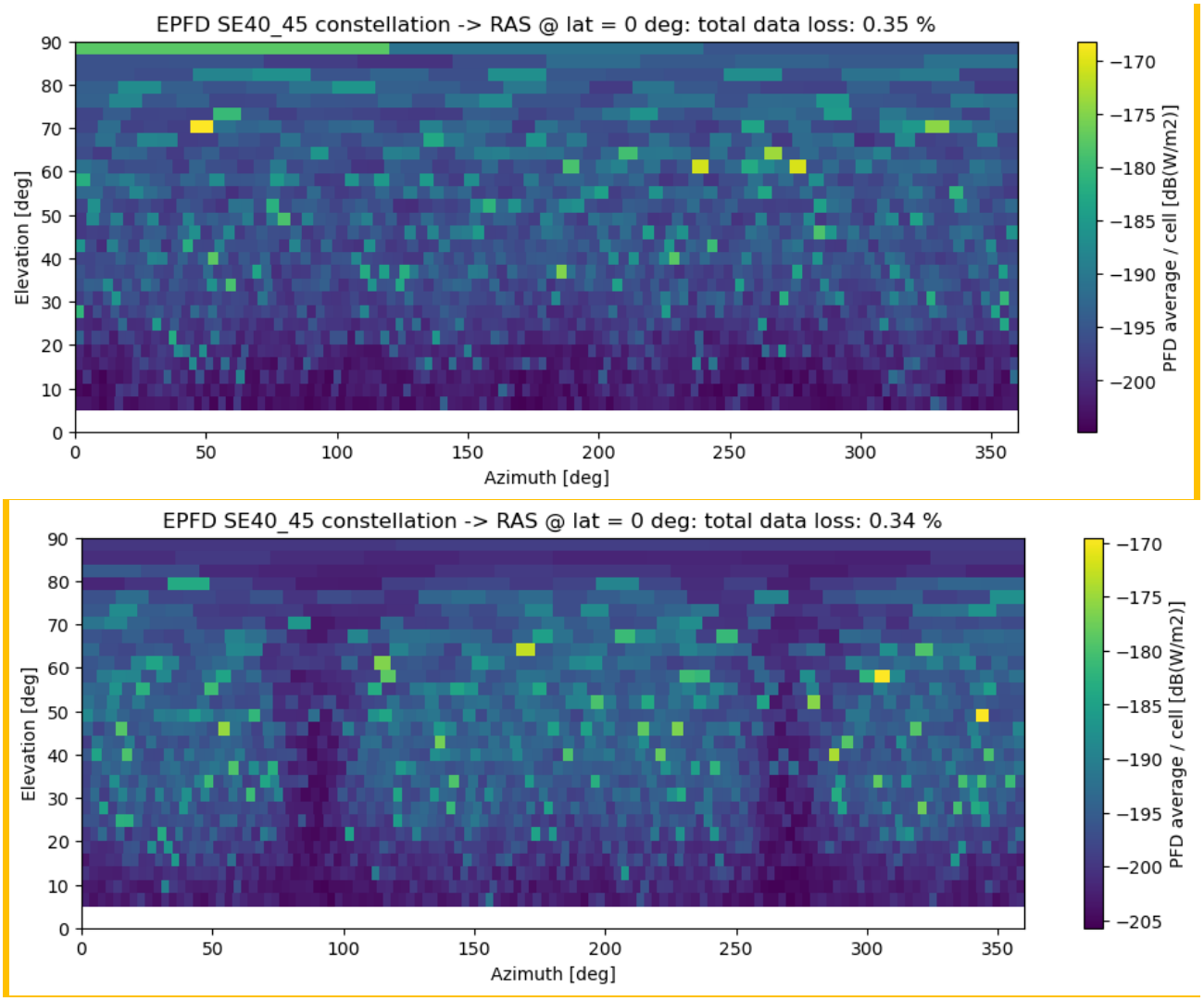

Figure 41: As Figure 40 but for a RAS site at a geographical latitude of 0°

Table 10: Data losses and margins for the simulations displayed in Figure 40 and Figure 41

Scenario	Observer latitude [deg]	Data loss [%]	Margin w.r.t. RAS [dB]
With geo-arc avoidance	0	$0.34^{+0.20}_{-0.19}$	$8.9^{+2.8}_{-1.7}$
Without geo-arc avoidance	0	$0.35^{+0.19}_{-0.17}$	$8.6^{+2.6}_{-1.6}$
With geo-arc avoidance	50	$1.12^{+0.24}_{-0.25}$	$2.9^{+0.8}_{-0.7}$
Without geo-arc avoidance	50	$1.11^{+0.25}_{-0.21}$	$2.8^{+0.9}_{-0.7}$

6.8 EFFECT OF SWITCHING OFF TRANSMISSIONS AROUND THE RADIO TELESCOPE BORESIGHT

A question that sometimes arises is, how much the radiation entering the RAS system via the radio telescope main beam contributes to the overall interference power (i.e. epfd values). This is relevant for several other topics, e.g.:

1 Is it necessary to run complex epfd simulations or would it suffice to study main-beam to main-beam coupling (and perhaps the likelihood of having a satellite crossing the RAS beam)?
2 How well would a mitigation technique work, where satellites cease transmission while flying through the pointing direction of the telescope and how large would such an avoidance area need to be?
3 Is the RAS antenna pattern given by Recommendation ITU-R RA.1631-0 [2] sufficiently precise – it obviously describes the main beam well enough, but how much depend the epfd results on the details in the near- and far-side lobes?

In the following, a first step towards answering these points shall be taken, by studying (by example) how much the epfd levels would change by blanking certain areas around the RAS boresight, i.e. by strictly turning off the transmissions of any satellite within a certain angle from the boresight of the RAS station. Again, the default satellite configuration (introduced in section 5.1.3) as well as a very small constellation (see section 6.6) is used for the simulations, both assuming isotropic transmitters (the satellite antenna patterns are assumed to play a minor role in the qualitative assessment of exclusion areas). In the former case, an *e.i.r.p.* of -30 dBm is utilised, in the latter case a value of –10 dBm is used. Both lead to a significant excess of the RAS thresholds. The simulations were then repeated but with the RAS antenna gain set to zero within certain angular separations around the telescope pointings, to see at what exclusion radius size the RAS thresholds would not be exceeded anymore. The separation angles were chosen as multiples of the half-power beam width (HPBW) of the RAS beam, which is about 0.15°, noting that the HPBW refers to a diameter, while the angular separations of the avoidance area are referring to a radius (around the boresight). As for the section 6.6, the results of the smaller and the default satellite configuration cannot be quantitatively compared since different e.i.r.p values have been considered for each.

To rule out that beamforming capabilities on the satellites would lead to completely different findings, a third scenario was simulated. This uses the default constellation but with the AAS antennas as described in section 6.7 (again with random beam pointings, but no geo arc avoidance was applied, and a maximum *e.i.r.p.* of -15 dBm). It has to be noted that absolute values of the data losses and margins between the default configuration with and without beamforming cannot be compared directly, only the relative effectiveness of the boresight avoidance.

In Table 11, the results of these simulations are compiled. It can be seen that the first step – excluding only the area with a diameter of twice the beam width, i.e. the main beam down to the first minima in the pattern – does not lead to a significant reduction in the data loss values. For the larger constellation, at least the margin is increased notably (by about 10 dB without beamforming, but only about 1.5 dB with beamforming), which has to do with the fact that the resulting cumulative distribution of the epfd values is very flat in this part of the curve (i.e. small changes in percentage are associated with large changes in the epfd values). How large the exclusion area needs to be, depends on the details of the satellite constellation but to reduce the margin by 20 dB, about 10 or more degrees of angular separation are required, in the cases studied here.

It is important to note that the results in Table 11 represent only an example for very specific constellation parameters. The findings will likely significantly change if parameters such as the number of satellites or the frequency will be different. Therefore, if the beam-avoidance mitigation technique is considered, calculations with the correct set of technical parameters and deployment numbers have to be performed.

Table 11: Results of epfd simulations for various exclusion areas around radio telescope boresight

Scenario	Avoidance radius around RAS boresight [°]	Data loss [%]	Margin w.r.t. RAS [dB]
Default constellation (484 satellites and Ptx = -30 dBm)	0	$46.12^{+0.82}_{-0.70}$	$-17.1^{+0.4}_{-0.3}$
	0.15	$45.87^{+0.53}_{-0.56}$	$-8.2^{+0.2}_{-0.2}$
	1.5	$7.19^{+0.50}_{-0.42}$	$-1.2^{+0.1}_{-0.0}$
	3	$0.00^{+0.00}_{-0.00}$	$1.5^{+0.0}_{-0.0}$

Scenario	Avoidance radius around RAS boresight [°]	Data loss [%]	Margin w.r.t. RAS [dB]
	6	$0.00^{+0.00}_{-0.00}$	$4.2^{+0.0}_{-0.1}$
	15	$0.00^{+0.00}_{-0.00}$	$7.2^{+0.1}_{-0.1}$
	30	$0.00^{+0.00}_{-0.00}$	$7.8^{+0.0}_{-0.0}$
	45	$0.00^{+0.00}_{-0.00}$	$8.0^{+0.0}_{-0.0}$
Small constellation (20 satellites and Ptx = -10 dBm)	0	$36.60^{+21.91}_{-17.99}$	$-18.6^{+2.5}_{-1.8}$
	0.15	$37.65^{+21.39}_{-19.72}$	$-18.4^{+3.0}_{-1.4}$
	1.5	$37.27^{+21.00}_{-18.74}$	$-11.3^{+0.7}_{-0.3}$
	3	$36.78^{+22.01}_{-18.61}$	$-8.0^{+0.9}_{-0.4}$
	6	$36.53^{+26.46}_{-18.44}$	$-4.6^{+1.4}_{-0.6}$
	15	$7.30^{+10.75}_{-7.30}$	$-0.5^{+2.2}_{-0.3}$
	30	$4.03^{+3.09}_{-4.03}$	$-0.4^{+2.4}_{-0.3}$
	45	$3.55^{+3.16}_{-3.55}$	$-0.3^{+2.0}_{-0.4}$
Default constellation with beamforming (484 satellites and max. *e.i.r.p.* = -15 dBm)	0	$69.40^{+5.29}_{-5.46}$	$-17.2^{+0.7}_{-0.8}$
	0.15	$68.79^{+5.54}_{-3.94}$	$-15.7^{+0.9}_{-0.7}$
	1.5	$63.15^{+4.72}_{-5.98}$	$-10.4^{+0.7}_{-0.6}$
	3	$55.82^{+5.56}_{-5.63}$	$-7.3^{+0.7}_{-0.6}$
	6	$42.23^{+7.84}_{-8.21}$	$-3.9^{+0.7}_{-0.7}$
	15	$0.18^{+0.10}_{-0.18}$	$0.5^{+0.9}_{-0.0}$
	30	$0.00^{+0.00}_{-0.00}$	$0.8^{+1.1}_{-0.1}$
	45	$0.05^{+0.05}_{-0.05}$	$1.0^{+0.9}_{-0.1}$

7 PRACTICAL SOURCES OF INFORMATION FOR EPFD CALCULATIONS

There is a question on where the information required to perform the epfd computation can be found. A part of that information is publicly available (during the submission process to ITU of non-GSO satellite system, the information that should be provided by the notifying administration of that non-GSO satellite system is described in Appendix 4 of the Radio Regulations). Another part is not and should preferably be provided by the non-GSO operators to ensure a maximum accuracy on the results. This section also explores some potential alternatives in case some information is missing.

7.1 NON-GSO INFORMATION AVAILABLE IN APPENDIX 4 DATA

When performing epfd computation for non-GSO constellations, detailed information about the non-GSO satellite system is needed, including operational parameters. Some of this information and parameters can be found in the data provided to ITU-R by the notifying administration of the non-GSO system (as specified in The ITU Radio Regulations, Appendix 4), and their ID is provided in Table 12.

Table 12: Sources of non-GSO operational parameters in ITU filings

Non-GSO operational parameter description	Details	Filing parameter ?	Parameter name in Appendix 4 data	Parameter units	Parameter id in filing information provided by notifying administration
PFD mask	Indicates, by latitude, the maximum power flux density that can be transmitted by a non-GSO satellite in the space-to-Earth direction	Not directly in Filing database, attached separately		dBW/m2/Ref_bw	
Non-GSO Tx Antenna Pattern		Not mandatory (overtaken by pfd mask in bands where Art. 22 applies)		no unit for pattern dBi for maximum gain	-B3c1 antenna radiation pattern ID -B3a1 maximum gain
Maximum number of non-GSO satellites operating co-frequency at latitude [lat]	Indicates the maximum quantity of satellites that can transmit signal over a given area on earth's surface	Yes	Nco [latitude]	Alphanumeric value	A.4.b.6.a.1
Minimum elevation angle	Specifies the minimum elevation angle under which an earth station cannot connect	Yes	ES_MINELEV	Degree	A.4.b.7.cbis

Non-GSO operational parameter description	Details	Filing parameter ?	Parameter name in Appendix 4 data	Parameter units	Parameter id in filing information provided by notifying administration
	to a given non-GSO satellite.				
GSO exclusion zone	Area on earth in which the non-GSO satellites cannot transmit to protect GSO service	Deduced from the pfd mask(s)	Alpha or X	Degree	
Frequency re-use scheme	Specifies the division of the frequency plan accessible to the non-GSO system (ex: 4-color scheme means that the bandwidth is shared in 4 portions)	No			
Tracking strategy	Indicates the conditions that a user earth station will follow to connect to the non-GSO satellites	No			
Duty Cycle / Activity factor	Specifies the portion of time during which the non-GSO satellites and the associated are transmitting	No			

7.1.1 Antenna Pattern

The antenna pattern can be part of Appendix 4, but it is not a mandatory information. Only the maximum gain (in-band) has to be provided. Antennas are generally optimised to be as directive as possible within the bands they are expected to transmit in, but this optimisation, which is done during the antenna subsystem overall design and production, has an impact on both the directivity and the polarisation in adjacent bands. It is therefore not possible to deduce from the already available data contained in Appendix 4 the radiation pattern in the RAS bands.

In consequence, the radiation pattern of the non-GSO systems in the RAS bands would need to be provided by the non-GSO system operator or its notifying administration.

It is worth to note that, when considering the case of emissions in RAS bands not directly adjacent to the transmitting bandwidths of the non-GSO systems in the space-to-Earth direction, a simple approach can be to

consider that in those bandwidths the non-GSO emissions follow an isotropic antenna pattern. But in this case also, the associated *e.i.r.p.* would need to be provided by the non-GSO system operator or its notifying administration.

7.1.2 Transmitted Power

The in-band transmitted power of a satellite is also provided in Appendix 4. However, there is no information given about the power transmitted outside of the bands filed by the satellite system. Recommendation ITU-R SM.1541-6 [35] aims at providing an envelope of those out-of-band (OOB) emissions but gives conservative results compared to actual systems OOB emission levels. This conservative aspect of Recommendation ITU-R SM.1541-6 [35] can be illustrated with the case of OneWeb.

Considering the appropriate parameters for Recommendation ITU-R SM.1541-6 (120 MHz of assigned band, spurious limit is equivalent to 40 dBsd) [35], the OOB emission mask shown in Figure 42 is obtained.

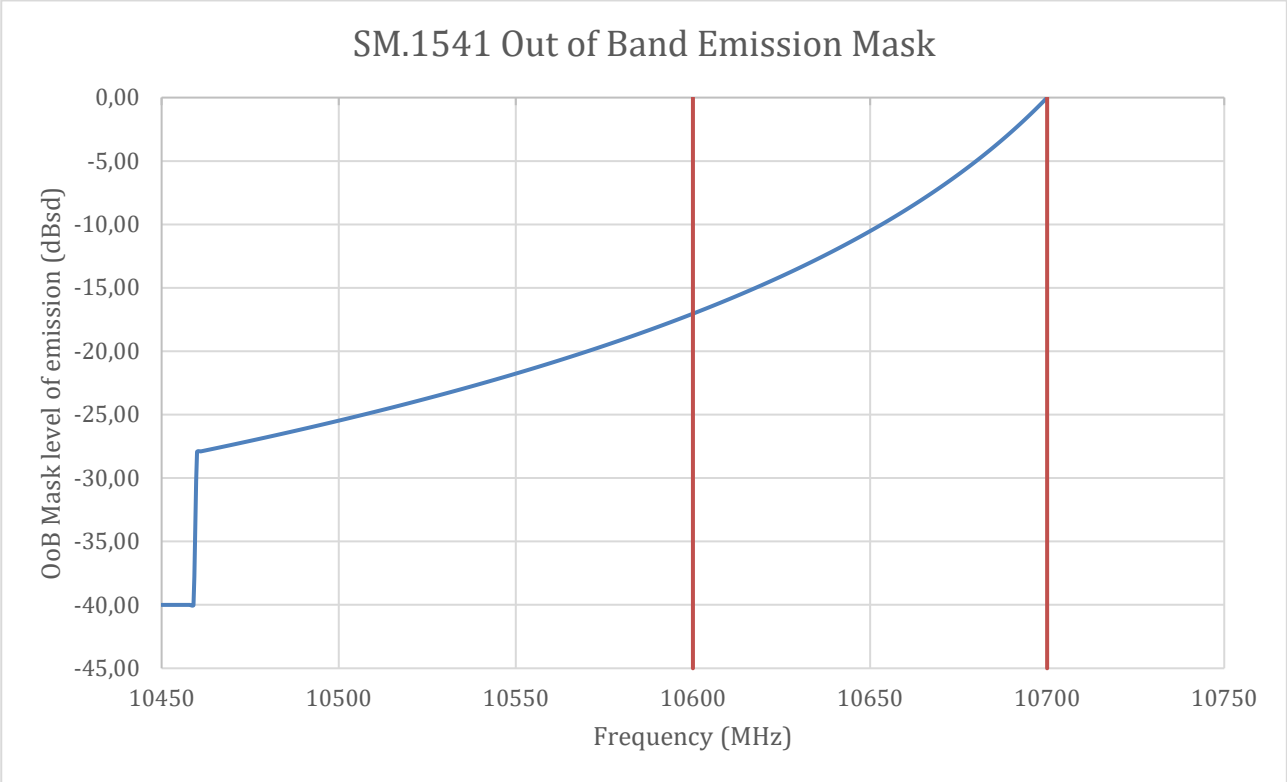

Figure 42: Out-of-band emission mask following Recommendation ITU-R SM.1541-6 [35]

The average attenuation in the 10.6-10.7 GHz bandwidth is of 7.1 dB.

Now, with the information publicly available in the OneWeb L5 satellite filing in Ku-band (beams TAR2 and TAR3), a maximum transmitted power spectral density of -72.3 dBW/Hz and a maximum gain of 25.9 dBi are indicated.

A bandwidth of 100 MHz (corresponding to the width of the adjacent RAS primary allocation), and an OOB attenuation of 7.1 dB as per Recommendation ITU-R SM.1541-6 [35] would correspond to an *e.i.r.p.* density of –72.3+10*log10(100 MHz) –7.1 + G= 0.6 + G dBW/100 MHz, where G is the average antenna gain in the 10.6-10.7 GHz band.

In ECC Report 271 [29], it was stated that the maximum e.i.r.p radiated within the RAS band and coming from the nearest channel would be of –5 dBW/100 MHz (still unacceptable for RAS).

It would mean that the average gain of the antenna in the 10.6–10.7 GHz would be –5.6 dBi. It would mean that the difference in term of gain is of more than 30 dB with the gain in the immediately adjacent channel (25.9 dBi, as indicated above), which is not realistic.

The conclusion is that the attenuation given by Recommendation ITU-R SM.1541-6 [35] is conservative. In the absence of OOB characteristics provided by the non-GSO system operator or its notifying administration, Recommendation ITU-R SM.1541-6 [35] can be used in a first approach, but to reach definitive conclusions, the exact characteristics should be used.

7.1.3 Number of satellites to consider and pointing strategy

In general, all the satellites above the horizon at the geographical position of a RAS station, transmitting in a frequency band adjacent or nearby to a RAS band, may contribute to the aggregate level of interference, as, due to the sensitivity of RAS receiving systems, their gains are non-negligible in any direction. The satellites below the minimum elevation angle of the RAS station may also contribute to the aggregate level of interference.

This is especially true if the non-GSO satellite emissions are assumed to follow an isotropic antenna pattern: in that case it can be considered that any satellite in visibility of the RAS station contributes unwanted received power at the RAS station if that satellite is active and transmitting.

If the antenna pattern is non-uniform, the pointing strategy, i.e. the procedure that determines the pointing direction of any satellite of the constellation at any given time, becomes highly relevant for the calculation of the epfd levels.

It is particularly important to know, at each moment, which satellites out of the entire constellation is transmitting in the area in which the RAS station resides, since they can be any of the non-GSO satellites which are simultaneously in visibility of the radio astronomy site and outside of the GSO avoidance arc. The quantity of satellites transmitting towards a given area on Earth's surface at the same time is determined by the "Nco" parameter (parameter A.4.b.7.a of the Radio Regulations, Appendix 4).

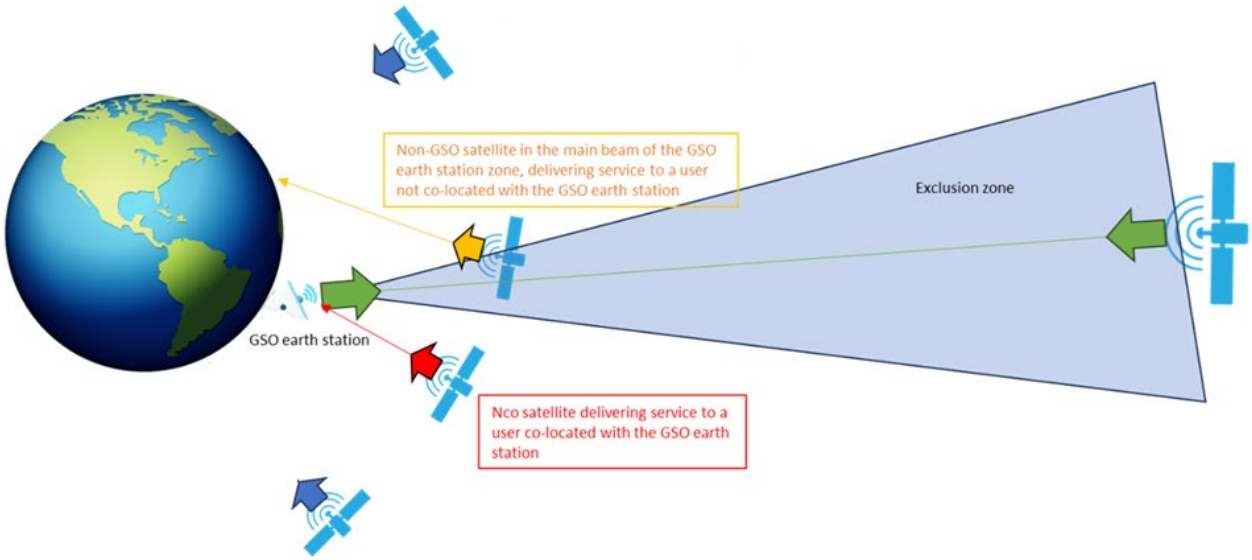

Figure 43: Illustration of Nco Parameter

7.1.4 Non-Nco satellites

It is also important to know the pointing direction of the remaining "non-Nco" satellites which are also in visibility of the radio astronomy site (as illustrated in Figure 43). It is relevant since they still emit a small, but significant amount of power in the direction of the RAS station, through their side and back lobes. The complete pointing strategy would therefore be, in principle, a requirement for the accurate computation of the average data loss of the RAS due to interference from satellite constellations, but, apart from the Nco parameter, no information with respect to the pointing strategy is provided by the notifying administration of the non-GSO system.

7.2 POTENTIAL ALTERNATIVES TO MISSING PARAMETERS

The accuracy of epfd and data loss calculations to determine the single entry or aggregate interference level of non-GSO systems on RAS depends on the available information on the parameters discussed in section 5.1.2. Not in all cases all the required information is available, in which case an alternative might be used. In section 5.1.2. existing recommendations for those parameters or their absence have been identified.

Table 13 summarises potential fallback options and corresponding recommendations and indicates if recommendations are missing. Note that when parameters have been provided directly by operators they should be used.

Table 13: Potential alternatives to missing parameters

Parameter description	Parameter	Recommendation	Potential fallback option
Telescope geographical position	Telescope geographical longitude	Not available	No fallback option. If telescope is not specified, choose a representative sample of filed radio telescopes and use values thereof
	Telescope geographical latitude	Not available	No fallback option. If telescope is not specified, choose a representative sample of filed radio telescopes and use values thereof
Telescope altitude		Not available	No fallback option. If telescope is not specified, choose a representative sample of filed radio telescopes and use values thereof
RAS station antenna pattern		Recommendation ITU-R RA.1631-0 [2]	Use Recommendation ITU-R RA.1631-0 [2] if the antenna diameter is known. If telescope is not specified, choose a representative sample of filed radio telescopes and use values thereof
RAS station minimum elevation		Indicated in ITU-R Resolution 739 (Rev. WRC-19)	If telescope is not specified, choose elevation limits for a representative sample of filed radio telescopes or 5° as indicated in ITU-R Resolution 739 (Rev. WRC-19)
Satellite constellation orbital parameters	Semi-major axis a	Not available	No fallback option. If systems are not described, choose a representative sample of filed satellite systems
	Eccentricity e	Not available	
	Inclination i	Not available	
	Longitude/right ascension of the ascending node Ω	Not available	
	Argument of perigee (ω)	Not available	
	True anomaly (v)	Not available	
Transmitted power		Recommendation ITU-R SM.1541-6 [35]	Use Recommendation ITU-R SM.1541-6 [35] for OOB transmission

Parameter description	Parameter	Recommendation	Potential fallback option
Satellite antenna pattern		Not available	Use Recommendation ITU-R S.1528 [38] below 30 GHz for in-band[4]
Satellite pointing strategy		Not available	If this cannot be deduced or a model is missing, different options are possible (e.g. nadir pointing, random pointing). For the Nco parameter in the epfd computation and the selection of the satellite(s) transmitting in the direction of the RAS site different options are possible (e.g. highest elevation, random).
Transmitted power duty cycle or activity factor		Not available	It may be assumed that the satellites of the non-GSO constellation are continuously transmitting, meaning that the activity factor is 100%
Frequency re-use scheme		Not available	As a worst-case assumption it can be assumed that all satellites of the non-GSO constellation are transmitting signal in the portion of bandwidth directly adjacent to the RAS service

[4] If no other information is available an omnidirectional pattern could be assumed for out of band emissions for some systems, but this would be worst-case.

8 CONCLUSIONS

The main goal of this report is to study the aggregation of received power from multiple satellite constellations into radio astronomy receiving systems. For this, the equivalent power flux density (epfd) method has been applied, which is described in detail in section 5.1. The threshold levels of interference detrimental to different types of radio astronomy observations (continuum observations, spectral line and VLBI observations) are provided in Recommendation ITU-R RA.769-2 [4]. The protection criterion, given in Recommendation ITU-R RA.1513-2 [5], is met when the data loss is less than 2% for an individual non-GSO satellite system, i.e. when less than 2% of the epfd samples over the entire sky, each averaged over 2000 s, exceed the threshold value given in Recommendation ITU-R RA.769-2, using the methodology given in Recommendation ITU-R M.1583-1 [7] and ITU-R S.1586-1. Recommendation ITU-R RA.1513-2 also specifies that a criterion of 5% is to be used for the aggregate data loss to the RAS due to interference from all networks. This Report also identifies the parameters of the radio astronomy station as well as the ones of the non-GSO satellite system(s) required in the analysis. Sensitivity analyses on some of those parameters are included as well.

To date, if technical parameters or deployment information (e.g. satellite antenna pointing directions) are not provided, no method is known to estimate the epfd and data loss at an RAS site caused by a single satellite system. Regarding aggregate data loss from multiple non-GSO satellite systems, it was found that it could not be directly inferred from the respective data losses corresponding to each of the individual non-GSO satellite system. The aggregate data loss needs to be calculated from the summation of epfd of all considered non-GSO satellite systems for each time sample.

This Report also includes examples, including data loss calculations, and investigates the dependency of the outcomes of the simulations on single parameters (section 6). Some key findings are as follows:

- the equatorial coordinate reference frame offers a potential alternative or complement to the usual calculations in the horizontal (topocentric) observer frame. Equatorial coordinates are more commonly used in astronomy to compensate for the Earth's rotation. Results in the equatorial and horizontal frames can differ, with the distribution of the power in the equatorial frame usually being smoother over the sky;
- boresight avoidance, which is the technique to switch off satellite transmissions when a satellite is moving through a RAS observing beam (assuming the beam pointing is known in real time) may help to mitigate interference and to reduce data loss but could require relatively large areas around the RAS beam to be kept free from transmission. Boresight avoidance would however always require close coordination between the operators of the non-GSO satellite system and all the RAS stations to be protected.
- the geo-arc avoidance concept, which is used to protect GSO from non-GSO systems, is estimated to have a limited impact on RAS epfd results and could be left out from calculations in order to simplify the studies.

The above findings are valid for the chosen example configurations and there may be certain sets of parameters and deployments for which different results could be obtained. Some of the required parameters are not publicly available, and the report lists examples of potential fall-back solutions that may be used when it is the case. Confidence in the results can only be achieved through the joint cooperation between radio astronomers and non-GSO system operators (and their respective notifying administrations), as they are the only ones in position to provide all the missing information on the operational characteristics of their respective systems.

ANNEX 1: LIST OF REFERENCES

[1] Recommendation ITU-R SA.509-3 (12/2013): "Space research earth station and radio astronomy reference antenna radiation pattern for use in interference calculations, including coordination procedures, for frequencies less than 30 GHz"

[2] Recommendation ITU-R RA.1631-0 (05/2003): “Reference radio astronomy antenna pattern to be used for compatibility analyses between non-GSO systems and radio astronomy service stations based on the epfd concept”

[3] Recommendation ITU-R S.1428-1 (02/2001): “Reference FSS earth-station radiation patterns for use in interference assessment involving non-GSO satellites in frequency bands between 10.7 GHz and 30 GHz”

[4] Recommendation ITU-R RA.769-2 (05/2003): “Protection criteria used for radio astronomical measurements”

[5] Recommendation ITU-R RA.1513-2 (03/2015): “Levels of data loss to radio astronomy observations and percentage-of-time criteria resulting from degradation by interference for frequency bands allocated to the radio astronomy service on a primary basis”

[6] Recommendation ITU-R RA.611-4 (03/2006): “Protection of the radio astronomy service from spurious emissions”

[7] Recommendation ITU-R M.1583-1 (10/2007): “Interference calculations between non-geostationary mobile-satellite service or radionavigation-satellite service systems and radioastronomy telescope sites”

[8] Recommendation ITU-R S.1586-1 (01/2007): “Calculation of unwanted emission levels produced by a non-geostationary fixed-satellite service system at radio astronomy sites”

[9] ITU-R Resolution 739 (Rev.WRC-19): “Compatibility between the radio astronomy service and the active space services in certain adjacent and nearby frequency bands”

[10] ECC Report 322: “Compatibility between the radio astronomy service and the active space services in certain adjacent and nearby frequency bands”, approved January 2022

[11] ECC Report 087: “Sharing studies between MES and existing terrestrial services in the bands already allocated to the MSS below 1 GHz”, approved June 2000

[12] Henry, C. 2020, “Kinéis raises 100 million euros to build and launch 25 IoT cubesats”, Spacenews, https://spacenews.com/kineis-raises-100-million-euros-to-build-and-launch-25-iot-cubesats/

[13] Voss, H. D., Dailey, J. F., Crowley, J. C., Nennett, B., White, A. J. 2014, “TSAT Globalstar ELaNa-5 Extremely Low-Earth Orbit (ELEO) Satellite”, 28th Annual AIAA/USU Conference on Small Satellites, https://digitalcommons.usu.edu/smallsat/2014/Workshop/3/

[14] FCC 2020, “FCC Authorizes Kuiper Satellite Constellation”, Federal Communications Commission, FCC-20-102, https://www.fcc.gov/document/fcc-authorizes-kuiper-satellite-constellation

[15] FCC 2018, “FCC Grants Kepler Communications Access to US Market”, Federal Communications Commission, FCC-18-162, https://www.fcc.gov/document/fcc-grants-kepler-communications-access-us-market

[16] Spina, N. 2020: “Application for market access authority for a non-geostationary satellite orbit system in Ka- and Ku-band frequencies”, Kepler Communications Inc., https://fcc.report/IBFS/SAT-LOA-20200526-00059/2379224.pdf

[17] FCC 2023: "Petition for Declaratory Ruling to Modify the U.S. Market Access Grant for the OneWeb Ku-band and Ka-Band NGSO FSS System”, Federal Communications Commission, FCC DA 23-362, https://www.fcc.gov/document/partial-grant-oneweb-ngso-modification-application

[18] FCC 2021: “FCC Grants SpaceX's Satellite Broadband Modification Application”, Federal Communications Commission, FCC-21-48, https://www.fcc.gov/document/fcc-grants-spacexs-satellite-broadband-modification-application

[19] SpaceX 2021, “Request for Modification of the Authorization for the SpaceX NGSO Satellite System”, IBFS File No. SAT-MOD-20200417-00037

[20] Telesat modifies its constellation 2378318.pdf (fcc.report)

[21] FCC Report - TELESAT LOW EARTH ORBIT NON-GEOSTATIONARY SATELLITE SYSTEM TECHNICAL INFORMATION SUPPLEMENT TO SCHEDULE

[22] Report ITU-R SM.2091-0 (2007): “Studies related to the impact of active space services allocated in adjacent or nearby bands on radio astronomy service”

[23] Recommendation ITU-R SM.1542-0 (07/2001): “The protection of passive services from unwanted emissions”

[24] Recommendation ITU-R SM.1633-0 (06/2003): “Compatibility analysis between a passive service and an active service allocated in adjacent and nearby bands”

[25] ECC Report 171: “Impact of unwanted emissions of Iridium satellites on radioastronomy operations in the band 1610.6-1613.8 MHz”, approved October 2011

[26] ECC Report 226: “Unwanted emissions of IRIDIUM satellites in the band 1610.6-1613.8 MHz, monitoring campaign 2013”, approved January 2015

[27] ECC Report 247: “Description of the software tool for processing of measurements data of IRIDIUM satellites at the Leeheim station”, approved October 2020

[28] ECC Report 349: “Unwanted emissions of IRIDIUM NEXT satellites in the band 1610.6-1613.8 MHz, monitoring campaign of November 2020 to May 2021”, approved February 2023

[29] ECC Report 271: “Compatibility and sharing studies related to NGSO satellite systems operating in the FSS bands 10.7-12.75 GHz (space-to-Earth) and 14-14.5 GHz (Earth-to-space)”, approved January 2018 and latest amended April 2021

[30] Python Software Foundation 2024, “Python”, Python Software Foundation, https://www.python.org/

[31] Project Jupyter 2024, “Jupyter”, Project Jupyter, https://jupyter.org/

[32] Winkel, B. 2024, “Pycraf”, GitHub, Inc., https://github.com/bwinkel/pycraf

[33] Winkel, B. 2024, “cysgp4”, GitHub, Inc., https://github.com/bwinkel/cysgp4

[34] Recommendation ITU-R M.2101-0 (02/2017): “Modelling and simulation of IMT networks and systems for use in sharing and compatibility studies”

[35] Recommendation ITU-R SM.1541-6 (08/2015): “Unwanted emissions in the out-of-band domain”

[36] Richter, C., Teichert, B., Pavelka, K. 2021, “Astronomical Investigation to Verify the Calendar Theory of the Nasca Lines”, Applied Sciences. 11. 1637. 10.3390/app11041637

[37] Recommendation ITU-R S.1325-3 (10/2003): ”Simulation methodologies for determining statistics of short-term interference between co-frequency, codirectional non-geostationary-satellite orbit fixed-satellite service systems in circular orbits and other non-geostationary fixed-satellite service systems in circular orbits or geostationary-satellite orbit fixed-satellite service networks”

[38] Recommendation ITU-R S.1528-0 (06/2001): “Satellite antenna radiation patterns for non-geostationary orbit satellite antennas operating in the fixed-satellite service below 30 GHz”